Structural plasticity and dynamic selectivity of acid-sensing ion channel - toxin complexes

by

Isabelle Rhyssa Joe Eduria Baconguis

A dissertation

Presented to the Neuroscience Graduate Program
and the Oregon Health and Science University
School of Medicine
in partial fulfillment of the
requirements for the degree of

Doctor of Philosophy

November 2012

School of Medicine

Oregon Health & Science University

CERTIFICATE OF APPROVAL

This is to certify that the Ph.D. dissertation of

ISABELLE BACONGUIS

has been approved on November 14, 2012

Advisor, Eric Gouaux, PhD

Member and Chair, Craig Jahr, PhD

Member, Show-Ling Shyng, PhD

Member, Francis Valiyaveetil, PhD

Member, William Zagotta, PhD

TABLE OF CONTENTS

Chapter 2

Structural plasticity and dynamic selectivity of acid sensing ion channel–spider toxin complexes 32

Acknowledgments

The success of this work would not have been possible without the encouragement and support from many individuals. I take this opportunity to express my gratitude to the Gouaux lab, past and present members, for the inspiration and entertainment. I especially would like to show my greatest appreciation to my mentor, Eric Gouaux, for his tremendous patience, trust, and invaluable guidance. It has been a great honor and privilege to work with all of them. Special thanks to the members of my thesis committee for their consistent support by providing constructive criticism and offering encouragement. Lastly, I am incredibly grateful to my family and friends for their understanding and endless support.

List of Tables

List of Figures

List of Abbreviations

AMPA	α-amino-3-hydroxy-5-methyl-4-isoxazolepropionic acid
APBS	Adaptive Poisson-Boltzmann Solver
APETx2	*Anthopleura elegantissima* toxin 2
ASIC	Acid-sensing Ion Channel
ASIC1mfc	Chicken acid-sensing ion channel subtype 1 minimal functional construct, residues 1-467
ATP	Adenosine triphosphate
cASIC1a	Chicken acid-sensing ion channel subtype 1 isoform a
CCP4	Collaborative Computational Project Number 4
CHO	Chinese Hamster Ovary cell
COOT	Crystallographic Object-Oriented Toolkit
DDM	*n*-dodecyl β-D-maltoside
DEG	Degenerin
DMPC	1,2-dimyristoyl-*sn*-glycero-3-phosphocholine
DTT	Dithiothreitol
EDTA	Ethylenediaminetetraacetic acid
ENaC	Epithelial Sodium Channel
FaNaCh	Phenylalanine-Methionine-Arginine-Phenylalanine-amide-activated Sodium Channel
FSEC	Fluorescence-detection Size-exclusion Chromatography
GFP	Green Fluorescent Protein
GMQ	2-Guanidine-4-methylquinazoline
HERG	Human Ether-à-go-go-Related Gene
ICK	Inhibitor Cystine Knot
lASIC1	Lamprey Acid-sensing Ion Channel subtype 1
LTP	Long-term Potentiation
MEC-4	Mechanosensory Channel subtype 4
MitTx	*Micrurus tener tener* Toxin
MME	Monomethyl Ether
MTS	Methanethiosulfonate
NCS	Non-crystallographic Symmetry
NMDA	*N*-methyl-D-aspartate
NMDG	*N*-methyl-D-glucamine
P2X4	Purinergic Receptor subtype 4
PcTx1	*Psalmopoeus cambridgei* Toxin 1
PEG	Polyethylene Glycol
PHENIX	Python-based Hierarchical ENvironment for Integrated Xtallography
rASIC	Rat Acid-sensing Ion Channel
sPLA2	Secreted phospholipase class A, cleaves the SN-2 acyl chain
TLS	Translation Libration Screw
TM1	Transmembrane Domain 1
TM2	Transmembrane Domain 2

TPEN	N,N,N'N'-tetrakis(-)[2-pyridylmethyl]-ethylenediamine
zfP2X4	Zebra Fish Purinergic Receptor subtype 4
Δ13	Chicken Acid-sensing Ion Channel Residues 14-463
ΔASIC1	Chicken Acid-sensing Ion Channel Residues 26-463

Abstract

Designed to detect pH fluctuations, acid-sensing ion channels began as mystifying molecules, initially known to only gate upon proton binding. However, recent studies unveiled a new mode of gating, independent of pH, thus revealing new roles in which they participate in the central and peripheral nervous systems. Harboring a large extracellular domain and anchored to the membrane bilayer with six transmembrane domains, these channels desensitize on a timescale of seconds, thus complicating structural studies investigating mechanisms underlying ion channel gating. To stabilize the activated state of the channel, I utilized potent and highly specific toxins and determined crystal structures of acid-sensing ion channel 1a in complexes with PcTx1 and MitTx, toxins identified from the venom of spider and snake, respectively, locking the channel in distinct open conformations. The structures illustrate that toxins bind at the subunit interface. Whereas the small PcTx1 binds near the acidic pocket, forming contacts between the thumb and finger domains, the heterodimeric MitTx boasts a large footprint, spanning from the top of the thumb domain down to the wrist region. Structural comparison between the toxin-bound states and the desensitized state reveal a structurally conserved scaffold in the upper palm domain and dynamic regions in the lower palm, thumb, and finger domains. PcTx1 primarily binds near the top of the thumb and upper palm domain, allowing for the lower palm domain to rearrange in a pH-dependent manner. By contrast, MitTx is wedged between two subunits near the lower palm domain, stabilizing the blanket of β-sheets in a pH-independent manner. The movements arising from toxin binding include 'flexing' of the lower palm domain, gating the channel through direct links to the transmembrane domains and contacts in the wrist region. Flexing of the lower palm domain induces an expansion in the extracellular vestibule that is proportional to the degree of rotation of the transmembrane domain, which

moves in an iris-like fashion. The distinct transmembrane arrangements of the toxin complexes reveal continuous pores with different ion selectivities, and mapped Cs^+ sites suggest that ions must be in a hydrated complex to successfully traverse the ion channel, consistent with a barrier mechanism for ion selectivity. Together, these structural and functional studies elucidate mechanisms of toxin binding, channel gating and ion selectivity and provide a foundation for therapeutic studies.

Chapter 1

Introduction

It was not until the late 1880's when the idea of neurons as individual entities that serve as building blocks of the nervous system was conceived, a principle that embodies the 'neuron doctrine' to which modern neuroscience adheres. Fighting the popular reticular theory and benefitting from Camillo Golgi's black reaction, a method for staining cells, Santiago Ramón y Cajal emphasized to the scientific community that individual neurons possess not only a soma but also processes, dendrites and axons, as Golgi had previously observed. Most importantly, Ramón y Cajal demonstrated that neurons extend cellular processes to other cells, forming discontinuous networks. The fundamental concept of the reticular theory centers on the idea that nervous impulse is propagated through diffusion within intertwining complex networks. By contrast with the reticular theory, the neuron theory requires an alternative mechanism to explain how neurons propagate information with each other, the requirement of a structure which we now identify as the synapse.

At the synapse, electrical and chemical signals converge for successful communication between structurally individual neurons. These signals are the consequence of biochemical and biophysical activities of many different types of proteins, some of which are ion channels. Ion channels comprise a large family of integral membrane proteins with different channel 'personalities' ranging from voltage-sensitivity to ligand recognition. The focus of this dissertation is to understand the relationships between atomic structure and biological function in a class of ligand-gated ion channels called acid sensing ion channels or ASICs. At the present time, the only known endogenous activating ligands for ASICs are protons. How these channels detect protons at the synapse, respond by altering their molecular conformation, reveal a pore that minimizes the amount of energy for ions to cross

the hydrophobic bilayer, and then reorganize to be equipped to detect a successive wave of protons, has left the field confounded.

Tackling questions that focus on the relationships between atomic structure and biological activity demands efforts from scientists from different fields. Generations of scientists have provided building blocks to surmount this wall of uncertainty ranging from physics to behavior. Specifically, structural biology has taken advantage of the fruits of labor generated by physicists to visualize macromolecules using x-ray crystallography. Though membrane proteins are often perceived as surly beasts that cannot be tamed for x-ray crystallographic studies, multiple advances have facilitated the crystallization of membrane proteins, resulting in a rapid growth of membrane protein structures and consequently, an increase in our understanding of ion channel function. To contribute to the understanding of how ASICs function in the nervous system, I have combined electrophysiology and x-ray crystallography for functional and structural analysis.

Acid-sensing ion channels (ASICs), members of the ENaC/DEG superfamily

The discovery more than 30 years ago by Krishtal and Pidoplichko unlocked a field of ion channels, the 'receptor for protons'[1, 2]. It was not until 15 years ago, however, with elegant studies pioneered by Lazdunki's group, that the ASIC genes were cloned, thus providing the first view of their primary structures and the inner workings of this class of ion channel[3]. ASIC1 was first thought to be the founding member of the ASIC family as defined by its novel amino acid sequence and proton-sensitive physiological properties and it was thus the first subunit to be crowned as an acid-sensing ion channel[3]. ASIC2 was actually the first ASIC gene to be cloned yet at the time it was initially believed to represent a mammalian equivalent of the *C. elegans* degenerin channel[4]. Because of its lower sensitivity

to protons, however, it was not immediately identified as an acid-sensing ion channel. The continuous application of molecular biological methods unearthed several other members of the ASIC family, which are now classified as members of a large class of ion channels deemed the ENaC/DEG superfamily[5-14]. Focusing mainly on the acid-sensing ion channels, it is not known whether only protons are the sole or even primary ligands of these ion channels. Nevertheless, the array of recently described biological roles and the litany of modulators of ASICs continue to expand, thus emphasizing that this class of ion channels is important to the development and function of the nervous system.

Cloned in the 1990's, the ENaC/DEG ion channels have so far been identified in insects, mollusks, nematodes, and mammals [15-20]. With a wide tissue distribution, these ion channels exhibit functional heterogeneity ranging from ligands to physiological properties, but what they do have in common are that they are amiloride-sensitive, voltage-independent, Na^+-selective channels[21]. Found only in vertebrates [5-14], ASICs are coded by four genes which give rise to six different subunits (ASIC1a, ASIC1b, ASIC2a, ASIC2b, ASIC3, and ASIC4) that form homomeric channels, except for ASIC2b and ASIC4, which assemble with other subunits to form heteromeric channels (**Figure 1.1**). They are found in the central and peripheral nervous systems with ASIC1a as the most abundant ASIC subunit in the central nervous system [3, 22, 23].

The crystal structures of chicken acid-sensing ion channel 1a

Prior to the determination of the first crystal structure of chicken ASIC1a (cASIC1a) in 2007 by the Gouaux group, various studies proposed that ASICs form tetrameric ion channels or even higher oligomeric assemblies. These hypotheses were shattered when the crystal structure at 1.9 Å resolution unambiguously demonstrated the trimeric assembly of

the channel [24] (PDB code: 2QTS). Over the following years other studies using methods such as atomic-force microscopy have solidified the conclusion that the ENaC/DEG superfamily are trimeric ion channels [25]. In addition to resolving the subunit stoichiometry, the first structure revealed a large extracellular domain linked to six transmembrane domains. In the initial crystal structure, the three-fold symmetry is preserved in the extracellular region of the ion channel yet upon transition to the membrane spanning region, the membrane domains are not arranged in a three-fold symmetrical fashion.

Each subunit resembles a hand clenching a ball and thus the subdomains have been defined as the thumb, finger, knuckle, upper and lower palm domains, the latter of which converge to the wrist region (**Figure 1.2**). The crucial wrist region is located at the interface where the extracellular domain, stapled together by multiple disulfide bonds, is in direct contact with the transmembrane domain and is proposed to be crucial for gating the ion channel. Moreover, the initial ASIC1a structure revealed clusters of negatively charged residues within a concave pocket defined by the thumb and finger domains and near a subunit interface, a region defined as the 'acidic pocket'. Together, the structure provided the first glimpse of a possible mechanism of proton sensing and the subsequent structural rearrangements required to gate the channel. To accomplish this high-resolution visualization, however, 26 residues at the N-terminus and 63 residues at the C- terminus were deleted, rendering the ion channel nonresponsive to low pH applications in patch-clamp electrophysiology experiments.

To preserve proton-dependent ion channel gating, the Gouaux group subsequently generated a new construct that included the full N-terminus, resulting in an ion channel that demonstrated wild-type like gating and ion selectivity. Similar to the first crystal structure,

crystals of this 'minimal functional construct' grew at low pH thus the resulting structure was proposed to represent a desensitized conformation [26] (PDB code: 3HGC) (**Figure 1.3**). This new desensitized state structure showed symmetrical arrangements of the transmembrane domains, by contrast with the asymmetric arrangement observed in the first crystal structure. The new structure also provided a map within the transmembrane domain that is perhaps involved in the desensitization of the channel which is called the desensitization gate, defined only by TM2 from all three subunits and forming an ~8 Å thick occlusion flanked by Asp 433 and Gly 436 on the extracellular and intracellular sides, respectively. In addition, the structure mapped possible cation-binding sites in the transmembrane region coordinated by the negatively charged side chains of Asp 433. Furthermore, the Gouaux group made side-by-side comparison with the first crystal structure of an ATP-gated zebrafish P2X4 receptor [27] and found that though these channels are unrelated, they display similar principles of channel architecture and perhaps gating [26]. Most importantly, the first two crystal structures of ASICs provided numerous opportunities for relating structural and functional studies by different groups, and these opportunities, in turn, have substantially advanced our understanding of ASICs and of the ENaC/DEG superfamily of ion channels[21] [28, 29].

ASIC gating

Each ASIC subunit confers different kinetics of activation and desensitization onto assembled trimeric ion channels [30] and accordingly different homomeric ASICs and different combinations of subunits forming heteromeric channels possess unique activation and desensitization profiles. ASICs undergo considerable changes in conformation during gating [31-33]. Studies using different approaches found evidence for structural movements

in the extracellular domain including the use of MTS reagents to investigate the accessibility of specific residues in the lower palm domain in ASIC3[32] or the manipulation of temperature slowing the rate of gating of DEG and ENaCs [31]. These indirect studies suggested that conformational changes in the extracellular domain of the ion channel were coupled with channel gating.

Several recent studies by two research groups using different orthologs of ASICs provided compelling evidence for dramatic movements occurring in the extracellular domain. Based on observations derived from the crystal structures of cASIC1a, Gründer's group postulated that the platforms of β-sheets that encapsulate the central vestibule region must undergo rearrangements during gating as they are directly linked to the transmembrane domains [34]. They observed that the β1-β2 linker region must assume distinct, state-dependent conformations based on accessibility studies with cysteine-modifying reagents. Reagents could only access the residues when the channel adopts a closed conformation. Furthermore, using pairs of cysteine residues as atomic rulers, they were able to detect dramatic rearrangements between the β1-β2 linkers and the β11-β12 linkers because introducing cysteines at these regions resulted in spontaneous disulfide formation stabilizing the desensitized state of the channel. These results indicated that linker regions that bridge the upper and lower regions of the extracellular domain are crucial in coupling ligand binding and gating of the ion channel.

In agreement with these observations, Canessa's group examined the roles of residues also in the vicinity of the linkers investigated by Gründer's group and found that changing the properties of side chains at these sites also modifies channel behavior [35, 36]. In the β1-β2 linker region, altering the residues from a hydrophobic side chain to a polar side

chain stabilizes the closed conformation of the channel by reducing the affinity of the channel for protons[35]. Furthermore, changing the properties of the side chain in the neighboring β11-β12 linker, which the crystal structure has been shown to be in close proximity to the β1-β2 linker, also stabilizes the closed conformation of the channel [36]. Therefore, modifying residues at the β1-β2 and β11-β12 linkers alters the channel behavior and implies that these regions undergo crucial structural changes upon gating the channel.

While the studies of Gründer and Canessa noted above show that modification of amino acid side chains in the linker regions alter the pH-dependent properties of the channel, recent studies demonstrate that ligands other than protons can modulate ASIC activity in a pH-independent manner by way of interactions with residues in the central vestibule. Reminiscent of observations from studies using cysteine-based modification with acidic residues in the central vestibule [37], the small molecule GMQ and the polyamine agmatine activate ASIC3 at physiological pH range [38]. Paradoxically, amiloride has also been shown to activate ASIC3 within physiological pH values [37], thus suggesting that in the presence of specific 'effector' molecules, ASICs can gate independent of pH. Because GMQ, amiloride, and agmatine are thought to bind in the central vestibule, which is encased by β-sheets that include the β1-β2 and β11-β12 linkers and the lower palm domain, these regions must be crucial in gating the channel in a pH-dependent or -independent manner.

In prescient experiments that preceded the cASIC1a structure, McCleskey's group scanned residues located immediately after TM1 and found that Glu 79 (rat ASIC1a numbering), when mutated to cysteine (E79C), only reacts to cysteine-modifying reagents when the channel is closed but not when desensitized, indicating different conformations between the two states [32]. Furthermore, covalent modification of the E79C mutant has a

slowed desensitization rate when compared to wild-type channel. Surprisingly, the unmodified E79C mutant desensitizes faster than the wild-type channel, thus reinforcing the conclusion that Glu 79 plays a crucial role in channel gating.

Locating residues involved in pH-sensing in ASICs has been challenging, especially when different combinations of ASIC subunits produce different ion channel properties. Glu 79 likely participates in pH sensing, not only because of experiments mentioned above but also because of its location within the functionally crucial lower palm domain, as shown in the crystal structures. Although it is not well understood as to whether the ionization characteristics of Glu 79 defines the desensitization properties of ASICs, simulation studies calculating pKa values of acidic residues throughout the extracellular domain of ASICs have indicated that Glu 79 is the most highly perturbed ionizable residue in the lower palm domain and perhaps important to proton sensing [39].

The central vestibule region is not the only possible proton sensing domain within the large extracellular domain. The first crystal structure revealed a cluster of acidic residues located in what is now called the acidic pocket and that was proposed to include at least a portion of the proton sensor. It is certainly a most enticing proposition because the acidic pocket rests atop the finger and thumb domains, where domain movements could be transduced via the wrist region, through close contacts between aromatic residues, Tyr 72 and Trp 288, that together act as clasps between the extracellular and the transmembrane regions. Indeed, mutations at the putative proton-sensing domain modify the affinity for protons but they do not completely eliminate the ability for the channel to sense pH fluctuations [24]. Nevertheless, supporting the conclusion that the Tyr 72 and Trp 288 aromatic residues in the wrist region are crucial for gating the channel are experiments which

show that perturbing these residues results in a dramatic shift of the apparent proton affinity to acidic conditions as well as a substantial change in the activation and desensitization properties of the channel [40]. But based on results for investigating residues crucial in sensing protons and domains important in gating the channel, ASICs are more complex in that they do not contain one domain focused on proton sensing and it is possible that their main function is not restricted to proton sensing. Perhaps they are a little more promiscuous and besides protons, they detect other molecules that are released at or are present with the synapse that modulate ion channel gating at typical physiological pH values.

Like the extracellular domain, the transmembrane domain is sensitive to perturbations. The degenerin site, located in the second transmembrane region (TM2), is one of the most studied sites on the DEG/ENaC ion channel family because of its profound effect in channel gating when modified by mutagenesis and the resulting cell-damaging consequences [41, 42]. A mutation at this site on degenerin channels of *C. elegans* that replaces an Ala with larger residues has been found to cause neurodegeneration[17, 18]. The phenotype for this mutant is a constitutively active channel. ENaCα, which has a Ser at the degenerin site, and ASIC2, with a Gly, exhibit similar channel kinetics as the degenerin channels when mutations are introduced [41, 42]. These mutations entail replacing small residues such as Gly and Ala with residues that have larger side chains, such as Thr and Phe, suggesting that steric hindrance occurs in the TM domain destabilizing the closed state of the channel [18, 43, 44].

Though the role of a bulky side chain within TM2 demonstrates a prominent role in favoring the open state of ENaC/DEG channels, TM1 exhibits a larger role in destabilizing the closed conformation within the ASIC subfamily. The biphasic current property of

ASIC3, comprising of a transient and a sustained current, presents ample opportunity for examining structural elements within the transmembrane region that prevents the channel from inactivating. Designing chimeras of ASIC1 and ASIC3 isolated the cytosolic N-terminus and TM1 domain as essential for generating sustained currents[45]. Supporting this notion, sequence alignment of lamprey ASIC1 (lASIC1) and rASIC highlight a crucial position in TM1 near the extracellular vestibule region, Trp 64 in lASIC1 but an Arg 64 in rat, which determines the stability of the open conformation of lASIC1. lASIC1 does not desensitize rapidly with continued application of protons, unlike rASIC1, but replacing Trp 64 with arginine results in a desensitizing lASIC1[46]. In summary, the roles that the transmembrane regions play in channel activity can best be summarized as opposing forces where TM1 destabilizes while TM2, forming the desensitization gate [26], stabilizes the closed conformation of the ion channel.

The highly conserved TM2 of the ENaC/DEG is residence to the putative selectivity filter, the region of the transmembrane ion channel that discriminates between monovalent cations [4, 41, 47-56]. The permeability ratio between Na^+ and K^+ within the family vary with ENaC being the most selective for Na^+ and strongly inhibited by K^+ ions[57, 58]. Because residues in TM2 are highly conserved, the observed differences in ion selectivity between the members of the ENaC/DEG superfamily suggest that other factors contribute to defining the ion selectivity of a particular family member. Perturbations at the degenerin site and at the desensitization gate of ASICs, a site at which a Cs^+ ion was mapped [26], do not alter selectivity and thus imply that these sites are not part of the selectivity filter. Instead, mutations at these sites in ASICs alter gating properties with the Asp 433 likely playing a role in the stability of the shut ion channel gate [47]. Mutations that alter ion

selectivity are focused on three residues, glycine, alanine and serine, located near the cytoplasmic end of TM2 and defined by residues 443-445 in cASIC1a. Mutations at these sites readily alter selectivity of the channel to be more nonselective. Though highly conserved, TM2 is not the only crucial domain for selectivity because different subunits behave differently. In fact, studies have indicated that residues preceding TM1 are also crucial for ion selectivity and are within a region that varies greatly across different subunits in the ASIC family. Furthermore, the pre-TM1 region is home to the important 'HG' sequence, a dipeptide motif conserved in all ENaC/DEG family members [59, 60]. Though its role is not at all understood, it is thought to be crucial in channel gating and ion selectivity. Thus the differences in gating and selectivity properties can be attributed to the less conserved TM1 within the ASIC family.

ASIC modulators

Divalent cations

Acid-sensing ion channels are modulated by divalent cations like Ca^{2+} and Zn^{2+} whereby the specific action of the cation depends on the subunit content of channels [3, 61, 62]. Whereas low concentrations of zinc inhibit ASIC1a, high concentrations of zinc potentiate ASIC2a [63-65]. ASIC channels in the brain are predominantly homomeric ASIC1a or heteromeric ASIC1a/ASIC2a assemblies. The differential regulation that is dependent upon the subunit content of the channels results in an interesting property of heteromeric ASIC1a/ASIC2a channels whereby they are inhibited at low concentrations of zinc but are potentiated at high concentrations [63, 66]. The inhibition by zinc of ASIC1a-containing receptors has been narrowed down to one residue located in the finger domain, Lys 133 of murine ASIC1 [63]. Interestingly, K133 in human ASIC1a is also involved in

channel potentiation by zinc [66, 67]. As for ASIC2a, site-directed mutagenesis of 10 histidines pinpointed two residues, His 162 and His 339, that are central to zinc potentiation [64]. While investigating these sites on ASIC2a, the crucial role of His 72 as the main protein sensor of ASIC2a was also uncovered [64].

The mechanism by which zinc modulates ASIC channels was best examined using ASIC1a-ASIC2a heterotrimeric channels which are differentially modulated at low and high concentrations of zinc [64]. The balance between the two different actions of zinc is best described by a model where there is a high affinity, inhibitory site and a low affinity site that diminishes the inhibitory action of the high affinity site. Consistent with this model, one observes a potentiation of the current upon increasing the zinc concentration yet this increase is best thought of as simply a relief of inhibition. Alternatively, this model is exemplified by comparing the effects of zinc in the absence and presence of a zinc chelator TPEN. The potentiating effects of zinc are only observed only in the absence of TPEN whereas in the presence of TPEN, zinc does not potentiate the activity of the channel [63].

In addition to the diametrically opposing regulation by zinc, the gating behavior of ASICs is interwoven with a balancing act between protons and Ca^{2+}, where the former favors the open and desensitized states while the latter promotes stabilization of the closed state [3, 68-71]. Studies propose that Ca^{2+} [72-74] stabilizes the closed state of the ion channel via two distinct mechanisms: allosteric binding and pore blocking [68, 69, 71]. The pore-blocking mechanism was based on a study focusing on ASIC3 and argued that Ca^{2+} and protons compete for the same binding site and that activation of the channel is mainly due to relief of the Ca^{2+} block. The implication of this model is that activation of the channel does not require extensive conformational movements in order to allow ion flux. The basis

of this hypothesis was further supported by the fact that ASIC3 exhibits a noninactivating current in the presence of low concentrations of calcium at physiological conditions. While this model has several appealing elements, it is not clear how channel activity is potentiated when the proton concentration is increased. To explain the irregularities with the first model, another study postulated that Ca^{2+} modulates via two mechanisms: allosteric binding and Ca^{2+} block. Canessa's group showed that despite mutation of the Ca^{2+} binding site residue Glu 425 [69](rASIC1a numbering), a residue located near the extracellular mouth of ion channel pore [26], the calcium-dependent shift of channel activation is preserved, thus supporting a role of a second, allosteric Ca^{2+} binding site. While the role of Glu 426 in the modulation of ASIC gating by Ca^{2+} is well-characterized [69], the residues involved in the allosteric mechanism, however, have not been identified [71].

Amiloride and derivatives

Amiloride is the classic open channel blocker of the ENaC/DEG superfamily with the highest affinity for ENaCs, blocking ion channel activity at nanomolar concentrations, though studies have shown that aside from pore blocking, amiloride also binds in the extracellular domain exhibiting a paradoxical role by potentiating channel activity [16, 75-79]. By contrast, amiloride blocks different isoforms of ASICs in the micromolar range [3, 4, 29, 80]. Whereas ENaC differentiate between different amiloride derivatives, exhibiting the highest affinity for phenamil, ASICs poorly discriminate between various amiloride derivatives, thereby emphasizing the substantial differences in the pharmacology of ion channel blockers acting on ENaCs and ASICs [81]. With amiloride as the most effective and well-characterized blocker to date for the ENaC/DEG family, its action on ENaC depends on two components within the molecule, the guanidinium and the pyrazine ring.

Addition of benzyl and phenyl group to the guanidium side increases affinity suggesting a hydrophobic patch proximal to the amiloride binding site that can further stabilize the interaction in the pore [81]. Various efforts of designing higher affinity compounds for ASICs derived from amiloride [82, 83] have yielded improved blocker potency but none possess the specificity and affinity of amiloride for ENaCs.

Peptide toxins

PcTx1

The mechanisms by which ions and inhibitors modulate ASICs and other members of this large family have fueled curiosity due to the wide variety of functions and diseases in which these ion channels are involved. While amiloride blocks ASIC activity in a voltage-dependent manner, ASIC1a is specifically inhibited by psalmotoxin 1 (PcTx1) in a voltage-independent manner. PcTx1 is 40-amino acid peptide that demonstrates promise for developing new therapeutic strategies. Found in the venom of a South American tarantula *Psalmopoeus cambridgei* [84, 85], it is a potent, specific, and reversible inhibitor of homomeric rASIC1a, blocking the current at pH 6 with an IC_{50} of 0.9 nM. The peptide contains 9 basic residues, has a pI of 10.38 in its native form, and consists of three disulfide bridges, three anti-parallel β sheets, and a protein fold called an inhibitor cystine knot (ICK) }[85]. Electrophysiology, binding assays and chimeras of ASIC1a and ASIC1b in rat models (rASIC) have suggested that it binds at a site in the extracellular domain [86]. The toxin increases the channel affinity for protons, pushing the channel towards a desensitized state, resulting in its inhibition [87]. Binding of toxin to ASIC1a is state-dependent, favoring the desensitized and open states [88].

APETx2

Isolated from sea anemone, *Anthopleura elegantissima*, APETx2 is a 42-amino acid peptide stapled by three disulfide bonds to form four β sheets encompassing a fold classified as all-β [89]. While adopting the same fold as APETx1, the two toxins greatly differ in that APETx1 targets potassium channels Kv3.4 and HERG, whereas APETx2 specifically targets ASIC3 [89] . Unlike PcTx1, which binds specifically to homomeric ASIC1a channels with nanomolar affinity, APETx2 can bind to ASIC3 heteromeric forms but at a lower affinity, and has no effect on ASIC2a/ASIC3 channels. Similar to the actions of amiloride, APETx2 can only block the fast peak current of ASIC3 and it has no effect on the noninactivating sustained current [90]. It is still unknown as to how APETx2 inhibits ASIC3 activity.

MitTx

In 2011, a new toxin which targets ASICs was identified from the venom of the Texas coral snake by the Julius lab [91]. The toxin, deemed MitTx, is of a heterodimeric complex of Kunitz-type and phospholipase-like subunits, α and β, respectively. Both subunits must be present in order to affect gating of ASICs. The heterodimer complex is most potent with ASIC1a and ASIC1b with an EC_{50} of 9 nM. Bohlen et al. suggested that this effect on the channel is mainly limited by the formation of the toxin complex. More importantly, the toxin complex appears to stabilize an open state of ASIC. Furthermore, the complex blocks psalmotoxin effects suggesting that toxins compete for the same site or that the binding of one toxin allosterically hinders the binding of the other by changing the properties of the site.

Mambalgins

Following the discovery of heterodimeric peptide toxin from coral snakes, Lazdunki's group once again revealed a new toxin isolated from the black mamba [92]. Like APETx2, the toxin exhibits analgesic effects but with a potency similar to morphine without the negative side effects. The findings of this study support the possibilities that ASIC1a is crucial in the pain pathway and thus a target for therapeutic strategies.

Other modulators

ASICs are sensitive to endogenous molecules like big dynorphin and dynorphin A by reducing proton affinity of steady-state desensitization by binding in the extracellular domain. Studies show that big dynorphin and PcTx1 antagonize each other's effects on ASICs suggesting that they either compete for the same site or one allosterically hinders the binding of the other [93]. Like the opioid peptides, RFamides also reduce proton affinity of steady-state desensitization and slow the rate of desensitization by binding in the extracellular domain [94-100]. Besides neuropeptides, polyamines like spermine and agmatine also modulate ASIC activity [38, 72, 101]. Whereas spermine stabilizes the closed/resting state of the channel, agmatine activates ASIC at physiological pH conditions. Whereas agmatine is proposed to bind in the nonproton ligand binding domain of ASIC located in the lower palm domain, the binding sites of dynorphin and spermine are still unknown.

ASIC and the central nervous system

The role of ASICs in the central nervous system is still unknown but manipulations that modify expression of ASICs result in significant effects that include changes in synaptic properties in different regions of the brain [22, 102-105]. With ASIC1 as the most

abundantly expressed subunit in the brain in particular regions of strong synaptic inputs, co-localizing with PSD-95, a known scaffolding protein at the postsynaptic density (PSD), ASICs are implicated in synaptic transmission [106-108]. Consequently, ASICs have been implicated in synaptic plasticity, learning, and memory [108] . Though their role in long-term potentiation is not completely understood, previous studies have shown that their excitatory contribution during high-frequency stimulation in the hippocampus assists in neuronal depolarization, which is key in activating NMDA receptors, the principal players of LTP in CA1 neurons [108] . How ASICs are activated in these regions is still unknown but since vesicles are acidic in nature, it is likely that their release exposes the synapse to higher concentrations of protons, perhaps activating ASICs [109, 110].

However, excessive activation of ASICs through acidification is pathologic in the central nervous system [103]. Excessive influx of Ca^{2+} is the main cause in neurotoxicity during ischemic brain injury. Inhibition of the primary routes of Ca^{2+} influx, such as through glutamate receptors and voltage-gated Ca^{2+} channels, however, has not been effective [111-113]. Emerging studies have shifted attention towards ASIC1a because it is Ca^{2+}-permeable [103, 114-116]. During ischemic stroke, acidosis occurs [117, 118] inhibiting glutamate receptors such as *N*-methyl-D-aspartate receptors (NMDARs) [119, 120]. The acidic conditions that arise as a consequence of stroke are within the ASIC1a window of activation; therefore, ASIC1a is capable of permitting Ca^{2+} ions to permeate cells and trigger neurotoxic events. Inhibition by amiloride, and PcTx1 prevent cell death that occur during ischemic stroke [103], making ASIC1a a promising target for therapeutic intervention in stroke [119-121].

The strongest role yet to be determined of ASICs in the nervous system, however, is likely their function in fear-conditioning. Detected at highest density in the amygdala, ASIC1a specifically plays a key role in fear conditioning [22, 108, 122, 123]. Deleting the ASIC1 gene in brains of transgenic mice yields animals with a lack of fear-related responses while overexpression of ASIC1 reverses the phenotype. Interestingly, restoring ASIC1 expression into ASIC1 knockout mice, specifically in the amygdala, only rescues fear memory but not other fear-related phenotypes, emphasizing the global importance of ASIC1 in the fear circuit in the central nervous system [124]. Likely related to its role in the fear circuit, ASIC1 is proposed to be the chemosensor for carbon monoxide, a toxic substance that robustly elicits fear-related behaviors [125].

Contrasting with it excitatory role, ASICs also have been shown to play a protective role in epileptic conditions, shortening seizure duration, seizure severity, and promoting seizure termination [126]. The paradoxical role of ASIC is proposed to be due to its differential expression pattern whereby it shows higher expression in inhibitory interneurons in the hippocampus than in the excitatory pyramidal neurons. Consequently, activation of ASICs in the interneurons increases inhibitory tone, thus diminishing the pathophysiological events brought on by seizure-related conditions. This model proposes acidification as a path for seizure termination and therefore a strategy for therapeutic design through targeting of ASICs. Moreover, targeting ASIC1a by using PcTx1 helps to define which subunit(s) play a part in ameliorating the effects of experimental epilepsy.

ASIC and the peripheral nervous system

Dating back to the discovery of ASICs by Krishtal and Pidoplichko, ASICs have been proposed to play significant roles in pain sensation based on their location in dorsal

root and trigeminal neurons [1]. Although studies using knockout mice have led to inconclusive results in attempts to understand ASIC involvement in nociception in the central and nervous systems, specifically targeting ASIC activity through the use of blockers like amiloride and specific toxins like PcTx1, APETx2, MitTx2, and mambalgins have presented strong evidence that they play crucial roles in nociception. Advancement in our understanding of their roles elucidated by pain studies suggest that not only ASIC3 but also ASIC1a-containing channels participate in pain transduction pathways.

Significance

The first crystal structures of cASIC1a revealed a trimeric assemblage [24] which resolved subunit stoichiometry ambiguities stemming from studies of ENaCs and FaNaChs [127-130]. Furthermore, this initial structural study presented domain arrangement which provided clues as to how protons gate ASICs and how desensitization in ASICs occurs by way of complete pore occlusion and stabilization of a shut ion channel gate. Though these structures greatly contributed to the advancement of our understanding with the gating mechanism of ENaC/DEG family of channels, we have only begun to unravel their function. Recent discoveries of pH-independent modulation have enhanced the complexity of the channels but they have also opened a new window of views that suggest ASICs have prominent roles in the central and peripheral nervous systems. To further elucidate how ASICs function, this dissertation focuses on understanding the mechanism of gating through a combination of electrophysiology and x-ray crystallography to correlate structure and function of the cASIC1a in complexes with the toxins PcTx1 and MitTx.

Preview of the dissertation

Chapter two focuses on the cASIC1a –PcTx1 structure at two pH conditions, pH 7.25 and pH 5.5. Structural and functional analyses reveal that PcTx1 induces two different and pH-dependent conformations of cASIC1a. The structure at pH 7.25 demonstrates a large symmetrical open pore that is nonselective in nature as examined by electrophysiology with current reversing close to 0 mV. Contrasting with the pH 7.25 structure, the complex at low pH reveals a Na^+-selective pore that is asymmetric in nature and that perhaps resembles the transmembrane domain arrangements of the heterotrimeric ENaC. Both structures reveal similar interactions between the channel and PcTx1. The toxin molecule wedges into an amphipathic subunit interface, inserting its basic hairpin loop into the negatively-charged acidic pocket and burying a cluster of hydrophobic residues within hydrophobic contacts on the thumb domain. Difference anomalous maps using Cs^+ to map cation binding regions reveal common sites found in the wrist region from both high and low pH structures, at a site which I proposed stabilizes the open conformation of the channel.

Chapter three delineates the interaction of MitTx with cASIC1a at pH 5.5. Like PcTx1, MitTx opens cASIC1a but unlike the low pH structure with PcTx1, MitTx traps the channel in a symmetrical open conformation. Biionic experiments show that Cs^+ ions do not readily permeate through the channel and that the pore does not efficiently discriminate between Na^+ and K^+. Like PcTx1, MitTx wedges between subunits. To mimic cation coordination as accomplished by the Cs^+ ion in the PcTx1 structures, MitTx protrudes a lysine to coordinate with the same backbone oxygens in the wrist region, supporting our hypothesis that cation coordination in the wrist region is crucial in stabilizing an open

conformation of the transmembrane domains. Taken together, the PcTx1 and MitTx complexes with chicken ASIC1a provide new insights into the action of toxins on ASICs and, most importantly, on the fundamental relationships between atomic structure and biological function in ASICs and in the superfamily of ENaC/DEG ion channels.

Figures and legends

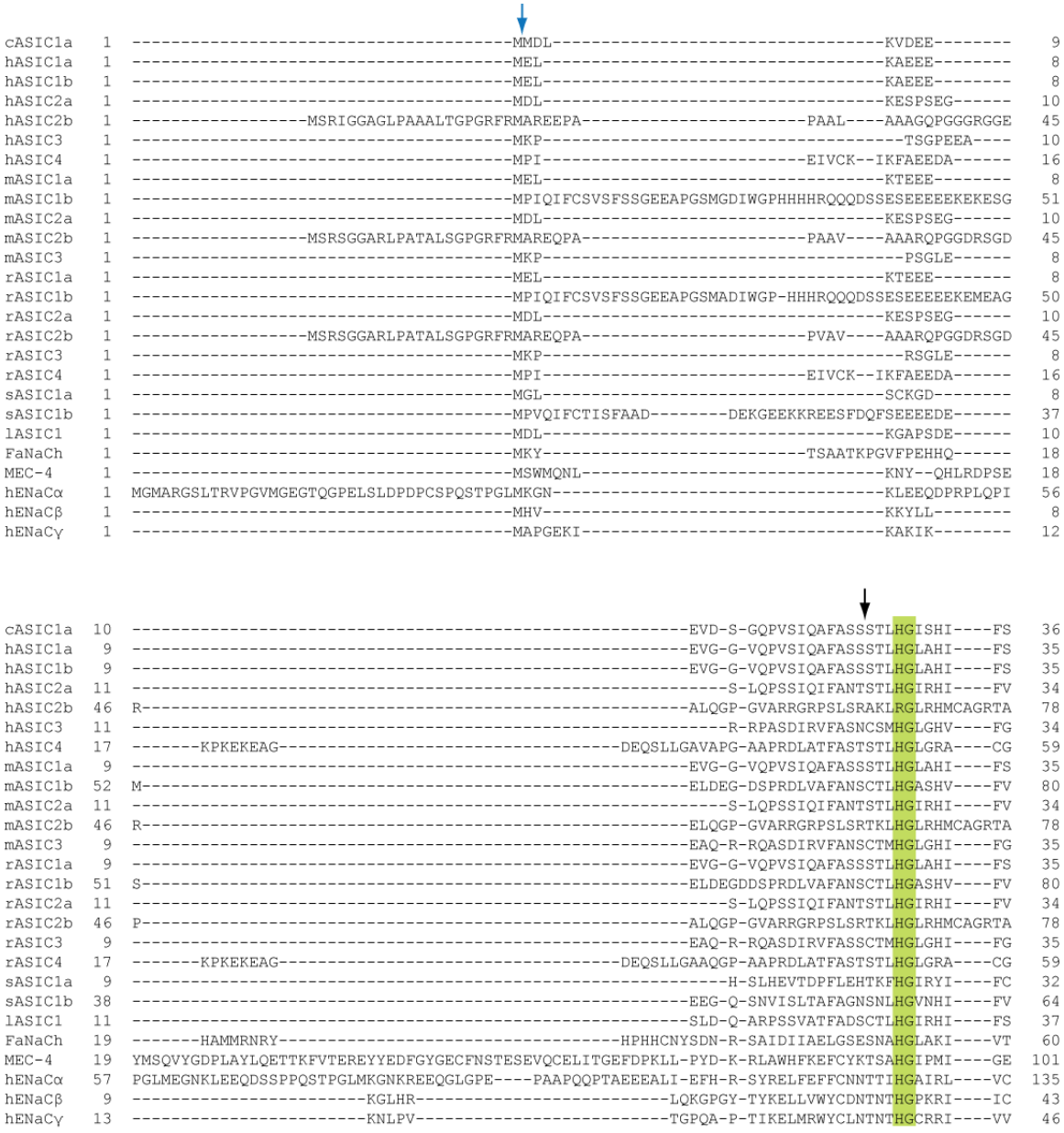

```
cASIC1a  37  YERLSLKRVVWALCFMGSLALLALVCTNRIQYYFLYPHVTKLDEVAA-TRLTFPAVTFCNLNEFRFSRVTKNDLYHA--GELLALLNNRY  123
hASIC1a  36  YERLSLKRALWALCFLGSLAVLLCVCTERVQYYFHYHHVTKLDEVAA-SQLTFPAVTLCNLNEFRFSQVSKNDLYHA--GELLALLNNRY  122
hASIC1b  36  YERLSLKRALWALCFLGSLAVLLCVCTERVQYYFHYHHVTKLDEVAA-SQLTFPAVTLCNLNEFRFSQVSKNDLYHA--GELLALLNNRY  122
hASIC2a  35  YGPLTIRRVLWAVAFVGSLGLLLVESSERVSYYFSYQHVTKVDEVVA-QSLVFPAVTLCNLNGFRFSRLTTNDLYHA--GELLALLDVNL  121
hASIC2b  79  AGGSFQRRALWVLAFCTSFGLLLSWSSNRLLYWLSFPSHTRVHREWS-RQLPFPAVTVCNNNPLRFPRLSKGDLYYA--GHWLGLLLPNR  165
hASIC3   35  PGSLSLRRGMWAAAVVLSVATFLYQVAERVRYYREFHHQTALDERES-HRLIFPAVTLCNINPLRRSRLTPNDLHWA--GSALLGLDPAE  121
hASIC4   60  PGPHGLRRTLWALALLTSLAAFLYQAAGLARGYLTRPHLVAMDPAAPAPVAGFPAVTLCNINRFRHSALSDADIFHL--ANLTGLPPKDR  147
mASIC1a  36  YERLSLKRALWALCFLGSLAVLLCVCTERVQYYFCYHHVTKLDEVAA-SQLTFPAVTLCNLNEFRFSQVSKNDLYHA--GELLALLNNRY  122
mASIC1b  81  EGGPGPRQALWAVAFVIALGAFLCQVGDRVAYYLSYPHVTLLDEVAT-TELVFPAVTFCNTNAVRLSQLSYPDLLYL--APMLGLDESDD  167
mASIC2a  35  YGPLTIRRVLWAVAFVGSLGLLLVESSERVSYYFSYQHVTKVDEVVA-QSLVFPAVTLCNLNGFRFSRLTTNDLYHA--GELLALLDVNL  121
mASIC2b  79  AGGSFQRRALWVLAFCTSLGLLLSWSSNRLLYWLSFPSHTRVHREWS-RQLPFPAVTVCNNNPLRFPRLSKGDLYYA--GHWLGLLLPNR  165
mASIC3   36  PGGLTLRRGLWATAVLLSLAAFLYQVAERVRYYGEFHHKTTLDERES-HQLTFPAVTLCNINPLRRSRLTPNDLHWA--GTALLGLDPAE  122
rASIC1a  36  YERLSLKRALWALCFLGSLAVLLCVCTERVQYYFCYHHVTKLDEVAA-SQLTFPAVTLCNLNEFRFSQVSKNDLYHA--GELLALLNNRY  122
rASIC1b  81  EGGPGPRQALWAVAFVIALGAFLCQVGDRVAYYLSYPHVTLLDEVAT-TELVFPAVTFCNTNAVRLSQLSYPDLLYL--APMLGLDESDD  167
rASIC2a  35  YGPLTIRRVLWAVAFVGSLGLLLVESSERVSYYFSYQHVTKVDEVVA-QSLVFPAVTLCNLNGFRFSRLTTNDLYHA--GELLALLDVNL  121
rASIC2b  79  AGGSFQRRALWVLAFCTSLGLLLSWSSNRLLYWLSFPSHTRVHREWS-RQLPFPAVTVCNNNPLRFPRLSKGDLYYA--GHWLGLLLPNR  165
rASIC3   36  PGGLTLRRGLWATAVLLSLAAFLYQVAERVRYYGEFHHKTTLDERES-HQLTFPAVTLCNINPLRRSRLTPNDLHWA--GTALLGLDPAE  122
rASIC4   60  PGPHGLRRTLWVLALLTSLAAFLYQAASLARGYLTRPHLVAMDPAAPAPVAGFPAVTLCNINRFRHSALSDADIFHL--ANLTGLPPKDR  147
sASIC1a  33  KRLSYQRRVLWLVAFLASFGLLCTWSSNRIRYLLSTPVHTKLHMIWA-KNLSFPAVTICNNNMLILRRMTKSDVYLT--GHWLGLLNESR  119
sASIC1b  65  EGGCGVRQVLWGCAFLSSLAIFLYQVMDRIMYYLEYHHITALDEMDS-PFMYFPAVTLCNFNRFRRSKITYPDLTFA--GSLMGYTEGMD  151
lASIC1   38  PGGLSVRRLLWLLAFLGSLSLLVLQSLDWVQYYLRYPCVTKQDEVST-PLTVFPAVTLCNLNEFRFSRMTRNDLYHA--GELLALLDERM  124
FaNaCh   61  SR-DTKRKVIWALLVIAGFTAATLQLSLLVRKYLQFQVVELSEIKDS-MPVQYPSVSICNIEPISLRTIRRMYFNNE--SQNLITWLRFI  146
MEC-4   102  AP-NVYYRAVWVVLFLGCMIMLYLNAQSVLDKYNRNEKIVDIQLKF--DTAPFPAITLCNLNPYKASLATSVDLVKRTLSAFDGAMGKAG  188
hENaCα  136  SQHNRMKTAFWAVLWLCTFGMMYWQFGLLFGEYFSYPVSLNINLNS--DKLVFPAVTICTLNPYRYPEIKEELEELD--RITEQTLFDLY  221
hENaCβ   44  EG--PKKKAMWFLLTLLFAALVCWQWGIFIRTYLSWEVSVSLSVGF--KTMDFPAVTICNASPFKYSKIKHLLKDLD--ELMEAVLERIL  127
hENaCγ   47  SR-GRLRRLLWIGFTLTAVALILWQCALLVFSF--YTVSVSIKVHF--RKLDFPAVTICNINPYKYSTVRHLLADLE--QETREALKSLY  129

cASIC1a 124  EI-------------------------PDTQT--ADEKQLEILQ-------------------------------------------  140
hASIC1a 123  EI-------------------------PDTQM--ADEKQLEILQ-------------------------------------------  139
hASIC1b 123  EI-------------------------PDTQM--ADEKQLEILQ-------------------------------------------  139
hASIC2a 122  QI-------------------------PDPHL--ADPSVLEALR-------------------------------------------  138
hASIC2b 166  TA-----------------------RPLVSELLRGDEPRRQWFR-------------------------------------------  186
hASIC3  122  HA-------------------------AFL---------RALGR-------------------------------------------  131
hASIC4  148  DG-------------------------------------------------------------------------------------  149
mASIC1a 123  EI-------------------------PDTQM--ADEKQLEILQ-------------------------------------------  139
mASIC1b 168  PG---------------------------VPL--APPGP-----------------------------------------------  177
mASIC2a 122  QI-------------------------PDPHL--ADPTVLEALR-------------------------------------------  138
mASIC2b 166  TA-----------------------RPLVSELLRGDEPRRQWFR-------------------------------------------  186
mASIC3  123  HA-------------------------AYL---------RALGQ-------------------------------------------  132
rASIC1a 123  EI-------------------------PDTQM--ADEKQLEILQ-------------------------------------------  139
rASIC1b 168  PG---------------------------VPL--APPGP-----------------------------------------------  177
rASIC2a 122  QI-------------------------PDPHL--ADPTVLEALR-------------------------------------------  138
rASIC2b 166  TA-----------------------RPLVSELLRGDEPRRQWFR-------------------------------------------  186
rASIC3  123  HA-------------------------AYL---------RALGQ-------------------------------------------  132
rASIC4  148  DG-------------------------------------------------------------------------------------  149
sASIC1a 120  SV-----------------------NPTAREI--LKDKRWKWFE-------------------------------------------  138
sASIC1b 152  LG---------------------------FQL--APSARN-----------------------------------------------  162
lASIC1  125  EI-------------------------VEPRF--ADAQVIAQLR-------------------------------------------  141
FaNaCh  147  QK-------------------------------------------------------------------------------------  148
MEC-4   189  GNKDHEEEREVVTEPPTTPAPTTKPARRRGKRD--LSGAFFEPGFARCLCGSQGSSEQEDKDEEKEEELLETTTKKVFNINDADEEWDGM  276
hENaCα  222  KYSSFT-------------TLVAGSRSRRDLRG--TLPHPLQRLRVPPPP-------------------------------------  256
hENaCβ  128  APELSH-------------ANATRNL----------NFSIWNHTPLVLIDERNPH---------------------------------  159
hENaCγ  130  GFPESR-------------KRREAESWNSVSEG--KQPRFSHRIPLLIFDQDEKG---------------------------------  169
```

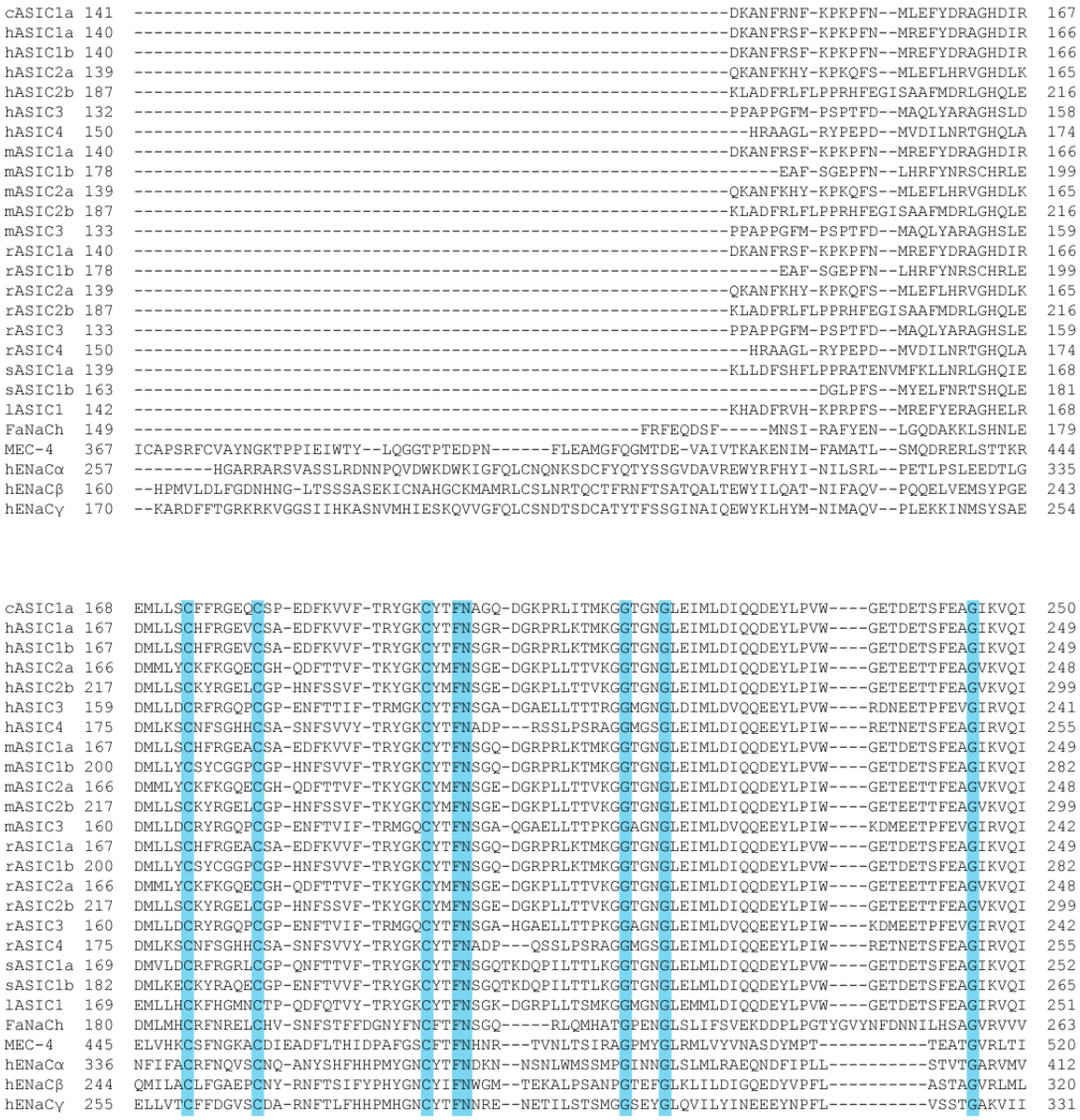
cASIC1a 141 ---------- DKANFRNF-KPKPFN--MLEFYDRAGHDIR 167
hASIC1a 140 ---------- DKANFRSF-KPKPFN--MREFYDRAGHDIR 166
hASIC1b 140 ---------- DKANFRSF-KPKPFN--MREFYDRAGHDIR 166
hASIC2a 139 ---------- QKANFKHY-KPKQFS--MLEFLHRVGHDLK 165
hASIC2b 187 ---------- KLADFRLFLPPRHFEGISAAFMDRLGHQLE 216
hASIC3 132 ---------- PPAPPGFM-PSPTFD--MAQLYARAGHSLD 158
hASIC4 150 ---------- HRAAGL-RYPEPD--MVDILNRTGHQLA 174
mASIC1a 140 ---------- DKANFRSF-KPKPFN--MREFYDRAGHDIR 166
mASIC1b 178 ---------- EAF-SGEPFN--LHRFYNRSCHRLE 199
mASIC2a 139 ---------- QKANFKHY-KPKQFS--MLEFLHRVGHDLK 165
mASIC2b 187 ---------- KLADFRLFLPPRHFEGISAAFMDRLGHQLE 216
mASIC3 133 ---------- PPAPPGFM-PSPTFD--MAQLYARAGHSLE 159
rASIC1a 140 ---------- DKANFRSF-KPKPFN--MREFYDRAGHDIR 166
rASIC1b 178 ---------- EAF-SGEPFN--LHRFYNRSCHRLE 199
rASIC2a 139 ---------- QKANFKHY-KPKQFS--MLEFLHRVGHDLK 165
rASIC2b 187 ---------- KLADFRLFLPPRHFEGISAAFMDRLGHQLE 216
rASIC3 133 ---------- PPAPPGFM-PSPTFD--MAQLYARAGHSLE 159
rASIC4 150 ---------- HRAAGL-RYPEPD--MVDILNRTGHQLA 174
sASIC1a 139 ---------- KLLDFSHFLPPRATENVMFKLLNRLGHQIE 168
sASIC1b 163 ---------- DGLPFS--MYELFNRTSHQLE 181
lASIC1 142 ---------- KHADFRVH-KPRPFS--MREFYERAGHELR 168
FaNaCh 149 ---------- FRFEQDSF-----MNSI-RAFYEN--LGQDAKKLSHNLE 179
MEC-4 367 ICAPSRFCVAYNGKTPPIEIWTY--LQGGTPTEDPN------FLEAMGFQGMTDE-VAIVTKAKENIM-FAMATL--SMQDRERLSTTKR 444
hENaCα 257 --------HGARRARSVASSLRDNNPQVDWKDWKIGFQLCNQNKSDCFYQTYSSGVDAVREWYRFHYI-NILSRL--PETLPSLEEDTLG 335
hENaCβ 160 --HPMVLDLFGDNHNG-LTSSSASEKICNAHGCKMAMRLCSLNRTQCTFRNFTSATQALTEWYILQAT-NIFAQV--PQQELVEMSYPGE 243
hENaCγ 170 --KARDFFTGRKRKVGGSIIHKASNVMHIESKQVVGFQLCSNDTSDCATYTFSSGINAIQEWYKLHYM-NIMAQV--PLEKKINMSYSAE 254
cASIC1a 168 EMLLSCFFRGEQCSP-EDFKVVF-TRYGKCYTFNAGQ-DGKPRLITMKGGTGNGLEIMLDIQQDEYLPVW----GETDETSFEAGIKVQI 250
hASIC1a 167 DMLLSCHFRGEVCSA-EDFKVVF-TRYGKCYTFNSGR-DGRPRLKTMKGGTGNGLEIMLDIQQDEYLPVW----GETDETSFEAGIKVQI 249
hASIC1b 167 DMLLSCHFRGEVCSA-EDFKVVF-TRYGKCYTFNSGR-DGRPRLKTMKGGTGNGLEIMLDIQQDEYLPVW----GETDETSFEAGIKVQI 249
hASIC2a 166 DMMLYCKFKGQECGH-QDFTTVF-TKYGKCYMFNSGE-DGKPLLTTVKGGTGNGLEIMLDIQQDEYLPIW----GETEETTFEAGVKVQI 248
hASIC2b 217 DMLLSCKYRGELCGP-HNFSSVF-TKYGKCYMFNSGE-DGKPLLTTVKGGTGNGLEIMLDIQQDEYLPIW----GETEETTFEAGVKVQI 299
hASIC3 159 DMLLDCRFRGQPCGP-ENFTTIF-TRMGKCYTFNSGA-DGAELLTTTRGGMGNGLDIMLDVQQEEYLPVW----RDNEETPFEVGIRVQI 241
hASIC4 175 DMLKSCNFSGHHCSA-SNFSVVY-TRYGKCYTFNADP---RSSLPSRAGGMGSGLEIMLDIQQEEYLPIW----RETNETSFEAGIRVQI 255
mASIC1a 167 DMLLSCHFRGEACSA-EDFKVVF-TRYGKCYTFNSGQ-DGRPRLKTMKGGTGNGLEIMLDIQQDEYLPVW----GETDETSFEAGIKVQI 249
mASIC1b 200 DMLLYCSYCGGPCGP-HNFSVVF-TRYGKCYTFNSGQ-DGRPRLKTMKGGTGNGLEIMLDIQQDEYLPVW----GETDETSFEAGIKVQI 282
mASIC2a 166 DMMLYCKFKGQECGH-QDFTTVF-TKYGKCYMFNSGE-DGKPLLTTVKGGTGNGLEIMLDIQQDEYLPIW----GETEETTFEAGVKVQI 248
mASIC2b 217 DMLLSCKYRGELCGP-HNFSSVF-TKYGKCYMFNSGE-DGKPLLTTVKGGTGNGLEIMLDIQQDEYLPIW----GETEETTFEAGVKVQI 299
mASIC3 160 DMLLDCRYRGQPCGP-ENFTVIF-TRMGQCYTFNSGA-QGAELLTTPKGGAGNGLEIMLDVQQEEYLPIW----KDMEETPFEVGIRVQI 242
rASIC1a 167 DMLLSCHFRGEACSA-EDFKVVF-TRYGKCYTFNSGQ-DGRPRLKTMKGGTGNGLEIMLDIQQDEYLPVW----GETDETSFEAGIKVQI 249
rASIC1b 200 DMLLYCSYCGGPCGP-HNFSVVF-TRYGKCYTFNSGQ-DGRPRLKTMKGGTGNGLEIMLDIQQDEYLPVW----GETDETSFEAGIKVQI 282
rASIC2a 166 DMMLYCKFKGQECGH-QDFTTVF-TKYGKCYMFNSGE-DGKPLLTTVKGGTGNGLEIMLDIQQDEYLPIW----GETEETTFEAGVKVQI 248
rASIC2b 217 DMLLSCKYRGELCGP-HNFSSVF-TKYGKCYMFNSGE-DGKPLLTTVKGGTGNGLEIMLDIQQDEYLPIW----GETEETTFEAGVKVQI 299
rASIC3 160 DMLLDCRYRGQPCGP-ENFTVIF-TRMGQCYTFNSGA-HGAELLTTPKGGAGNGLEIMLDVQQEEYLPIW----KDMEETPFEVGIRVQI 242
rASIC4 175 DMLKSCNFSGHHCSA-SNFSVVY-TRYGKCYTFNADP---QSSLPSRAGGMGSGLEIMLDIQQEEYLPIW----RETNETSFEAGIRVQI 255
sASIC1a 169 DMVLDCRFRGRLCGP-QNFTTVF-TRYGKCYTFNSGQTKDQPILTTLKGGTGNGLELMLDIQQDEYLPVW----GETDETSFEAGIKVQI 252
sASIC1b 182 DMLKECKYRAQECGP-ENFTVVF-TRYGKCYTFNSGQTKDQPILTTLKGGTGNGLELMLDIQQDEYLPVW----GETDETSFEAGIKVQI 265
lASIC1 169 EMLLHCKFHGMNCTP-QDFQTVY-TRYGKCYTFNSGK-DGRPLLTSMKGGMGNGLEMMLDIQQDEYLPVW----GETDETSFEAGIRVQI 251
FaNaCh 180 DMLMHCRFNRELCHV-SNFSTFFDGNYFNCFTFNSGQ-----RLQMHATGPENGLSLIFSVEKDDPLPGTYGVYNFDNNILHSAGVRVVV 263
MEC-4 445 ELVHKCSFNGKACDIEADFLTHIDPAFGSCFTFNHNR---TVNLTSIRAGPMYGLRMLVYVNASDYMPT----------TEATGVRLTI 520
hENaCα 336 NFIFACRFNQVSCNQ-ANYSHFHHPMYGNCYTFNDKN--NSNLWMSSMPGINNGLSLMLRAEQNDFIPLL----------STVTGARVMV 412
hENaCβ 244 QMILACLFGAEPCNY-RNFTSIFYPHYGNCYIFNWGM--TEKALPSANPGTEFGLKLILDIGQEDYVPFL----------ASTAGVRLML 320
hENaCγ 255 ELLVTCFFDGVSCDA-RNFTLFHHPMHGNCYTFNNRE--NETILSTSMGGSEYGLQVILYINEEEYNPFL----------VSSTGAKVII 331

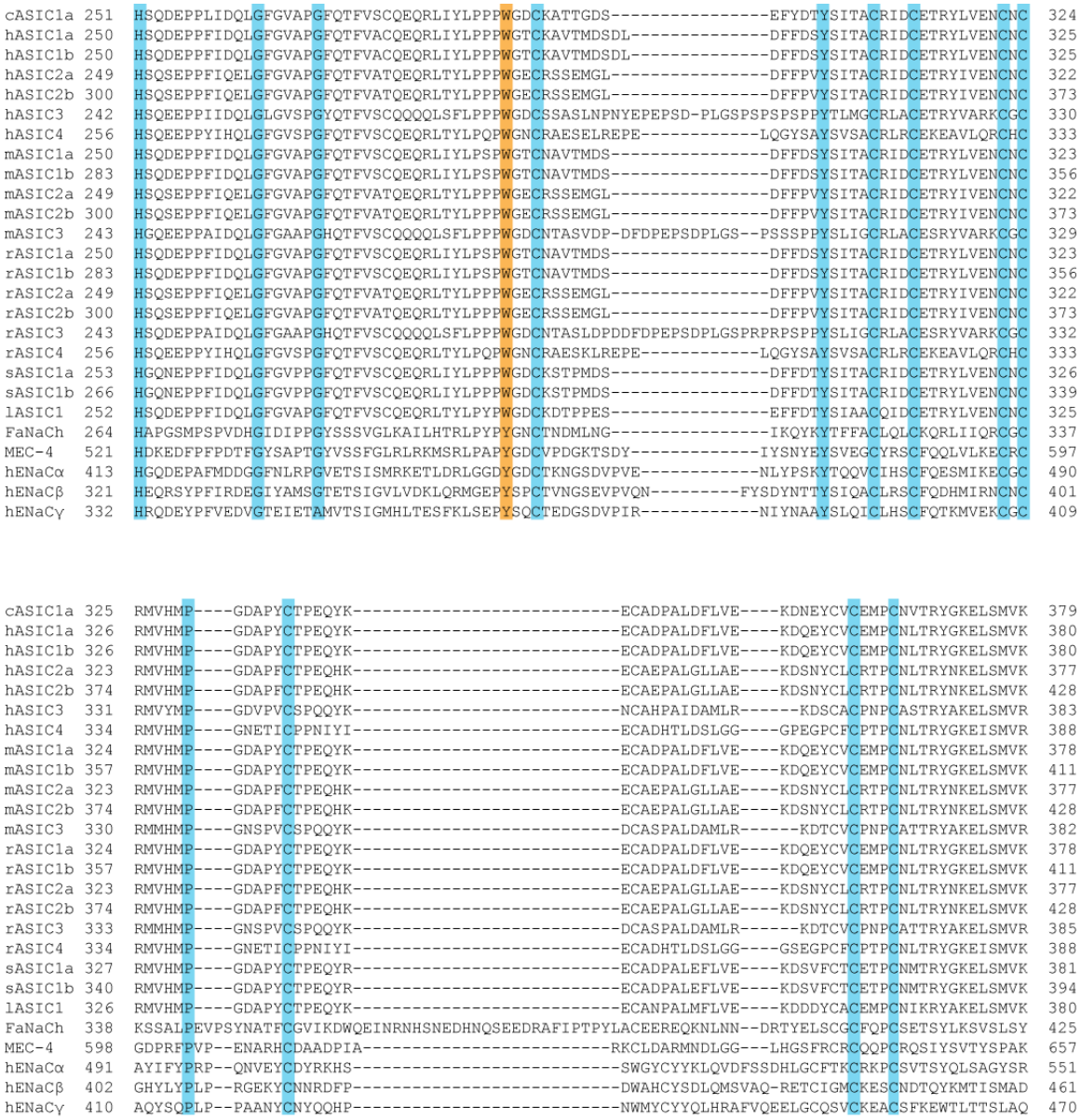
cASIC1a 251 HSQDEPPLIDQLGFGVAPGFQTFVSCQEQRLIYLPPPWGDCKATTGDS----------EFYDTYSITACRIDCETRYLVENCNC 324
hASIC1a 250 HSQDEPPFIDQLGFGVAPGFQTFVACQEQRLIYLPPPWGTCKAVTMDSDL----------DFFDSYSITACRIDCETRYLVENCNC 325
hASIC1b 250 HSQDEPPFIDQLGFGVAPGFQTFVACQEQRLIYLPPPWGTCKAVTMDSDL----------DFFDSYSITACRIDCETRYLVENCNC 325
hASIC2a 249 HSQSEPPFIQELGFGVAPGFQTFVATQEQRLTYLPPPWGECRSSEMGL----------DFFPVYSITACRIDCETRYIVENCNC 322
hASIC2b 300 HSQSEPPFIQELGFGVAPGFQTFVATQEQRLTYLPPPWGECRSSEMGL----------DFFPVYSITACRIDCETRYIVENCNC 373
hASIC3 242 HSQEEPPIIDQLGLGVSPGYQTFVSCQQQQLSFLPPPWGDCSSASLNPNYEPEPSD-PLGSPSPSPSPPYTLMGCRLACETRYVARKCGC 330
hASIC4 256 HSQEEPPYIHQLGFGVSPGFQTFVSCQEQRLTYLPQPWGNCRAESELREPE----------LQGYSAYSVSACRLRCEKEAVLQRCHC 333
mASIC1a 250 HSQDEPPFIDQLGFGVAPGFQTFVSCQEQRLIYLPSPWGTCNAVTMDS----------DFFDSYSITACRIDCETRYLVENCNC 323
mASIC1b 283 HSQDEPPFIDQLGFGVAPGFQTFVSCQEQRLIYLPSPWGTCNAVTMDS----------DFFDSYSITACRIDCETRYLVENCNC 356
mASIC2a 249 HSQSEPPFIQELGFGVAPGFQTFVATQEQRLTYLPPPWGECRSSEMGL----------DFFPVYSITACRIDCETRYIVENCNC 322
mASIC2b 300 HSQSEPPFIQELGFGVAPGFQTFVATQEQRLTYLPPPWGECRSSEMGL----------DFFPVYSITACRIDCETRYIVENCNC 373
mASIC3 243 HGQEEPPAIDQLGFGAAPGHQTFVSCQQQQLSFLPPPWGDCNTASVDP-DFDPEPSDPLGS--PSSSPPYSLIGCRLACESRYVARKCGC 329
rASIC1a 250 HSQDEPPFIDQLGFGVAPGFQTFVSCQEQRLIYLPSPWGTCNAVTMDS----------DFFDSYSITACRIDCETRYLVENCNC 323
rASIC1b 283 HSQDEPPFIDQLGFGVAPGFQTFVSCQEQRLIYLPSPWGTCNAVTMDS----------DFFDSYSITACRIDCETRYLVENCNC 356
rASIC2a 249 HSQSEPPFIQELGFGVAPGFQTFVATQEQRLTYLPPPWGECRSSEMGL----------DFFPVYSITACRIDCETRYIVENCNC 322
rASIC2b 300 HSQSEPPFIQELGFGVAPGFQTFVATQEQRLTYLPPPWGECRSSEMGL----------DFFPVYSITACRIDCETRYIVENCNC 373
rASIC3 243 HSQDEPPAIDQLGFGAAPGHQTFVSCQQQQLSFLPPPWGDCNTASLDPDDFDPEPSDPLGSPRPRPSPPYSLIGCRLACESRYVARKCGC 332
rASIC4 256 HSQEEPPYIHQLGFGVSPGFQTFVSCQEQRLTYLPQPWGNCRAESKLREPE----------LQGYSAYSVSACRLRCEKEAVLQRCHC 333
sASIC1a 253 HGQNEPPFIDQLGFGVPPGFQTFVSCQEQRLIYLPPPWGDCKSTPMDS----------DFFDTYSITACRIDCETRYLVENCNC 326
sASIC1b 266 HGQNEPPFIDQLGFGVPPGFQTFVSCQEQRLIYLPPPWGDCKSTPMDS----------DFFDTYSITACRIDCETRYLVENCNC 339
lASIC1 252 HSQDEPPFIDQLGFGVAPGFQTFVSCQEQRLTYLPYPWGDCKDTPPES----------EFFDTYSIAACQIDCETRYLVENCNC 325
FaNaCh 264 HAPGSMPSPVDHGIDIPPGYSSSVGLKAILHTRLPYPYGNCTNDMLNG----------IKQYKYTFFACLQLCKQRLIIQRCGC 337
MEC-4 521 HDKEDFPFPDTFGYSAPTGYVSSFGLRLRKMSRLPAPYGDCVPDGKTSDY----------IYSNYEYSVEGCYRSCFQQLVLKECRC 597
hENaCα 413 HGQDEPAFMDDGGFNLRPGVETSISMRKETLDRLGGDYGDCTKNGSDVPVE----------NLYPSKYTQQVCIHSCFQESMIKECGC 490
hENaCβ 321 HEQRSYPFIRDEGIYAMSGTETSIGVLVDKLQRMGEPYSPCTVNGSEVPVQN---------FYSDYNTTYSIQACLRSCFQDHMIRNCNC 401
hENaCγ 332 HRQDEYPFVEDVGTEIETAMVTSIGMHLTESFKLSEPYSQCTEDGSDVPIR----------NIYNAAYSLQICLHSCFQTKMVEKCGC 409
cASIC1a 325 RMVHMP----GDAPYCTPEQYK--------------------------ECADPALDFLVE----KDNEYCVCEMPCNVTRYGKELSMVK 379
hASIC1a 326 RMVHMP----GDAPYCTPEQYK--------------------------ECADPALDFLVE----KDQEYCVCEMPCNLTRYGKELSMVK 380
hASIC1b 326 RMVHMP----GDAPYCTPEQYK--------------------------ECADPALDFLVE----KDQEYCVCEMPCNLTRYGKELSMVK 380
hASIC2a 323 RMVHMP----GDAPFCTPEQHK--------------------------ECAEPALGLLAE----KDSNYCLCRTPCNLTRYNKELSMVK 377
hASIC2b 374 RMVHMP----GDAPFCTPEQHK--------------------------ECAEPALGLLAE----KDSNYCLCRTPCNLTRYNKELSMVK 428
hASIC3 331 RMVYMP----GDVPVCSPQQYK--------------------------NCAHPAIDAMLR------KDSCACPNPCASTRYAKELSMVR 383
hASIC4 334 RMVHMP----GNETICPPNIYI--------------------------ECADHTLDSLGG----GPEGPCFCPTPCNLTRYGKEISMVR 388
mASIC1a 324 RMVHMP----GDAPYCTPEQYK--------------------------ECADPALDFLVE----KDQEYCVCEMPCNLTRYGKELSMVK 378
mASIC1b 357 RMVHMP----GDAPYCTPEQYK--------------------------ECADPALDFLVE----KDQEYCVCEMPCNLTRYGKELSMVK 411
mASIC2a 323 RMVHMP----GDAPFCTPEQHK--------------------------ECAEPALGLLAE----KDSNYCLCRTPCNLTRYNKELSMVK 377
mASIC2b 374 RMVHMP----GDAPFCTPEQHK--------------------------ECAEPALGLLAE----KDSNYCLCRTPCNLTRYNKELSMVK 428
mASIC3 330 RMMHMP----GNSPVCSPQQYK--------------------------DCASPALDAMLR------KDTCVCPNPCATTRYAKELSMVR 382
rASIC1a 324 RMVHMP----GDAPYCTPEQYK--------------------------ECADPALDFLVE----KDQEYCVCEMPCNLTRYGKELSMVK 378
rASIC1b 357 RMVHMP----GDAPYCTPEQYK--------------------------ECADPALDFLVE----KDQEYCVCEMPCNLTRYGKELSMVK 411
rASIC2a 323 RMVHMP----GDAPFCTPEQHK--------------------------ECAEPALGLLAE----KDSNYCLCRTPCNLTRYNKELSMVK 377
rASIC2b 374 RMVHMP----GDAPFCTPEQHK--------------------------ECAEPALGLLAE----KDSNYCLCRTPCNLTRYNKELSMVK 428
rASIC3 333 RMMHMP----GNSPVCSPQQYK--------------------------DCASPALDAMLR------KDTCVCPNPCATTRYAKELSMVR 385
rASIC4 334 RMVHMP----GNETICPPNIYI--------------------------ECADHTLDSLGG----GSEGPCFCPTPCNLTRYGKEISMVK 388
sASIC1a 327 RMVHMP----GDAPYCTPEQYR--------------------------ECADPALEFLVE----KDSVFCTCETPCNMTRYGKELSMVK 381
sASIC1b 340 RMVHMP----GDAPYCTPEQYR--------------------------ECADPALEFLVE----KDSVFCTCETPCNMTRYGKELSMVK 394
lASIC1 326 RMVHMP----GDAPYCTPEQYK--------------------------ECANPALMFLVE----KDDDYCACEMPCNIKRYAKELSMVK 380
FaNaCh 338 KSSALPEVPSYNATFCGVIKDWQEINRNHSNEDHNQSEEDRAFIPTPYLACEEREQKNLNN--DRTYELSCGCFQPCSETSYLKSVSLSY 425
MEC-4 598 GDPRFPVP--ENARHCDAADPIA--------------------------RKCLDARMNDLGG---LHGSFRCRCQQPCRQSIYSVTYSPAK 657
hENaCα 491 AYIFYPRP--QNVEYCDYRKHS--------------------------SWGYCYYKLQVDFSSDHLGCFTKCRKPCSVTSYQLSAGYSR 551
hENaCβ 402 GHYLYPLP--RGEKYCNNRDFP--------------------------DWAHCYSDLQMSVAQ-RETCIGMCKESCNDTQYKMTISMAD 461
hENaCγ 410 AQYSQPLP--PAANYCNYQQHP--------------------------NWMYCYYQLHRAFVQEELGCQSVCKEACSFKEWTLTTSLAQ 470

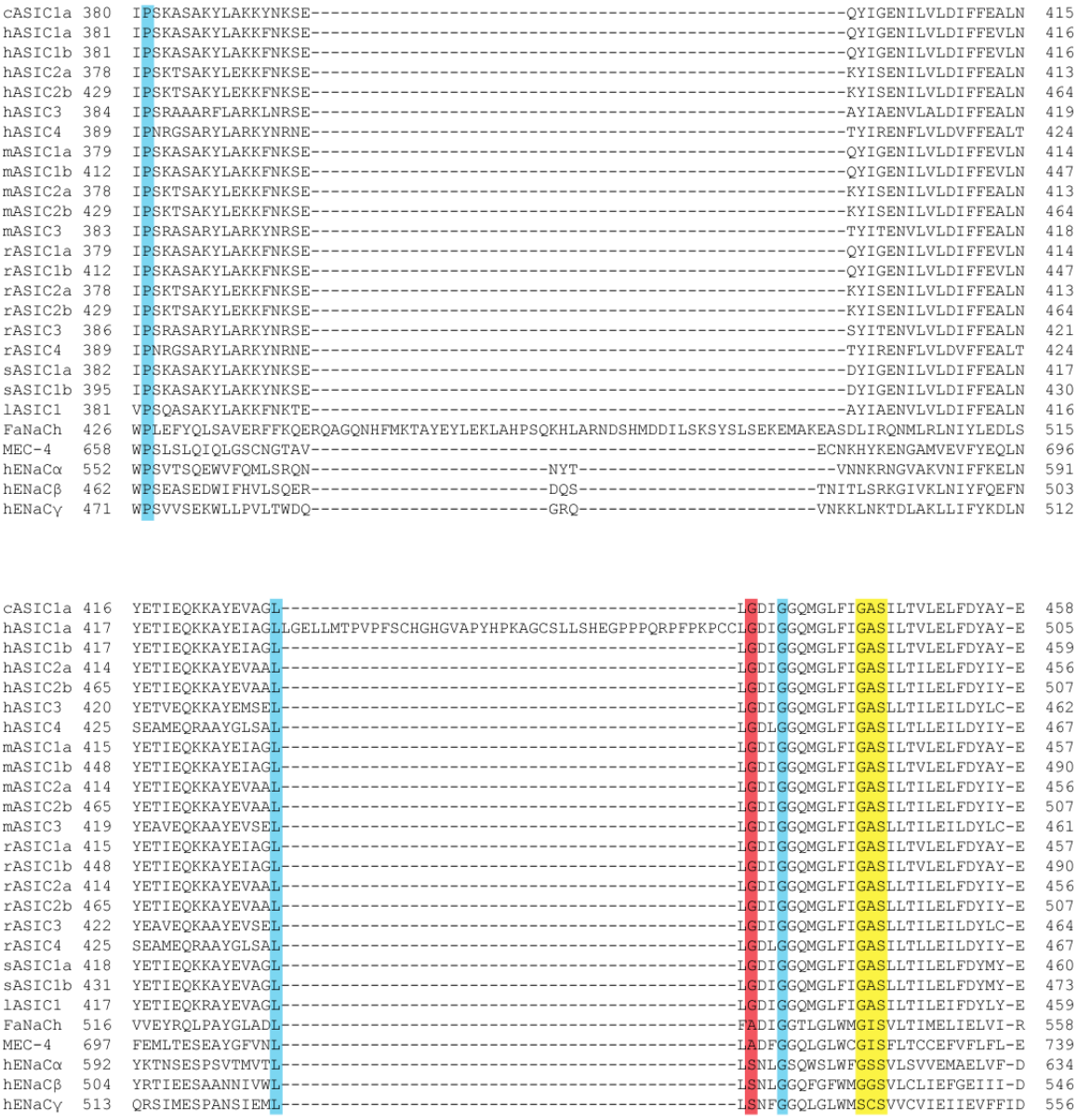
cASIC1a 380 IPSKASAKYLAKKYNKSE----------QYIGENILVLDIFFEALN 415
hASIC1a 381 IPSKASAKYLAKKFNKSE----------QYIGENILVLDIFFEVLN 416
hASIC1b 381 IPSKASAKYLAKKFNKSE----------QYIGENILVLDIFFEVLN 416
hASIC2a 378 IPSKTSAKYLEKKFNKSE----------KYISENILVLDIFFEALN 413
hASIC2b 429 IPSKTSAKYLEKKFNKSE----------KYISENILVLDIFFEALN 464
hASIC3 384 IPSRAAARFLARKLNRSE----------AYIAENVLALDIFFEALN 419
hASIC4 389 IPNRGSARYLARKYNRNE----------TYIRENFLVLDVFFEALT 424
mASIC1a 379 IPSKASAKYLAKKFNKSE----------QYIGENILVLDIFFEVLN 414
mASIC1b 412 IPSKASAKYLAKKFNKSE----------QYIGENILVLDIFFEVLN 447
mASIC2a 378 IPSKTSAKYLEKKFNKSE----------KYISENILVLDIFFEALN 413
mASIC2b 429 IPSKTSAKYLEKKFNKSE----------KYISENILVLDIFFEALN 464
mASIC3 383 IPSRASARYLARKYNRSE----------TYITENVLVLDIFFEALN 418
rASIC1a 379 IPSKASAKYLAKKFNKSE----------QYIGENILVLDIFFEVLN 414
rASIC1b 412 IPSKASAKYLAKKFNKSE----------QYIGENILVLDIFFEVLN 447
rASIC2a 378 IPSKTSAKYLEKKFNKSE----------KYISENILVLDIFFEALN 413
rASIC2b 429 IPSKTSAKYLEKKFNKSE----------KYISENILVLDIFFEALN 464
rASIC3 386 IPSRASARYLARKYNRSE----------SYITENVLVLDIFFEALN 421
rASIC4 389 IPNRGSARYLARKYNRNE----------TYIRENFLVLDVFFEALT 424
sASIC1a 382 IPSKASAKYLAKKYNKSE----------DYIGENILVLDIFFEALN 417
sASIC1b 395 IPSKASAKYLAKKYNKSE----------DYIGENILVLDIFFEALN 430
lASIC1 381 VPSQASAKYLAKKFNKTE----------AYIAENVLVLDIFFEALN 416
FaNaCh 426 WPLEFYQLSAVERFFKQERQAGQNHFMKTAYEYLEKLAHPSQKHLARNDSHMDDILSKSYSLSEKEMAKEASDLIRQNMLRLNIYLEDLS 515
MEC-4 658 WPSLSLQIQLGSCNGTAV----------ECNKHYKENGAMVEVFYEQLN 696
hENaCα 552 WPSVTSQEWVFQMLSRQN----------NYT----------VNNKRNGVAKVNIFFKELN 591
hENaCβ 462 WPSEASEDWIFHVLSQER----------DQS----------TNITLSRKGIVKLNIYFQEFN 503
hENaCγ 471 WPSVVSEKWLLPVLTWDQ----------GRQ----------VNKKLNKTDLAKLLIFYKDLN 512
cASIC1a 416 YETIEQKKAYEVAGL----------LGDIGGQMGLFIGASILTVLELFDYAY-E 458
hASIC1a 417 YETIEQKKAYEIAGLLGELLMTPVPFSCHGHGVAPYHPKAGCSLLSHEGPPPQRPFPKPCCLGDIGGQMGLFIGASILTVLELFDYAY-E 505
hASIC1b 417 YETIEQKKAYEIAGL----------LGDIGGQMGLFIGASILTVLELFDYAY-E 459
hASIC2a 414 YETIEQKKAYEVAAL----------LGDIGGQMGLFIGASILTILELFDYIY-E 456
hASIC2b 465 YETIEQKKAYEVAAL----------LGDIGGQMGLFIGASILTILELFDYIY-E 507
hASIC3 420 YETVEQKKAYEMSEL----------LGDIGGQMGLFIGASLLTILEILDYLC-E 462
hASIC4 425 SEAMEQRAAYGLSAL----------LGDLGGQMGLFIGASILTLLEILDYIY-E 467
mASIC1a 415 YETIEQKKAYEIAGL----------LGDIGGQMGLFIGASILTVLELFDYAY-E 457
mASIC1b 448 YETIEQKKAYEIAGL----------LGDIGGQMGLFIGASILTVLELFDYAY-E 490
mASIC2a 414 YETIEQKKAYEVAAL----------LGDIGGQMGLFIGASILTILELFDYIY-E 456
mASIC2b 465 YETIEQKKAYEVAAL----------LGDIGGQMGLFIGASILTILELFDYIY-E 507
mASIC3 419 YEAVEQKAAYEVSEL----------LGDIGGQMGLFIGASLLTILEILDYLC-E 461
rASIC1a 415 YETIEQKKAYEIAGL----------LGDIGGQMGLFIGASILTVLELFDYAY-E 457
rASIC1b 448 YETIEQKKAYEIAGL----------LGDIGGQMGLFIGASILTVLELFDYAY-E 490
rASIC2a 414 YETIEQKKAYEVAAL----------LGDIGGQMGLFIGASLLTILELFDYIY-E 456
rASIC2b 465 YETIEQKKAYEVAAL----------LGDIGGQMGLFIGASLLTILELFDYIY-E 507
rASIC3 422 YEAVEQKAAYEVSEL----------LGDIGGQMGLFIGASLLTILEILDYLC-E 464
rASIC4 425 SEAMEQRAAYGLSAL----------LGDLGGQMGLFIGASILTLLEILDYIY-E 467
sASIC1a 418 YETIEQKKAYEVAGL----------LGDIGGQMGLFIGASLLTILELFDYMY-E 460
sASIC1b 431 YETIEQKKAYEVAGL----------LGDIGGQMGLFIGASLLTILELFDYMY-E 473
lASIC1 417 YETIEQKRAYEVAGL----------LGDIGGQMGLFIGASILTILEIFDYLY-E 459
FaNaCh 516 VVEYRQLPAYGLADL----------FADIGGTLGLWMGISVLTIMELIELVI-R 558
MEC-4 697 FEMLTESEAYGFVNL----------LADFGGQLGLWCGISFLTCCEFVFLFL-E 739
hENaCα 592 YKTNSESPSVTMVTL----------LSNLGSQWSLWFGSSVLSVVEMAELVF-D 634
hENaCβ 504 YRTIEESAANNIVWL----------LSNLGGQFGFWMGGSVLCLIEFGEIII-D 546
hENaCγ 513 QRSIMESPANSIEML----------LSNFGGQLGLWMSCSVVCVIEIIEVFFID 556

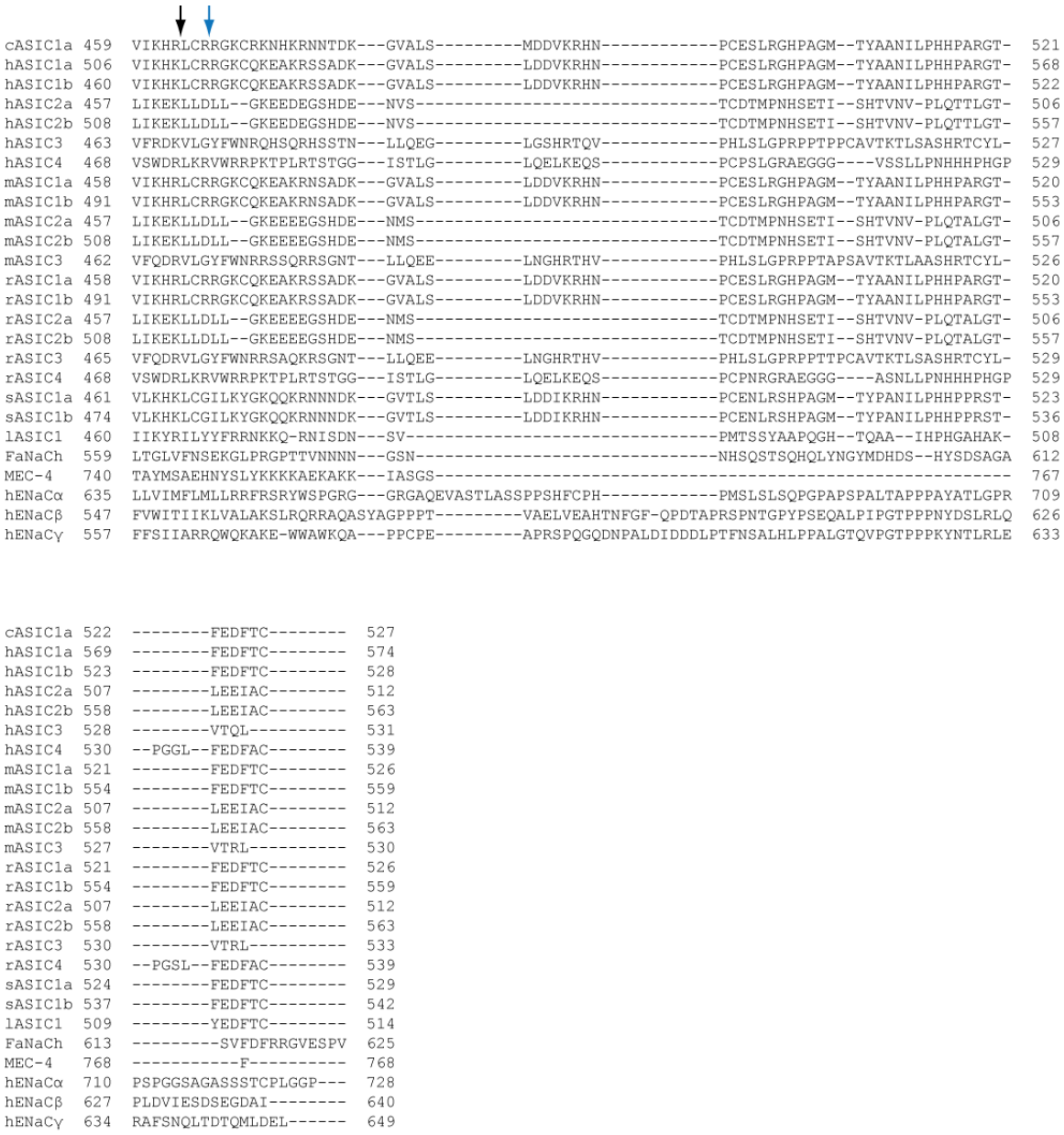

Figure 1.1 Sequence alignment

Figure 1.1 Sequence alignment. Sequence alignment of ASICs from chicken, human, mouse, rat, and lamprey, and several members of the ENaC/DEF family including FMRF-amide sodium channel (FaNaCh), degenerin channel (MEC-4), and human epithelial sodium channel (ENaC: α, β, and γ subunits). The sequences were aligned using PROMALS3D. Shading of residues are as follows: conserved residues are in blue, residues crucial for channel gating in the wrist region are orange, degenerin site is in red, selectivity filter in yellow, and 'HG' dipeptide motif in green. Black and blue arrows indicate N- and C- termini of ΔASIC1 and ASIC1mfc, respectively.

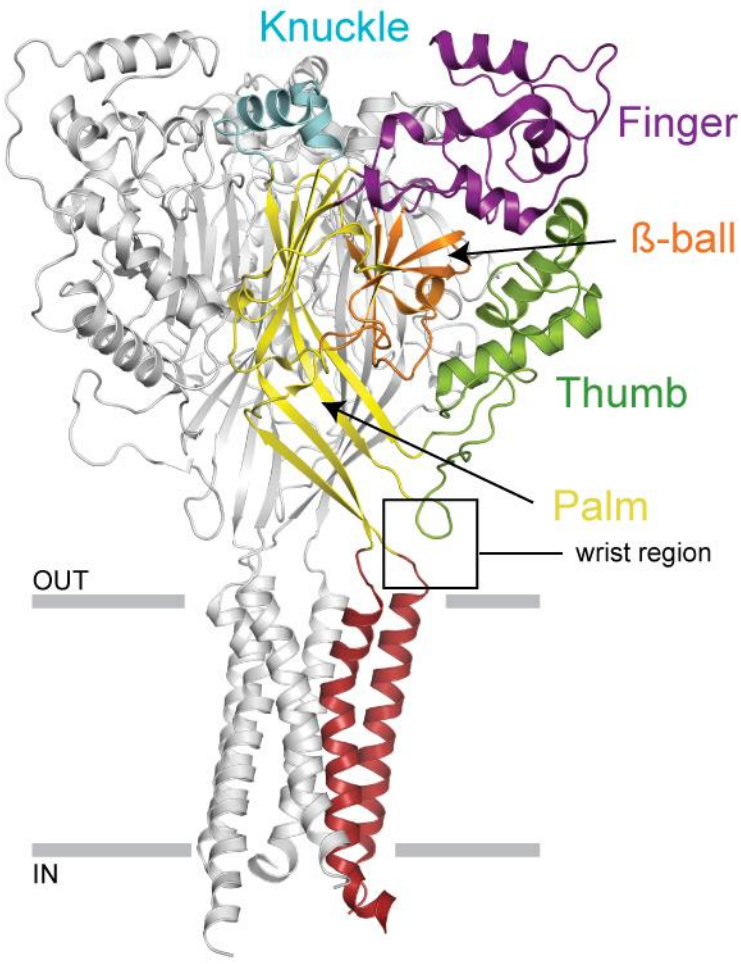

Figure 1.2. Crystal structure of ΔASIC1 at 1.9 Å. Domains of a single subunit are colored as follows: β-ball in orange, finger in purple, knuckle, in cyan, lower and upper palm domains in yellow, and thumb in green. Boxed region indicates the 'wrist' region.

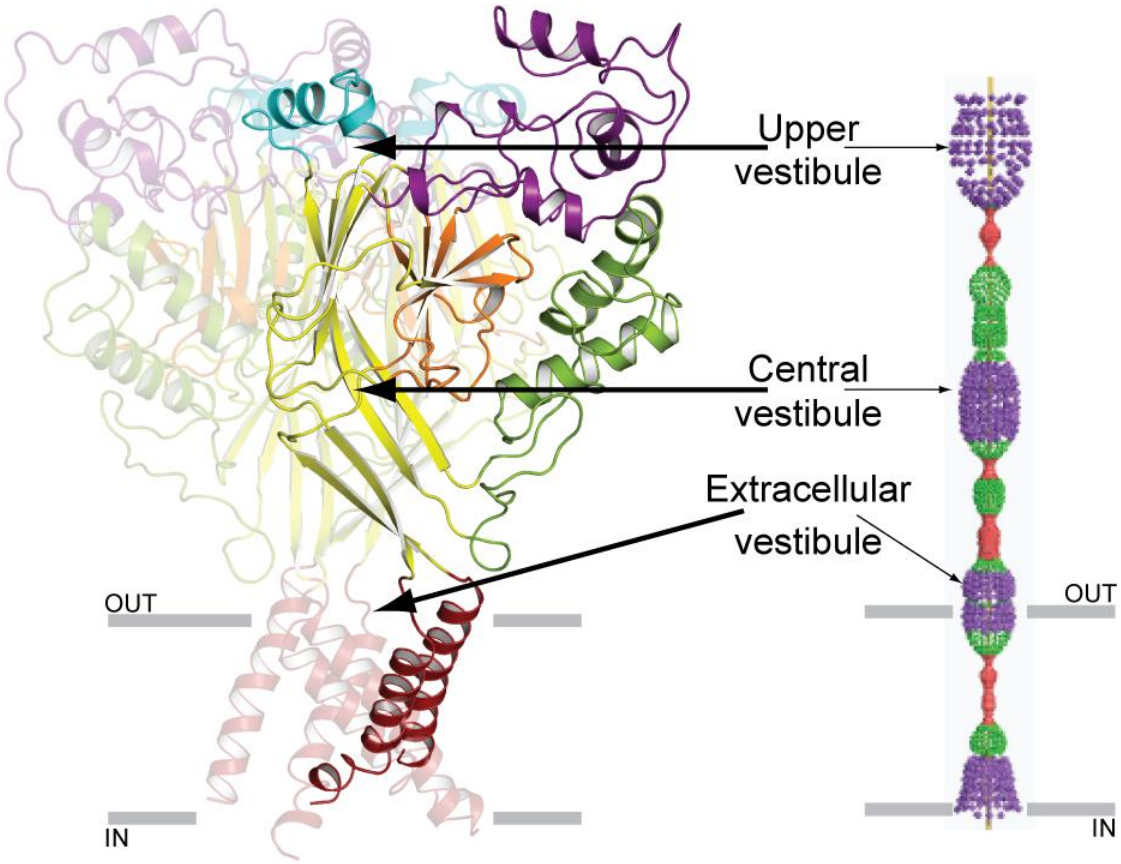

Figure 1.3. Crystal structure of ASIC1mfc demonstrating three-fold symmetry in the extracellular and transmembrane domains. Vestibule regions are labeled. The structure is proposed to be in a desensitized conformation. Shown on the left is a HOLE representation of the pore surface and dimension (red < 1.4 Å < green < 2.3 Å < purple).

Chapter 2

Structural plasticity and dynamic selectivity of acid sensing ion channel–spider toxin complexes

The contents of chapter two are published in modified form:

Baconguis, I. & Gouaux, E. Structural plasticity and dynamic selectivity of acid-sensing ion channel-spider toxin complexes. *Nature* 489, 400-5 (2012).

Author Contributions

I.B. and E.G. designed the project. I.B. performed protein purification, crystallography, and electrophysiology. I.B. and E.G. wrote and edited the manuscript, respectively.

Abstract

Acid sensing ion channels (ASICs) are voltage-independent, amiloride-sensitive channels implicated in diverse physiological processes ranging from nociception to taste. Despite the importance of ASICs in physiology, we know little about the mechanism of channel activation. Here we show that psalmotoxin activates non- and sodium-selective currents in chicken ASIC1a at pH 7.25 and 5.5, respectively. Crystal structures of ASIC1a – psalmotoxin complexes map the toxin binding site to the extracellular domain and illuminate how toxin binding triggers an expansion of the extracellular vestibule and stabilization of the open channel pore. At pH 7.25 the pore is ~10 Å in diameter whereas at pH 5.5 the pore is largely hydrophobic and elliptical in cross section with dimensions of ~5 by ~7 Å, consistent with a barrier mechanism for ion selectivity. These studies define mechanisms for activation of ASICs, illuminate the basis for dynamic ion selectivity and provide the blueprints for new therapeutic agents.

Introduction

Acid-sensing ion channels (ASICs)[80], members of the epithelial sodium channel/degenerin (ENaC/DEG) superfamily of cation channels[21, 28], open a transmembrane pore upon exposure to low pH[2]. Primarily found in the central and peripheral nervous systems[22, 23, 131], ASICs occupy diverse physiological roles that include nociception[91, 132], mechanosensation[132], synaptic plasticity, learning and memory[22], and fear conditioning[124]. The ASIC subfamily is coded by four genes which give rise to seven isoforms[133], of which ASIC1a is permeable to Na^+ and Ca^{2+} and is implicated in ischemic neuronal injury[103, 134]. The ENaC channel[28], found throughout the human body, is crucial to the regulation of blood pressure[135] and is directly involved in Liddle's syndrome[136] and pseudohypoaldosteronism[137].

ASICs and ENaCs are trimeric[24], voltage-independent and sodium-selective ion channels sensitive to the classic ENaC blocker amiloride[28, 80]. Whereas ASICs display a selectivity of Na^+:K^+ ranging from 3 to 30:1 and are inhibited by micromolar concentrations of amiloride, ENaCs harbor a preference for Na^+:K^+ of >100:1 and are blocked by nanomolar concentrations of amiloride[15, 21]. For both ASICs and ENaCs, Li^+ permeability is similar to that of Na^+ and monovalent ions larger than K^+, such as Cs^+, are generally impermeable[58]. However, the 'peak' and 'sustained' or 'steady state' ionic currents carried by ASICs display variable ion selectivity and blocker sensitivity[9, 13, 34, 37, 138, 139], properties reminiscent of the dynamic ion selectivity of trimeric P2X receptors[140]. At present there is no understanding of how ASICs adopt sodium-selective and non-selective conformations with differential sensitivity to the blocker amiloride.

Activation of the ion channel pore in ASICs is classically conditioned by drops in extracellular pH from ~7.5 to pH 4-6[2] with the currents of ASIC1a exhibiting rapid and nearly complete desensitization[3]. Psalmotoxin (PcTx1), classified as an inhibitor cystine knot toxin from a South American tarantula[84, 85], acts potently on ASIC1a, increasing the channel's affinity for protons[87] and, contingent on the species and splice variant of the channel, acts as an agonist, eliciting steady state current or as an antagonist, diminishing ion channel activation[88, 141]. The action of PcTx1 as an antagonist confers both analgesic[142] and neuroprotective[103] properties.

Here we report crystallographic and electrophysiological studies of the action of PcTx1 on chicken ASIC1a, showing the determinants of toxin binding, the mechanism by which toxin binding opens the ion channel, and the architecture of non- and Na^+-selective conformations of the ion channel pore. Our studies inform mechanisms of gating and permeation in ASICs and ENaC/DEG channels and lay a foundation for development of new molecules for modulation of ion channel activity.

Methods

Expression and purification

The construct Δ13 was derived from the chicken ASIC1 gene and was expressed as N-terminal fusion with octa-histidine-tagged GFP using baculovirus expression systems in insect cells and mammalian cells[143] with two thrombin sites and one thrombin site, respectively, encoded upstream of Δ13 generating a final protein sequence containing residues Gly 14 to Arg 463, verified by N-terminal amino acid sequencing. Protein expressed in insect cells was purified as described[26], while the Δ13 expressed in mammalian cells were collected by centrifugation (1000*g*) and sonicated in the presence of 150 mM NaCl, 20

mM Tris (pH 8.0) and protease inhibitors, then subsequently solubilized in 40 mM *n*-dodecyl β-D-maltoside (DDM) for 1 hour at 4°C. The solubilized material was clarified by centrifugation (19,000*g*) for 1 hour at 4°C and the supernatant was incubated with TALON resin for 1.5 hours at 4°C. Bound protein was then eluted with 150 mM NaCl, 20 mM Tris (pH 8.0), 250 mM imidazole, and 1 mM DDM. Cleavage of the histidine-tagged GFP was achieved by thrombin. The resulting Δ13 protein was further purified by size-exclusion chromatography using a mobile phase containing 150 mM NaCl, 20 mM Tris (pH 7.4), 1 mM DDM, 1mm DTT, and 1 mM EDTA. Peak fractions were collected and concentrated to 1.60 mg/mL based on A280 measurement. Synthetic psalmotoxin (Peptides International) was immediately added in a 6:1 molar ratio of toxin to channel prior to crystallization.

Crystallization

Crystals of the high pH form of the Δ13-PcTx1 complex were grown with a protein solution supplemented with 100 μM 1,2-dimyristoyl-*sn*-glycero-3-phosphocholine (DMPC) by way of vapor diffusion using a reservoir solution composed of 20 mM Tris (pH 7.25), 14-18% PEG 550 MME and drops composed of a ratio of 1.5:1 and 2:1, reservoir to protein, respectively, at 4 °C. For cryoprotection, crystals were soaked in reservoir solution supplemented with increasing concentrations of glycerol (15% v/v final concentration), 1 mM DDM, and 1 mM DMPC. For Cs^+ anomalous diffraction experiments, crystals were soaked in reservoir solutions supplemented with 300 mM CsCl, 500 uM DMPC and 1 mM DDM.

Crystals of the low pH form of the Δ13-PcTx1 complex were obtained by vapor diffusion in hanging drop configuration using a 1:2 reservoir to protein ratio at 4°C. The

reservoir solution typically contained 100 mM sodium acetate (pH 5.5) and 9-12% PEG 2000 MME. Cryoprotection was accomplished using reservoir solution supplemented with increasing concentrations of glycerol (20% v/v final concentration). For Cs^+ anomalous diffraction experiments, a modified reservoir solution was employed in which the sodium acetate was replaced by cesium acetate, and the solution was supplemented with 500 mM CsCl and 1 mM DDM.

Structure determination

X-ray diffraction data sets from crystals grown at pH 7.25 and belonging to the *R*3 space group were collected at the Advanced Light Source (beamline 5.0.2) and diffraction was measured to ~3.35 Å resolution. The best x-ray diffraction data sets from the C2 form, pH 5.5 crystals, were collected at the Advanced Photon Source (beamline 24ID-C) and scaled to ~2.80 Å resolution. Diffraction data for crystals soaked in cesium containing solutions were measured using low energy x-rays (9000 eV) at the Advanced Light Source. Diffraction data were indexed, integrated, and scaled using the HKL2000 software[144]. The structures were solved by molecular replacement using the program PHASER[145], with the extracellular domain coordinates of the ΔASIC1 structure[24] (PDB code: 2QTS) as a search probe. Resulting maps after molecular replacement showed strong density of psalmotoxin, and thus the toxin was fitted into the density at the subunit interface using the solution structure[85]. Iterative model building and refinement were performed using COOT[146] and PHENIX[147] package. Crystals in the *R*3 space group contained one subunit and one toxin in the asymmetric unit; consequently, the channel is built using the subunits and toxins related by crystallographic symmetry. Alternatively, crystals in the *C*2 space group contained one trimer and three toxins in the asymmetric unit. Manual building

of the transmembrane domains was guided by electron density maps calculated using the crystallographically refined coordinates of the extracellular domain - toxin complex. "Omit" electron density maps were calculated to validate residue registration, particularly with the transmembrane domains. Subsequent iterative cycles of model building and refinement were performed after building the transmembrane regions. Non-crystallographic symmetry (NCS) restraints were implemented in the extracellular domain and toxin for the low pH structure containing regions defined automatically by the PHENIX package to improve maps. These regions consist of residues 72-135, 138-153, 155-291, 303-331, 333-360, 362-386, and 388-427 in the extracellular domain and residues 2-38 in the toxin. As for the high pH structure, TLS parameters were refined with 7 TLS groups defined by PHENIX, which comprised of 5 groups in the ASIC subunit and 2 groups in the toxin. Structure validation was performed using MolProbity[148]. The low pH final model contains channel subunits with residues 50-454, 45-450 and 42-454 of A, B, and C chains, respectively and toxins with residues 2-38, 2-37, and 1-38 of M, N, and O chains, respectively. The high pH model contains residues 41-450 of the ASIC subunit, and 2-13 and 16-38 of the toxin. A region in the thumb domain of the high pH structure lacked electron density consisting of residues 298-301 and was omitted in the final structure. Pore surface and dimension were determined using the software HOLE[149], while the rotation axis shown in Figure 3a was analyzed using Dyndom[150].

Electrophysiology

Whole-cell recordings were carried out with CHO-K1 cells 24-48 hours after transfection by plasmid DNA encoding the Δ13 construct and GFP expressed from an internal ribosome entry site. Pipettes were pulled and polished to 2-3 MΩ resistance and

filled with internal solution containing (in mM): 150 KCl, 2 $MgCl_2$, 5 EGTA and 10 HEPES (pH 7.35). External solution contained (in mM): 150 NaCl, 2 $MgCl_2$, 2 $CaCl_2$, 8 Tris and 4 MES. For ion selectivity experiments, NaCl was substituted with equimolar concentrations of LiCl, KCl, CsCl, or NMDG in the external solution. Proton concentration-response profiles were recorded and normalized to maximal current generated by application of external solution buffered at pH 5.8, while the PcTx1 concentration-response curve was generated by normalizing to maximal current generated by application of 1 μM of toxin. All concentration-response curves were fitted to the Hill equation.

Results and discussion

Function and architecture of ASIC1a – PcTx1 complex

PcTx1 slows desensitization of ASIC and yields substantial steady state current when applied to ASIC1a/1b chimeras, and thus we asked whether PcTx1 stabilizes open channel states of cASIC1a[88]. We generated a cASIC1a construct for structural studies by removing 13 and 63 residues from the N- and C-termini respectively, yielding a channel with wild type-like electrophysiological properties (Δ13; **Figures 2.1 and 2.2**). Application of a pH 5.5 solution to Δ13 gives rapidly activating and desensitizing inward current while perfusion of a saturating PcTx1 solution at pH 7.25 elicits a current that activates and decays over a time scale of seconds to yield a steady state current (**Figures 2.3a and 2.4**). Subsequent application of saturating PcTx1 at pH 5.5 further activates peak current and steady state currents.

The Δ13-PcTx1 complex forms crystals at pH 7.25 (high pH) that belong to the *R*3 space group, diffract to ~3.3 Å resolution, and have a single ASIC subunit-toxin complex positioned on the 3-fold axis of crystallographic symmetry. Crystals grown at pH 5.5 (low

pH) belong to the *C*2 space group with an ASIC trimer and three toxin molecules in the asymmetric unit and a diffraction limit of ~2.8 Å resolution (**Figures 2.3b, c, d, and 2.5**). Structures of both crystal forms were solved by molecular replacement and refined to good crystallographic statistics (**Table 2.1 and 2.2**).

PcTx1 binds at subunit interfaces

The high and low pH channel-toxin complexes show three toxin molecules bound to the extracellular domain of each trimer at similar subunit interfaces ~45 Å from the transmembrane domain (**Figure 2.3**). PcTx1 molecules bury ~900 Å of solvent accessible surface area and make multiple ionic, polar and hydrophobic contacts consistent with studies mapping sites of channel-toxin interaction[86] (**Figure 2.6**) yet distinct from computational modeling of the channel-toxin complex[151, 152]. Docked on the thumb domain, toxin molecules form nonpolar interactions mediated by aromatic residues, and they nestle an arginine-rich hairpin between adjacent subunits, making polar interactions in the acidic pocket (**Figure 2.7**). Together, these interactions bridge the finger, β-ball, and thumb domains of one subunit and the palm domain of the adjacent subunit. Arg 26 of PcTx1 tunnels under the toxin β-sheet to hydrogen bond with the side chain carboxylate of Asp 350 of the thumb domain, which in turn interacts with Asp 238 and Arg 191 of the finger domain. In contrast, Arg 27 is oriented in the opposite direction, forming hydrogen bonds with backbone oxygens of Thr 215, Gly 216, and Gly 218 and also lying near the Glu 220-Asp 408 acidic pair, all on the palm domain of an adjacent subunit. Like Arg 27, Arg 28 interacts with backbone oxygens of Asp 238 and Thr 240 in the finger domain.

PcTx1 is further anchored on the thumb domain by an aromatic 'embrace' between Trp 7 and Trp 24 of PcTx1 and Phe 351 (**Figure 2.7**), a residue that when mutated in

human ASIC1a to leucine renders the channel insensitive to PcTx1[70]. Phe 351 is conserved in ASIC1 orthologs[24] and appears crucial to the specificity of PcTx1 to ASIC1 channels. Site-directed mutagenesis of PcTx1[151] previously implicated Trp 24, Arg 26, and Arg 27 as central to toxin specificity, consistent with our structures of the channel-toxin complex. In addition, a recent structure of PcTx1 in complex with a non functional construct of cASIC1a supports our definition of the toxin binding site [153].

Conformational changes in the extracellular domain

Structural comparisons of the high and low pH PcTx1-bound states with the desensitized state (PDB code: 3HGC) show that the upper palm β-strands and knuckle domains define a structurally conserved scaffold (**Figure 2.8**), reminiscent of the scaffold of P2X receptors[154]. Relative to the desensitized state, the lower palm domain and the wrist of the high pH Δ13-PcTx1 complex rotate by as much as ~13° around an axis positioned below the scaffold (**Figure 2.9a**). This rotation shifts subunit-subunit interfaces compared to those of the desensitized state structure, separating the thumb and palm domains of adjacent subunits by 2-3 Å and displacing the finger domains of the high and low pH complexes (**Figure 2.9a**).

The consequences of toxin binding are manifested in the flexing of a blanket of β-sheets encapsulating the negatively charged central vestibule[26], a cavity composed of the lower palm domains, poised between the toxin binding site and the wrist (**Figures 2.9a and 2.10**). With the Cα atom of Val 75 as a landmark, the distances between adjacent subunits are ~11 Å and ~12 Å in the low and high pH structures, respectively; upon formation of the desensitized state, the distance diminishes to ~7 Å. Chemical modification of the E79C mutant of ASIC3[32], a residue equivalent to Glu 80 in cASIC1a and predicted to face the

interior of the central vestibule, slows the rate and extent of channel desensitization, consistent with the notion that the central vestibule contracts upon transition from the PcTx1-bound states to the desensitized state. Small molecules that activate[139] or potentiate the steady state current of ASIC3[36, 138], respectively, bind within the central vestibule[139], or at the subunit interface near Ala 82, and stabilize the central vestibule in an expanded conformation, recalling the ATP-dependent expansion of the extracellular vestibule of P2X receptors[154].

A striking conformational change in the palm domain, common to both PcTx1 complexes and located within the β1-β2 linker, is a ~180° flip of the Thr 84-Arg 85 peptide bond (**Figure 2.11**), inducing a shift of β1 away from the equivalent β-sheet of the adjacent subunit. In addition, Ala 413, Leu 414, and Asn 415 in the β11-β12 linker in the high pH structure adopt conformations in which the side chains of Leu 414 and Asn 415 have effectively swapped positions (**Figures 2.9b and 2.12**). Indeed, the Cα atoms of residues Ala 82 and Ala 413 are farther apart in the high pH state (8.1 Å), in comparison to the low pH state (6.4 Å), consistent with the notion that a disulfide can form between the equivalent residues in shark ASIC1b, stabilizing the channel in the desensitized state[34] (**Figure 2.13**). Studies at sites equivalent to Leu 86, a residue that interacts with Leu414 in the high pH Δ13-PcTx1 state, and Asn 415 reinforce the conclusion that the β1-β2 and β11-β12 linkers are crucial to gating[35, 36, 46].

The structures of the high and low pH Δ13-PcTx1 complexes suggest molecular mechanisms underlying the pH dependent conformations of the β1-β2 and β11-β12 linkers. We speculate that at high pH, the carboxyl group of Glu 80 is ionized, favoring an expanded conformation of the central cavity (**Figure 2.10**). As the pH drops, acidic residues in the

vestibule bind protons, allowing Glu 80 and adjacent residues to adopt a 'contracted' central vestibule conformation. In fact, the distance between Cα of Glu 80 and Glu 412, residues that flank both linkers, diminishes from 14.1 Å to 11.3 Å in the high and low pH states, respectively. Neutralization of Glu 80 by mutation to Ala results in a channel that desensitizes ~40-fold more rapidly than the parent construct and that does not yield measureable steady state current upon application of PcTx1 at pH 7.25 (**Figure 2.14**), thus underscoring the role that titratable residues play in pH dependent conformational changes of the central vestibule.

A highly conserved non polar residue in the β11-β12 linker, Leu 414, is also important to the conformational transitions of the central vestibule. In the high pH Δ13-PcTx1complex, Leu 414 interacts with Leu 86 of the β1-β2 linker. Upon transition to the low pH Δ13-PcTx1 complex and to the desensitized state, however, Leu 414 forms multiple hydrophobic contacts involving Leu 281, Ile 306, and Val 368 of the adjacent subunit. In addition, Asn 415 hydrogen bonds with Tyr 416 and the backbone nitrogen of Ala 83 in the β1-β2 linker (**Figure 2.12c, d**). Together, these rearrangements highlight the importance of the β1-β2 and β11-β12 linkers and nearby subunit interfaces to conformational transitions of the central vestibule.

Ion channel at high pH

The high pH Δ13-PcTx1 complex harbors a cavernous, 3-fold symmetric pore in which TM2 resides on the periphery of the pore and lines the ion channel together with TM1 (**Figure 2.15a, b**). In comparison to the desensitized state, a kink in TM2 at Asp 433 results in an effective rotation of the cytoplasmic end of TM2 by ~90° around the 3-fold axis and a tilting of TM2 by ~50°; movements in TM1 are smaller, characterized by a ~20°

rotation around the 3-fold axis. Collectively, these movements rupture intrasubunit interactions between TM1 and TM2 and completely disrupt intersubunit contacts between TM2 segments that define the closed, desensitized channel gate, yielding sparse intersubunit and hydrophobic contacts between TM1 and TM2 mediated primarily by Ile 66 and Ile 434, and Val 46 and Ile 446 in the high pH complex (**Figure 2.16**).

The large TM pore of the pH 7.25 PcTx1 complex, with a diameter of ~10 Å near Asp 433 (**Figutr 2.17**), led us to probe the selectivity of the Δ13-PcTx1 complex using bi-ionic patch clamp electrophysiology (**Figure 2.15c, d**). At neutral pH, the channel-toxin complex does not discriminate between Li^+, Na^+, K^+, and Cs^+, and we suggest that these ions permeate through the pore in a fully hydrated state. Furthermore, *N*-methyl-D-glucamine (NMDG), with a radius of ~4.0 Å, permeates through the ion channel and application of 500 μM amiloride only blocks 10% of the steady-state current (**Figure 2.18**). This non selective behavior of the Δ13-PcTx1 complex is reminiscent of the non selective behavior previously observed in steady state currents of wild type ASIC3 and in the degenerin mutants of ASICs[9, 13], and of the pore-dilated behavior of trimeric P2X receptors[140].

Architecture of low pH ion channel pore

The TM helices of each subunit in the low pH Δ13-PcTx1 complex not only adopt different conformations but they also occupy distinct positions relative to the pore axis (**Figure 2.15e, f**). TM2 segments of subunits A and B bend and 'stretch' at residues 433-435, similar to conformations observed in the high pH structure. In comparison to the desensitized state, the TM1 helices of the low pH complex rotate by 9-12° around the pore axis and the TM2 helices of subunits A, B and C tilt by ~47°, 65° and 30°, respectively. Thus

the TM2 helices adopt an orientation nearly perpendicular to the membrane plane, reminiscent of the TM conformation of the low pH ΔASIC1 structure[24].

TM2 of the C subunit adopts a straight α-helix, resulting in a ~4 residue displacement along the pore axis relative to subunits A and B, shifting subunit C toward the extracellular side of the membrane, thus conferring axial asymmetry onto the pore. This asymmetry has precedent in chemical modification studies of ENaC which were interpreted in terms of a model in which the β subunit is displaced along the pore axis by about 1 turn of an α-helix[155]. The axial displacement of the TM's gives rise to a striking constellation of hydrophobic contacts mediated by the staggered arrangement of Leu 440 and Leu 447 of subunits B and C that resembles a leucine zipper motif (**Figure 2.19a, b**). The extensive contacts between the TM2 domains of the B and C subunits give rise to TM1 of subunit B residing on the periphery of the ion channel domain, while the proximity of TM2 of subunits A and C shields TM1 of subunit C from exposure to the pore. The remaining 4 TM segments line the pore and participate in intersubunit interactions that include contacts between Val 46 (C) and Ile 446 (A), as observed in the high pH structure (**Figure 2.19c, d**). The exposure of portions of TM1 from subunit A to the pore concurs with the results from accessibility studies of TM1 residues of FaNaC[156], a peptide-gated channel, but stands in contrast to cysteine-directed chemical modification studies of lamprey ASIC[48], which suggest that TM2 primarily lines the pore. Determining how the conformation of the asymmetric pore in the low pH Δ13-PcTx1 complex is related to the conductive pore of the Δ13 construct upon activation by protons will require additional studies. Nevertheless, we note that ENaCs likely harbor an asymmetric pore based on variable reactivity of cysteine residues at equivalent sites on different subunits[155] and that the extensive intra- and

intersubunit interactions between TM1 and TM2 seen in the low pH Δ13-PcTx1 complex renders asymmetric pore formation favorable.

Low pH pore is sodium selective

The low pH complex harbors an elliptical pore with a region of constriction spanning a helical turn and located approximately halfway along the transmembrane domain, primarily lined by hydrophobic side chains of Leu 440 (**Figure 2.20**). The position of the constriction exposes the putative amiloride binding site, Gly 439 and the 'GAS' selectivity tract, to the extracellular side of the membrane, consistent with the inhibitory mechanism of amiloride as an open channel blocker[157]. Strikingly, ion channel blockers of ASICs and ENaCs, including amiloride, are characteristically planar, non-symmetric molecules that roughly mirror the shape of the extracellular portion of the low pH pore (**Figure 2.20**).

To assess the properties of the Δ13-PcTx1 ion channel pore at low pH, we determined its ion selectivity properties and found that the complex remains selective for Na^+ and Li^+ with a selectively for Na^+ over K^+ of 10:1 (**Figure 2.15g**). Because the pore is primarily lined by hydrophobic residues at the constriction point (**Figure 2.15h**), we assume that Na^+ ions are hydrated when traversing the pore. We suggest that the pore discriminates ions by the size of a fully or partially hydrated ion and that the mechanism underlying ion selectivity is best described by a barrier model. Indeed, Hille proposed that sodium selective pores have a rectangular cross section with dimensions of 3.2 Å by ~5.2 Å, large enough to allow one sodium ion and one water molecule to percolate but too small to allow passage of hydrated potassium ions[158]. The elliptical outline of the constriction in the low pH Δ13-PcTx1 structure is in general accord with the proposed geometry of a Na^+-selective pore albeit larger, with constrictions of ~5 Å by ~7 Å at Leu 440 of subunit C and of ~4 Å by 10

Å at Leu 440 of subunits A and B (**Figure 2.20**). The extent to which the mechanism of Na^+-selectivity upon proton activation, in the absence of PcTx1, hinges on Leu 440 and on the low pH Δ13-PcTx1 conformation requires further experimentation. Nevertheless, mutation of Leu 440 to Ala or Ser (**Figure 2.21**) demonstrates that Leu 440 is crucial to the formation and function of the ion channel pore based on the reduced activity of the mutants compared to the parent construct.

Ion binding sites

To map ion binding sites we soaked crystals in solutions containing Cs^+, a voltage-dependent, open channel blocker of the Δ13 construct (**Figure 2.22**). Inspection of anomalous difference electron density maps revealed a site (6-12 σ) in each subunit, common to the high and low pH Δ13-PcTx1 crystal forms and located at the interface between the wrist and the extracellular end of TM1 (**Figure 2.23a and 2.24**). In both crystal forms, the backbone carbonyl oxygens of Leu 71, Tyr 72, Pro 287, and Trp 288 coordinate Cs^+ (**Figure 2.23b**). Interestingly, the three crystallographically independent Cs^+ sites in the *C2* structure vary in strength, with subunit C having the weakest signal, thus suggesting that the binding of ions to these sites is influenced by the variation in TM1/wrist conformation between subunits. Because Cs^+ soaking experiments with crystals of the desensitized state failed to reveal ion binding to this site, and TM1 (C) in low pH Δ13-PcTx1 state harbors the weakest Cs^+ site, we suggest the occupancy of the site is state dependent, with ion binding favored when the pore is in an open state, augmenting interactions between Tyr 72 and Trp 288.

We identified two Cs^+ sites in the electrostatically negative mouth of the pore, near Asp 433 in the *C2* structure (**Fig 2.23c, d**), a residue implicated in stabilization of the open state yet not crucial to ion selectivity[48]. Ions at these sites are ~5 Å from the closest

protein residues consistent with the notion that they are low affinity, transiently occupied cation sites bound by water-mediated contacts. We did not observe anomalous difference density features deeper into the pore, perhaps because the hydrophobic pore is devoid of favorable binding sites and the structural analysis was carried out in the absence of a membrane potential.

Summary and Conclusion

Mechanism

We used PcTx1 to stabilize open states of the Δ13 construct at high and low pH. Comparison of the open state and desensitized state structures defines the upper palm and knuckle as a structural scaffold and the lower palm as a conformationally flexible, proton-sensitive domain at the core of ion channel gating (**Figure 2.10**). The finger and thumb domains flank the palm domain, harbor binding sites for protons and PcTx1 and modulate movements of the lower palm domain by alterations in intersubunit contacts. In the open conformations, the subunit interface between the thumb and the palm domain separates while the extracellular and transmembrane domain interface forming the extracellular vestibule expands. The presence of a modulator, such as PcTx1, precludes 'collapse' of the thumb – palm subunit interface to a desensitized state conformation. The motions of the lower palm domain converge at the wrist region, inducing radial and rotational movements of the transmembrane domains, gating the ion channel (**Figures 2.25 and 2.26**).

Conclusion

Our functional and structural studies of the chicken ASIC1a complex with PcTx1 at two proton concentrations provide new insights into how the movements of the multiple

domains of ASICs are coupled to ligand and pH dependent gating. Channel opening is correlated to the expansion of the extracellular vestibule and to rearrangements at subunit interfaces, movements coupled to the ion channel pore by the direct connections of extracellular β-strands to the transmembrane α-helices and also by the non covalent contacts between the thumb and wrist region, a previously unrecognized site of cation binding in the open state. The non selective and sodium selective states of the ion channel pore illustrate how transmembrane helices can rearrange to form a large, non selective pore at high pH and a small, asymmetric and sodium selective channel at low pH Together, these studies illuminate mechanisms of gating and selectivity in ASIC/ENaC/DEG channels.

Acknowledgements

We appreciate assistance in the initial characterization of the action of PcTx1 on chicken ASIC1a by D. Samways and T. Egan, mass spectrometry analysis by D. King, together with comments from C. Jahr. We are grateful to K.C. Garcia (Stanford), C. Lee and A. Goehring for assistance with protein expression in mammalian cells. We thank L. Vaskalis for assistance with figures, H. Owen for help with manuscript preparation, H. Krishnamurthy for assistance in initial data collection, and Gouaux lab members for helpful discussion. This work was supported by an individual National Research Service Award from the National Institute of Neurological Disorders and Stroke (I.B.) and the NIH (E.G.). E.G. is an investigator with the Howard Hughes Medical Institute.

Tables

Table 2.1 Data collection and refinement statistics (High pH)

	Δ13-PcTx1	Cs^+
Data collection		
Beamline	ALS 5.0.2	ALS 5.0.2
Space group	*R3*	*R3*
Cell dimensions		
a, *b*, *c* (Å)	131.5, 131.5, 129.9	131.8, 131.8,129.5
α, β, γ (°)	90.0, 90.0, 120.0	90.0, 90.0, 120.0
Wavelength (Å)	1.000	1.378
Resolution (Å)*	50.0-3.35 (3.47-3.35)	50.0-4.25 (4.40-4.25)
R_{sym} or R_{merge}*	0.064 (0.904)	0.072 (0.503)
$I/\sigma I$*	22.9 (1.4)	22.3 (1.9)
Completeness (%)*	95.4 (97.0)	99.7 (98.9)
Redundancy*	4.1 (4.0)	5.4 (4.0)
Refinement		
Resolution (Å)	3.35	
No. reflections	11369	
$R_{work/}$ R_{free}	0.216/0.281	
No. atoms		
Total	3203	
Δ13	2947	
PcTx1	256	
Chloride	n/a	
Solvent	n/a	
B-factors (Å^2)		
Total	161.20	
Δ13	159.03	
PcTx1	186.18	
Chloride	n/a	
Solvent	n/a	
R.m.s deviations		
Bond lengths (Å)	0.009	
Bond angles (°)	1.283	
Ramachandran		
Most favored (%)	96.1	
Allowed (%)	3.9	
Disallowed (%)	0	

*Highest resolution shells are shown in parentheses.

Table 2.2 Data collection and refinement statistics (Low pH)

	Δ13-PcTx1	Cs^+
Data collection		
Beamline	APS 24-ID-C	ALS 5.0.2
Space group	*C2*	*C2*
Cell dimensions		
a, *b*, *c* (Å)	232.3, 108.7, 126.4	232.9, 109.6, 127.4
α, β, γ (°)	90.0, 119.8, 90.0	90.0, 119.3, 90.0
Wavelength (Å)	0.979	1.378
Resolution (Å)*	50.0-2.80 (2.85-2.80)	50.0-4.10 (4.17-4.10)
R_{sym} or R_{merge}*	0.069 (0.581)	0.145 (0.491)
$I/\sigma I$*	20.9 (1.9)	8.60 (2.0)
Completeness (%)*	99.9 (99.3)	99.3 (95.5)
Redundancy*	3.8 (3.7)	3.6 (3.2)
Refinement		
Resolution (Å)	2.80	
No. reflections	63727	
R_{work}/ R_{free}	0.202/0.231	
No. atoms		
Total	10557	
Δ13	9519	
PcTx1	879	
Chloride	3	
Solvent	156	
B-factors (Å^2)		
Total	71.14	
Δ13	71.42	
PcTx1	70.78	
Chloride	77.93	
Solvent	56.37	
R.m.s deviations		
Bond lengths (Å)	0.007	
Bond angles (°)	1.120	
Ramachandran		
Most favored (%)	98.2	
Allowed (%)	1.8	
Disallowed (%)	0	

*Highest resolution shells are shown in parentheses.

Figures and legends

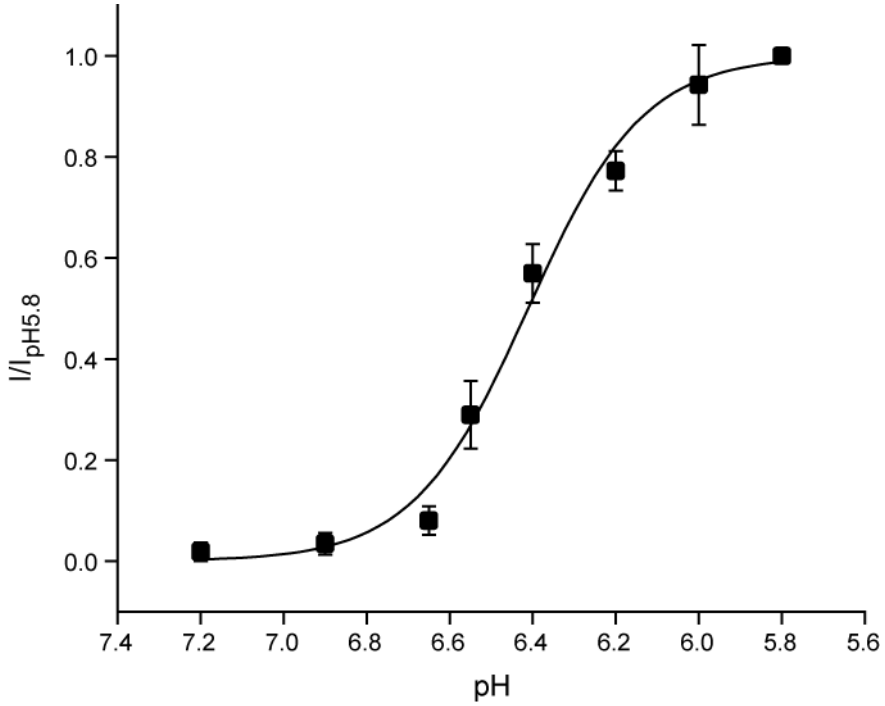

Figure 2.1. Characterization of the Δ13 chicken ASIC1a construct. Normalized pH concentration-response of the Δ13 construct expressed in Chinese hamster ovary (CHO) cells yields a pH50 of 6.41 ± 0.02 with a Hill slope, n = 3.1. Error bars indicate SEM for 4 CHO cells.

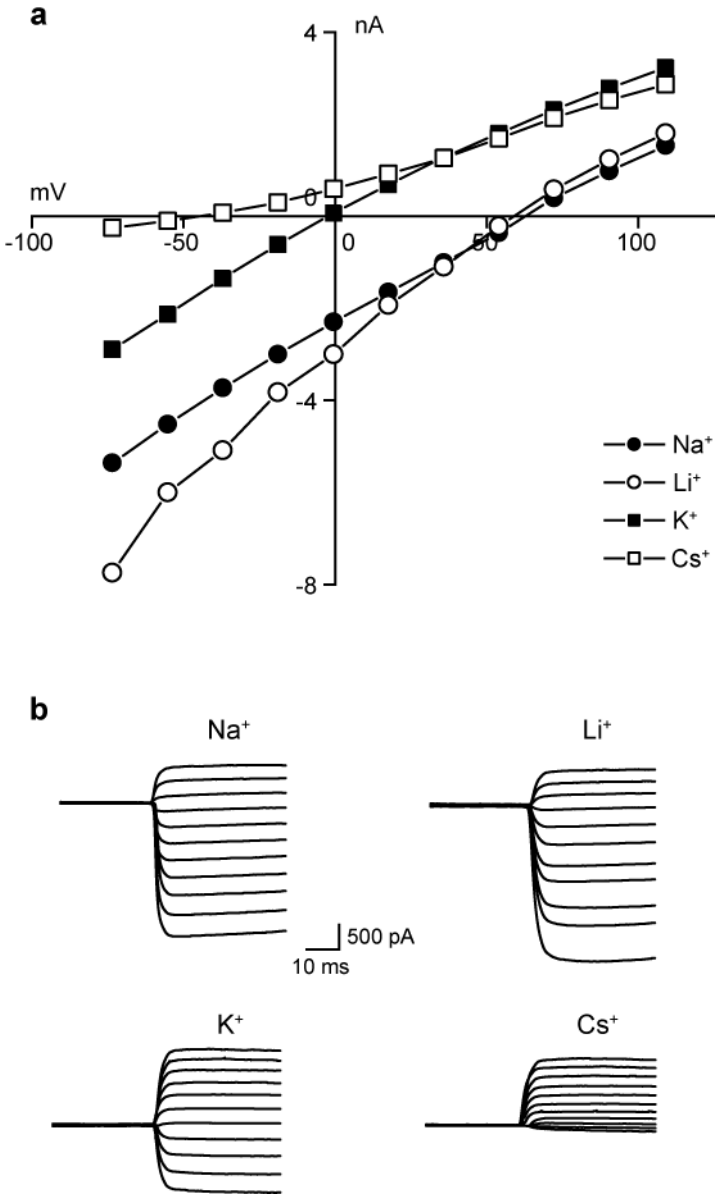

Figure 2.2. Selectivity of Δ13 construct probed by bi-ionic current-voltage experiments. a, I-V curves of Δ13 with external solutions containing 150 mM of Na+, Li+, K+, or Cs+. **b**, Representative whole-cell patch records at stepped holding potentials from -80 mV to +120 mV. Pipette solution contains 150 mM KCl.

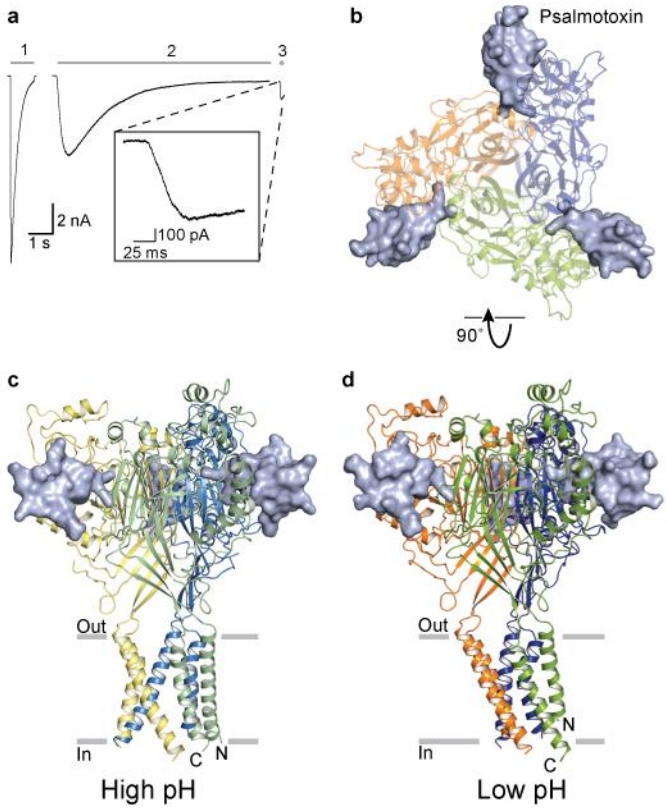

Figure 2.3. PcTx1 activates the chicken ASIC1a Δ13 construct. a, Whole-cell, patch-clamp current traces of activation by steps into pH 5.5 (1), pH 7.25 and 1 μM PcTx1 (2), and pH 5.5 and 1 μM PcTx1 (3). Inset, current trace of step into pH 5.5 and 1 μM PcTx1. **b,** Structure of low pH Δ13-PcTx1 complex viewed from the extracellular side. **c**, **d**, High pH **(c)** and low pH **(d)** complexes viewed parallel to the membrane. Each subunit is in a different color and toxin is in solvent-accessible surface representation.

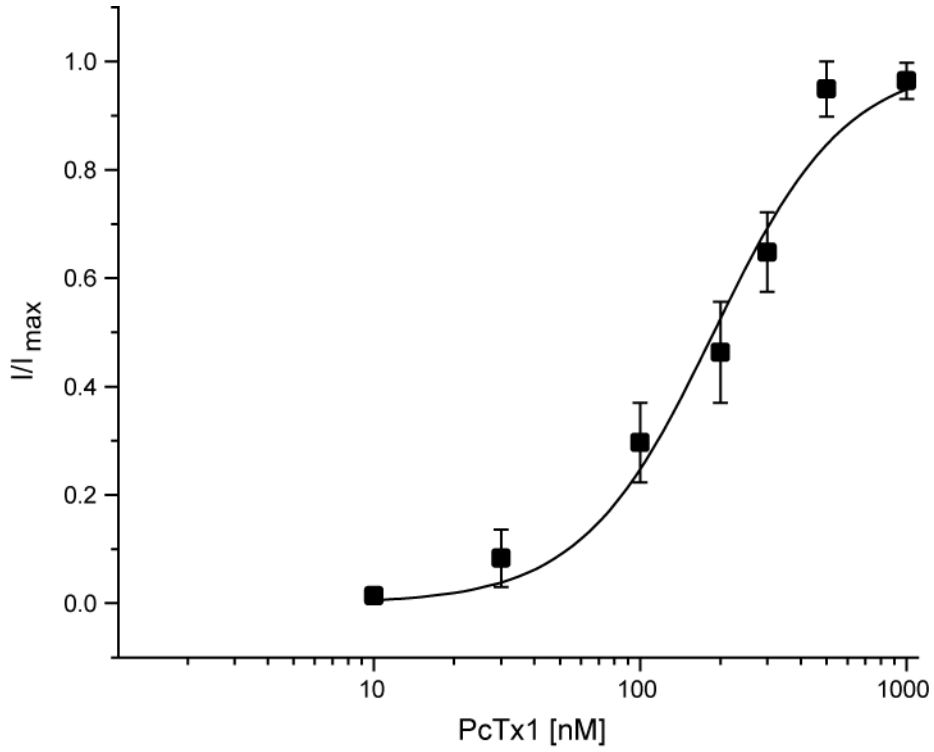

Figure 2.4. PcTx1 activates Δ13 at pH 7.4. Normalized PcTx1 concentration-response relationship of the Δ13 construct yields an EC50 of 188.6 ± 17.8 nM with a Hill slope, n, of 1.75. Error bars indicate SEM for 3 CHO cells.

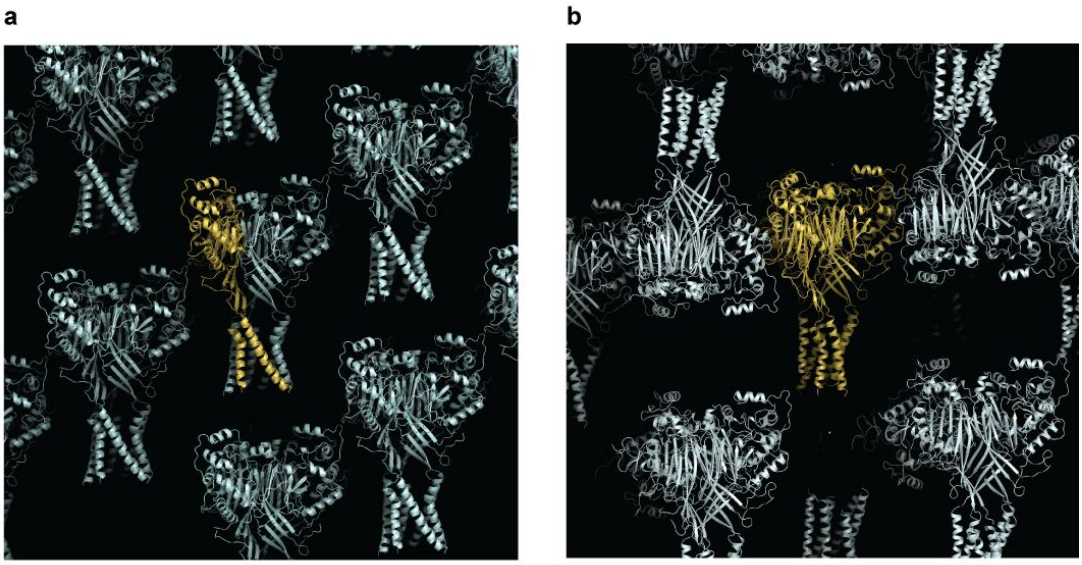

Figure 2.5. Crystal packing of Δ13-PcTx1 complexes. a, **b**, Molecules in the Δ13-PcTx1 crystal lattice at high pH **(a)** and at low pH **(b)** in the R3 and C2 space groups, respectively. The view is perpendicular to the a-c plane. A crystallographically unique subunit **(a)** or a trimeric channel **(b)** are gold, respectively, while symmetry-related molecules are in pale cyan. Note that the TM domains do not participate in direct lattice contacts and thus we suggest crystal lattice interactions do not directly influence the conformation of TM domains.

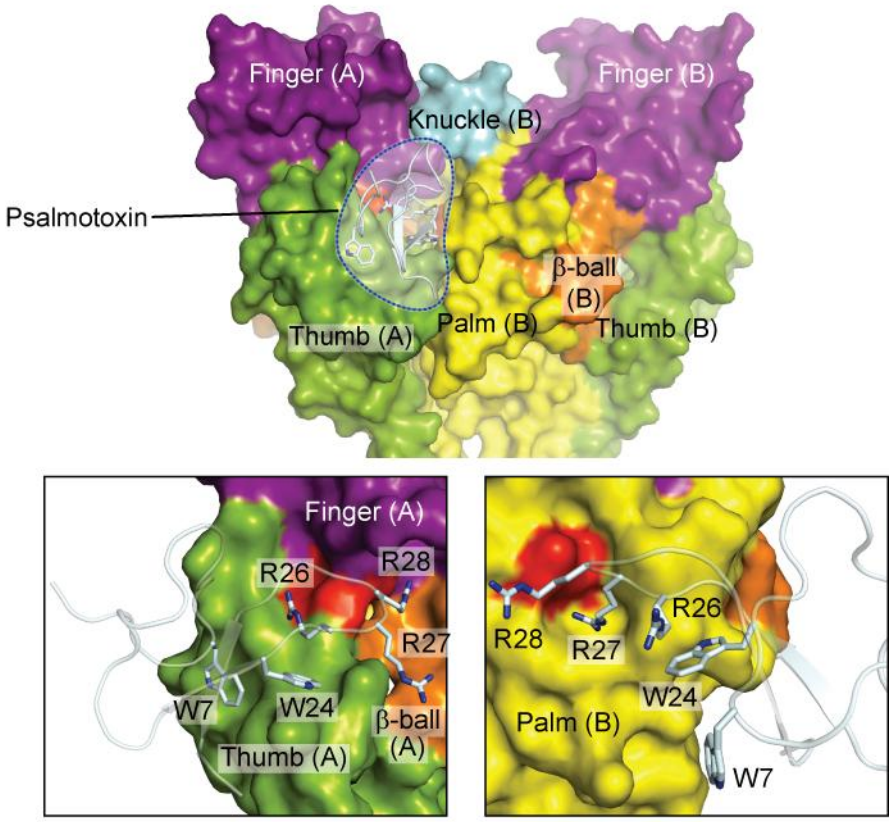

Figure 2.6. PcTx1 binds at subunit interfaces. The Δ13 structure is in solvent-accessible surface representation and colored according to domain organization. Upper panel, toxin is indicated by the blue dashed line. Lower panels, subunit interfaces surrounding the toxin binding site viewed from subunit B (left) and subunit A (right). Acidic pairs are in red. Toxin is in cartoon representation.

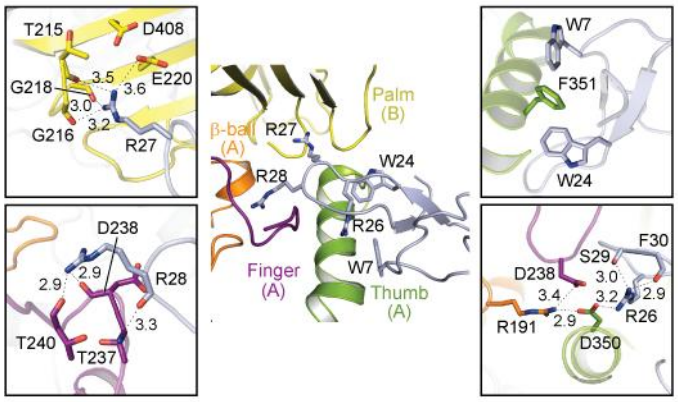

Figure 2.7. Extensive interactions adhere PcTx1 to the Δ13 ion channel. Close-up views of toxin-binding site of the low pH complex. Dashed lines indicate possible hydrogen bonds.

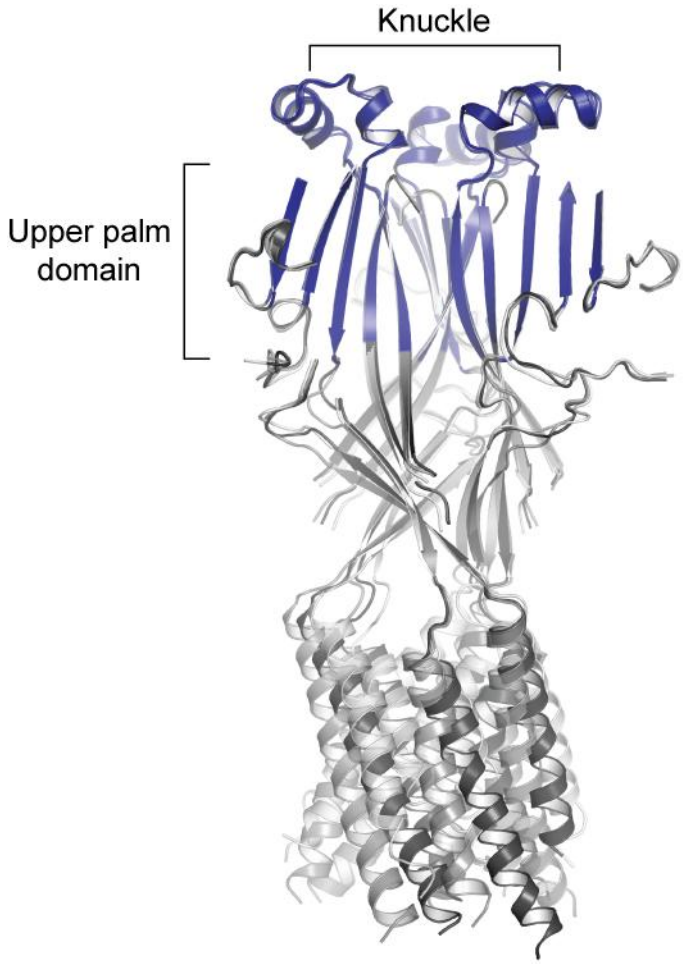

Figure 2.8. The upper palm and knuckle domains are a structural scaffold. The high pH and low pH structures are superimposed on the desensitized structure using Cα positions of all three subunits in the trimers. The regions shown in blue, which are composed of the knuckle domain and β3, β6, β9(270-275), β10(373-379), and β11 of the palm domain, adopt similar conformations in all three structures and thus define a structurally invariant scaffold domain. The desensitized state is in light gray, high pH in gray, and the low pH in dark gray. The finger and thumb domains are omitted for clarity.

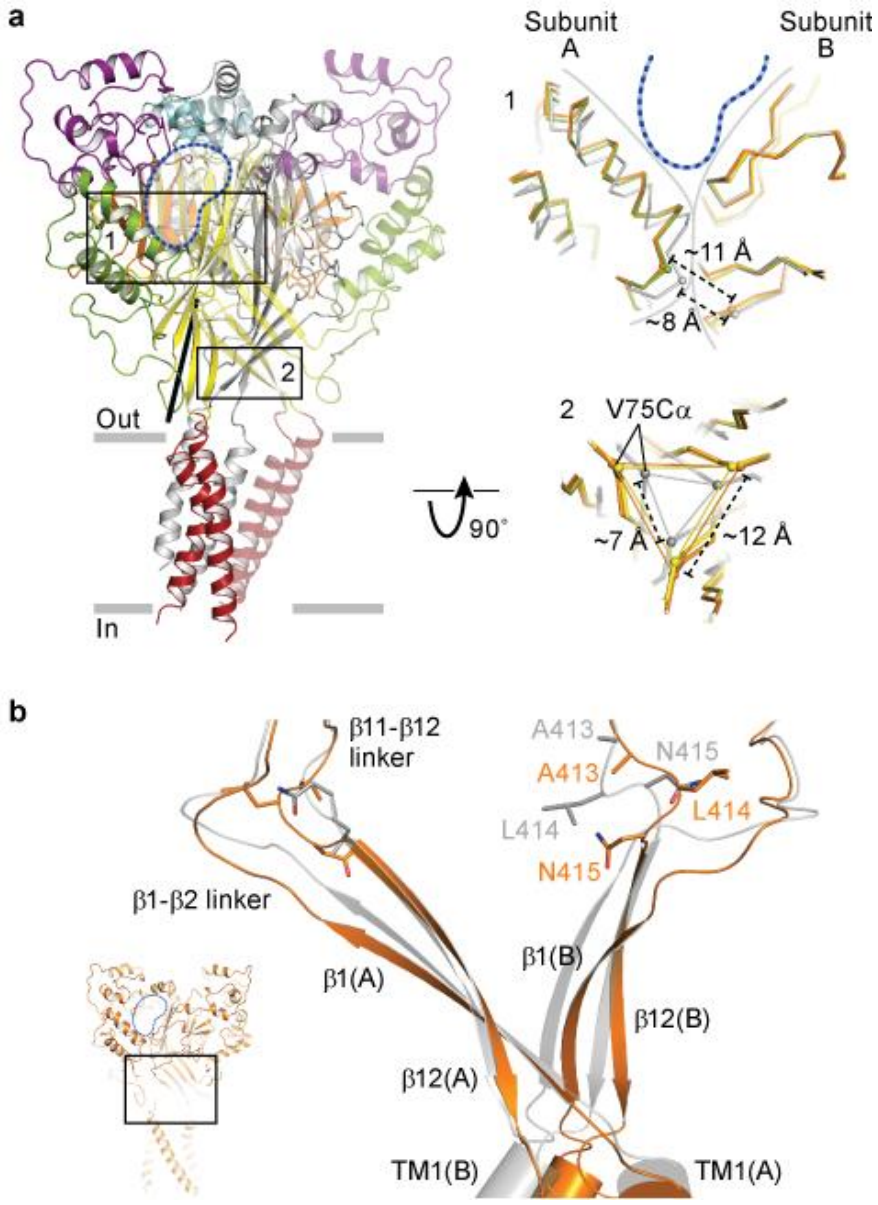

Figure 2.9. Conformational changes in the extracellular domain.

Figure 2.9. Conformational changes in the extracellular domain. a, Low pH Δ13-PcTx1 structure is in cartoon representation and colored as in Figure 2.6. Black line indicates the axis around which the lower palm domain and the wrist region rotate following superpositions of the desensitized and open state structures. Close-up views of selected regions are boxed. The low pH complex is colored by domain, the high pH complex is orange, and the desensitized state (PDB code: 3HGC) is gray. Approximate position of PcTx1 is indicated by blue dashed lines and the boundaries between adjacent subunits is shown by solid gray lines. Measured Cα distances are between residues Asn 357 (A) and Arg 85 (B) in box 1. In box 2 the distances are between Val 75 Cα atoms on adjacent subunits. **b**, Close-up view of strands β1 and β12, the β 1- β 2/ β 11- β 12 linkers and the extracellular boundary of the TM domains from two subunits of the high pH Δ13-PcTx1 complex (orange) and the desensitized state (gray) following superposition of the respective scaffold domains. Inset shows location of close-up view in the context of the entire channel.

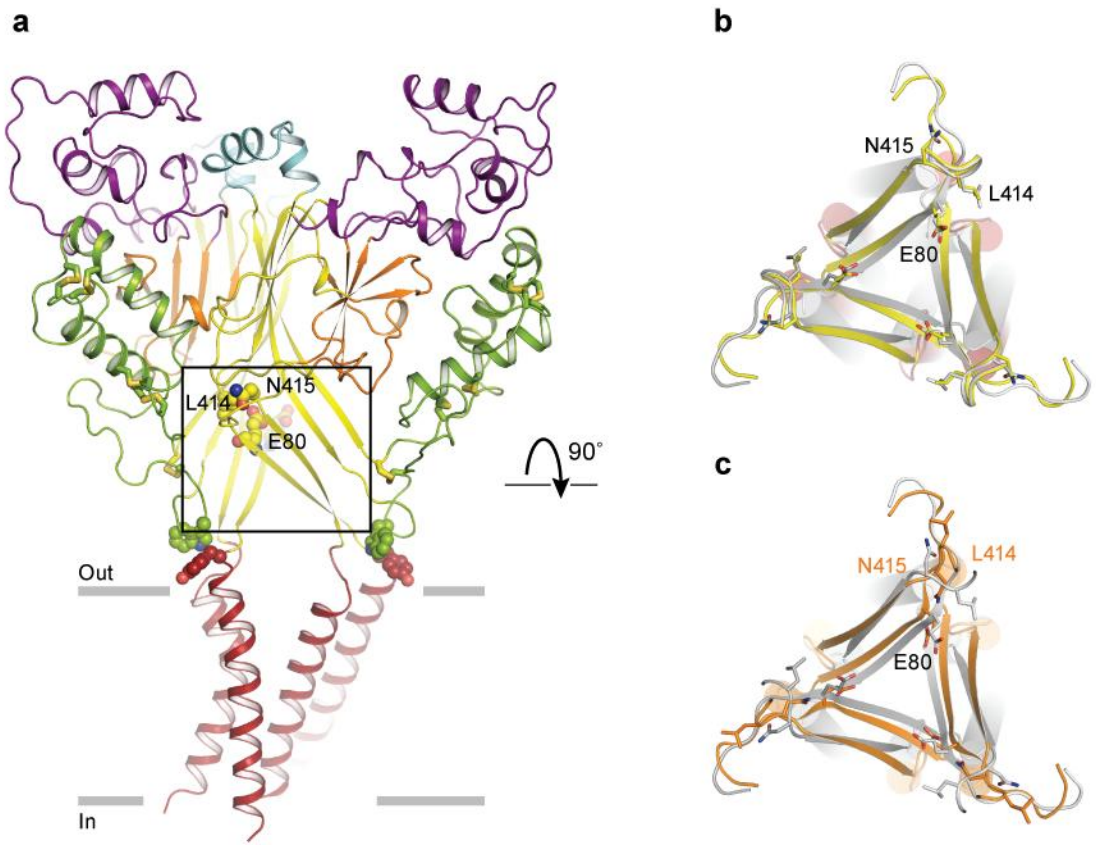

Figure 2.10. Conformational changes in the vestibule region. a, Two subunits of the low pH structure are shown for clarity and in cartoon representation, colored according to structural domains as in Figure 2 in the main text. Residues Glu 80, Leu 414, and Asn 415 are shown in spheres. **b**, **c**, Close-up view of the vestibule region viewed from the extracellular side showing how flexing of β1 and β12 expands the vestibule. Side chains of Glu 80, Leu 414, and Asn 415 are shown in stick representation. The desensitized state is colored gray, the low pH structure is yellow **(b)** and the high pH structure is orange **(c)**.

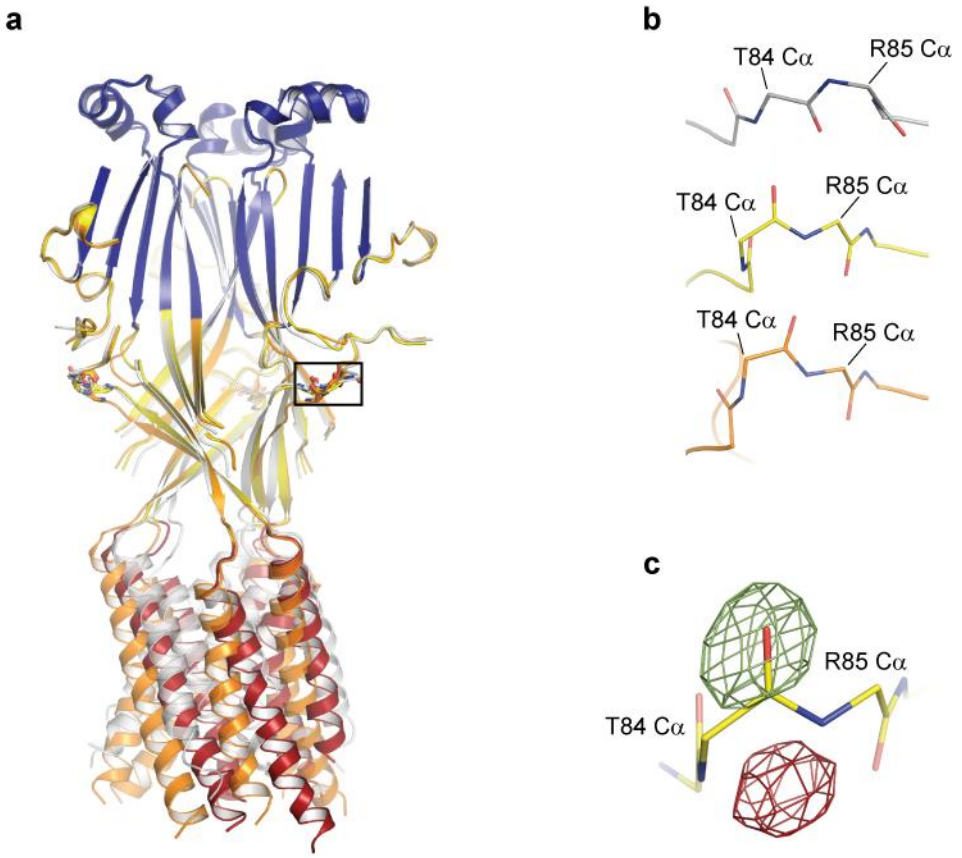

Figure 2.11. Peptide plane flip in the β1-β2 linker.

Figure 2.11. Peptide plane flip in the β1-β2 linker. a, The high pH (orange) and low pH structures (colored by domain as in Figure 2) are superimposed on the desensitized structure (gray) using Cα positions of all three subunits in the trimers and shown in cartoon representation. The finger and thumb domains are omitted for clarity. **b**, Close-up view of main chain in sticks representation of residues 83-85 in the β1-β2 linker (boxed region of panel a) of desensitized state (top), low pH (middle), and high pH (bottom) structures. **c**, Fo-Fc map contoured at 6σ. Map was calculated using unflipped peptide plane between Thr 84 and Arg 85, as observed in the desensitized state structure. The structure shown is of the flipped peptide plane of the toxin-bound low pH structure. Green and red mesh correspond to positive and negative peaks, respectively.

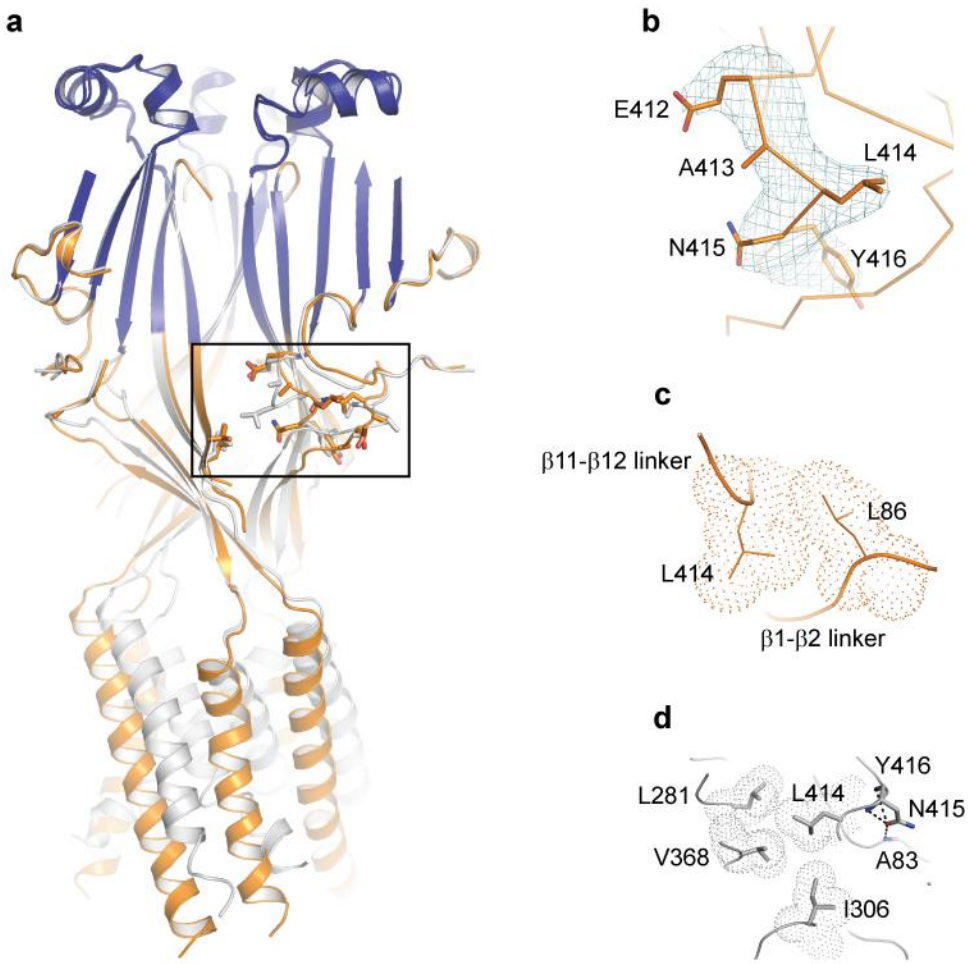

Figure 2.12. Side chain and main chain swap in the β11-β12 linker. **a**, Cartoon representation of the desensitized state structure (gray) and high pH toxin-bound structure (orange) are shown with the finger and thumb domains omitted for clarity. Residues involved in main chain swap are in the boxed region (a) and shown in sticks representation. **b**, Fo-Fc 'omit' map contoured at 3.5 σ. Map was calculated using a high pH model with residues 412-416 omitted. Model shown contains residues 412-416 as present in the final refined structure. **c**, **d**, Hydrophobic interactions mediated by Leu 414 in the high pH structure **(c)** and in the desensitized state structure **(d)**. Residues involved are shown in sticks and dots representation. Hydrogen bonding interactions involving Asn 415 are shown as dashed lines **(d)**.

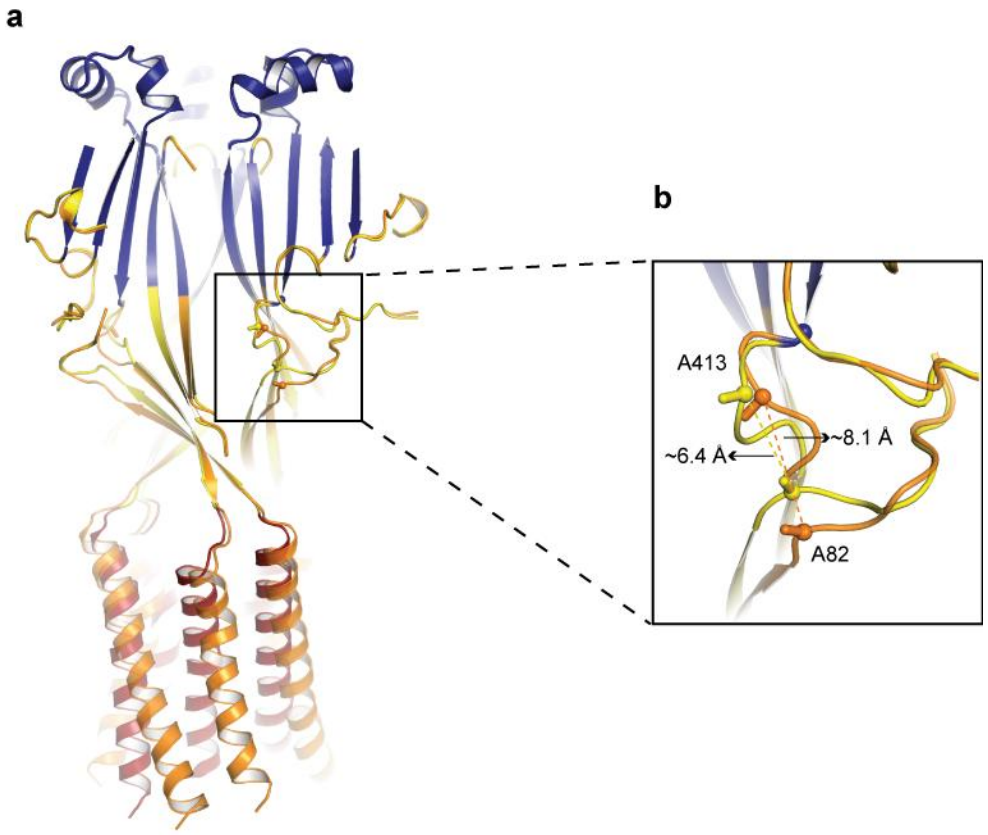

Figure 2.13. Conformational changes in the β1-β2 and β11-β12 linkers. a, Cartoon representation of the high pH (orange) and low pH (colored by domain as in Figure 2) are shown with the finger and thumb domain omitted for clarity. Residues involved in main chain swap are in the boxed region and shown in sticks representation. **b,** Close-up view of boxed region illustrating difference in Cα distances between residues Ala 82 and Ala 413.

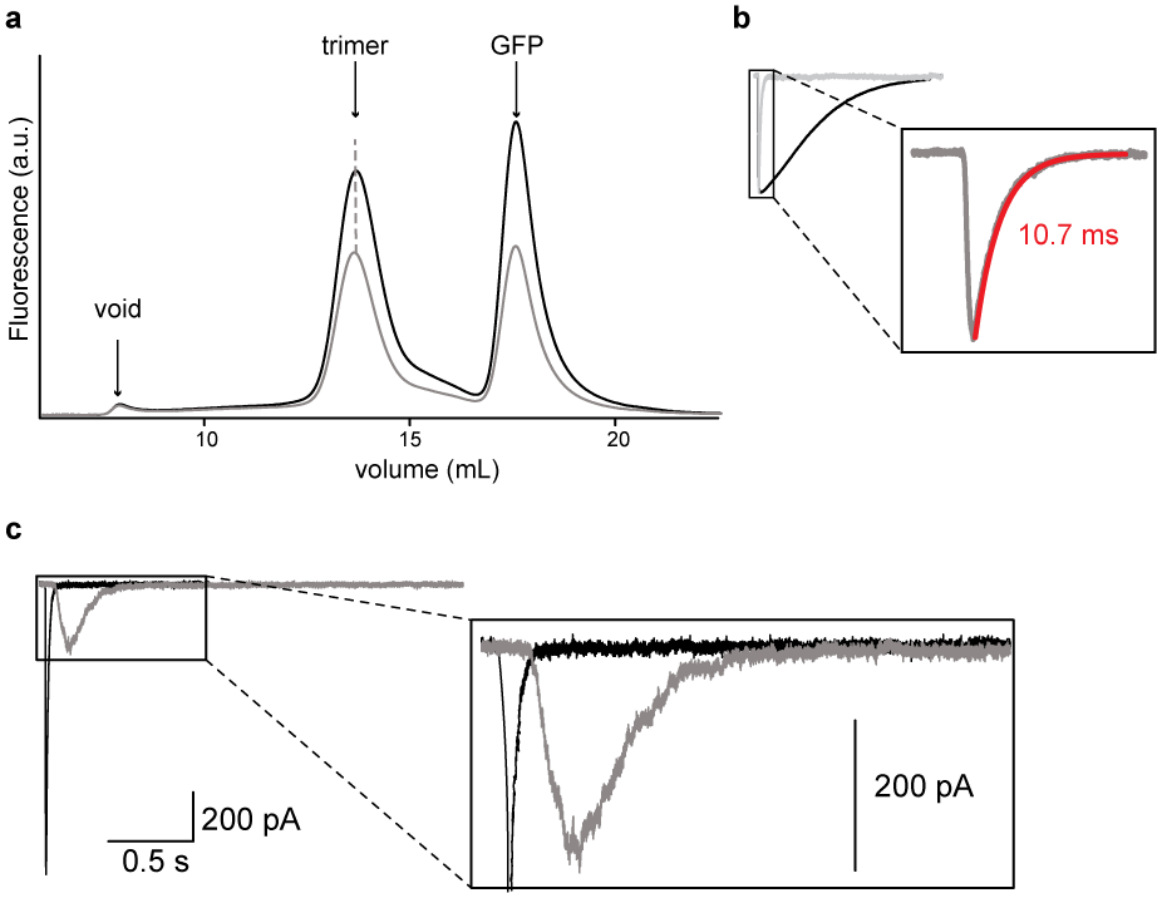

Figure 2.14. Characterization of E80A by FSEC and electrophysiology. a, Fluorescence-detection size-exclusion chromatography traces of Δ13 (black) and Δ13-E80A (gray). Peaks of trimeric ASIC and adventitiously cleaved GFP are labeled. **b**, Normalized representative current traces of Δ13 (black) and Δ13-E80A (gray). Channels were opened by a step to pH 5.5 from pH 8.0. Inset, current trace of Δ13-E80A with time constant (red) of ~10 ms (Δ13, time constant of ~400 ms). **c**, Activation of Δ13-E80A at pH 7.25 + 1 uM PcTx1 (gray) generates a peak current that is 25% of the pH 5.5 peak amplitude (black). Both currents rapidly desensitize.

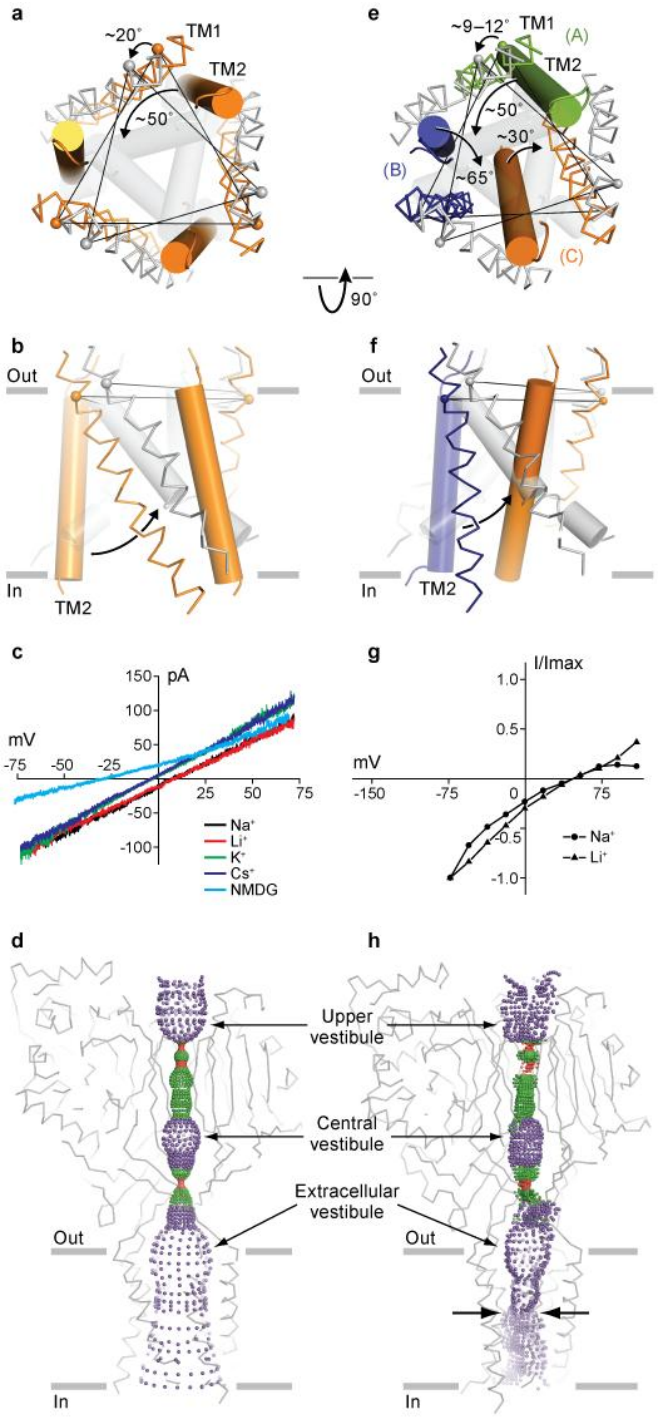

Figure 2.15. Structural rearrangements and ion selectivity of the transmembrane pores

Figure 2.15. Structural rearrangements and ion selectivity of the transmembrane pores. a, **b**, Comparison of transmembrane domains from the high pH (orange) and desensitized (gray) state structures with TM1 in ribbon and TM2 in cylinder representation. Transmembrane domains are viewed from the extracellular side **(a)** and parallel to the membrane **(b)**. **c**, Current/voltage experiment showing that at neutral pH the Δ13-PcTx1 complex forms a non selective cation channel. **d**, Mapping of solvent accessible pathway along the 3-fold axis shows that the high pH complex has a large, transmembrane pore. The occluded pathway along the 3-fold in the extracellular domain suggests that ions access the pore by way of lateral fenestrations. **e, f.** A comparison of the transmembrane domains from the low pH complex, where each subunit is in a different color. The desensitized state is gray. TM1 and TM2 segments are in ribbon and cylinder representations, respectively. Transmembrane domains are viewed from the extracellular side **(e)** and parallel to the membrane **(f)**. **g,** Current/voltage experiment demonstrating that the ion channel of the low pH □ 13-PcTx1 complex is sodium selective. **h**, Mapping of a solvent accessible pathway along the pseudo 3-fold axis of the low pH complex shows that it has an asymmetric ion channel pore and a constriction (opposing arrows) halfway across the bilayer. Maps of solvent-accessible pathways (d and h) were generated using the HOLE software (red < 1.4 Å < green < 2.3 Å < purple).

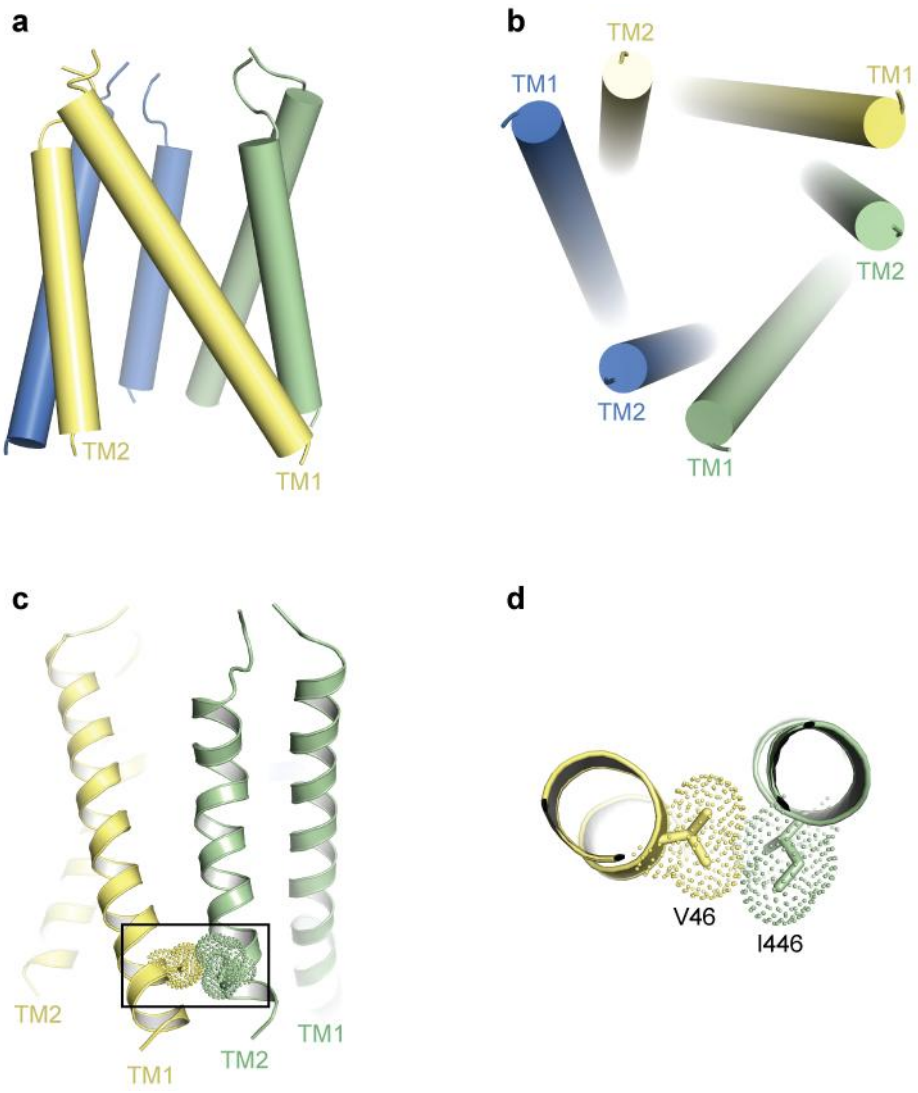

Figure 2.16. Transmembrane domain swap in the high pH, R3 space group structure. **a**,**b**, Cylindrical representation of the transmembrane domains of the high pH structure viewed parallel to the membrane **(a)** and perpendicular to the membrane, from the intracellular side **(b)**. **c**, Intersubunit interactions include hydrophobic contacts between Val 46 (TM1) of one subunit and Ile 446 (TM2) of the adjacent subunit. **d**, Close-up view of **(c)** from the extracellular side. Side chains are in sticks and dots representation.

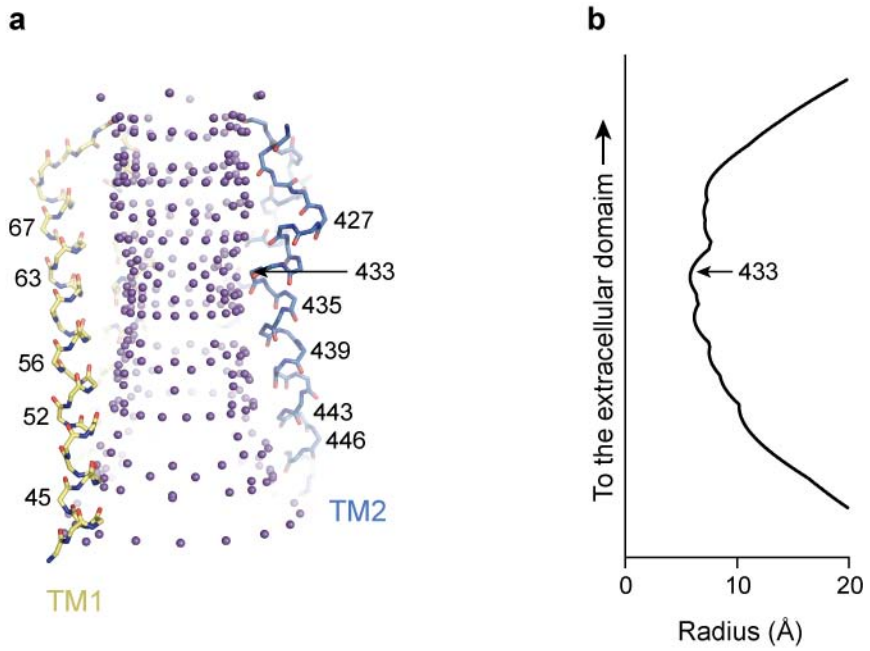

Figure 2.17. High pH complex has a large pore. a,b, Calculation of the pore radius of high pH structure using HOLE software. **(a)** Outlines of the transmembrane pore of the high pH complex as defined by HOLE where the purple sphere marks indicate a pore radius greater than 2.3 Å. Main chain in sticks representation is shown with one subunit omitted for clarity. **(b)** Pore radius is plotted along the three-fold axis. Smallest pore diameter is ~10 Å and occurs at residue 433.

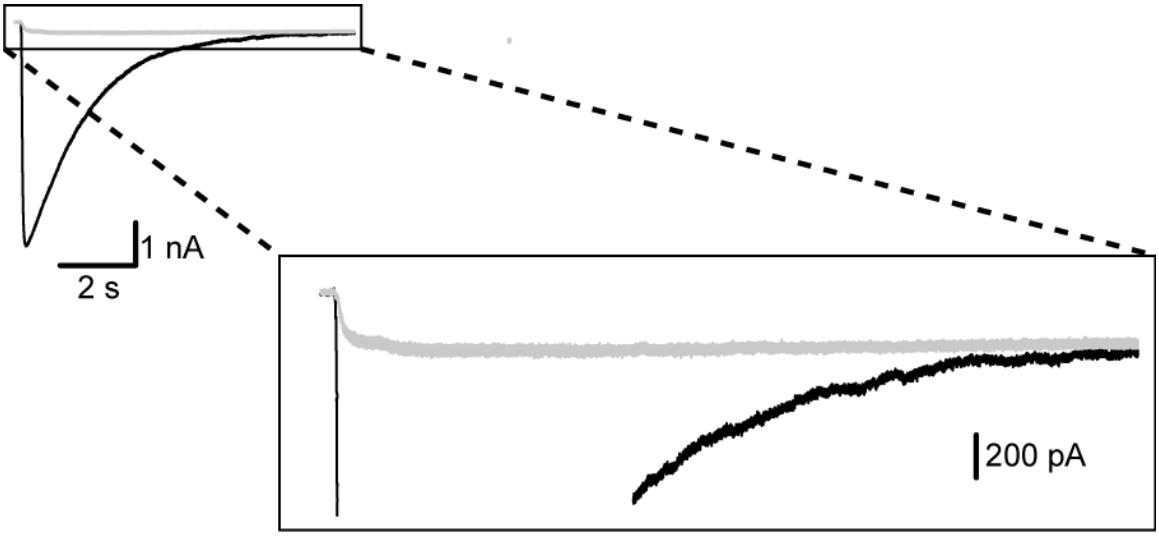

Figure 2.18. Amiloride block of toxin-mediated current at pH 7.25. A 500 uM concentration of amiloride blocks (gray trace) 95% of the peak current mediated by activation of Δ13 with pH 7.25 and 1 uM PcTx1, but only blocks 10% of the steady-state current.

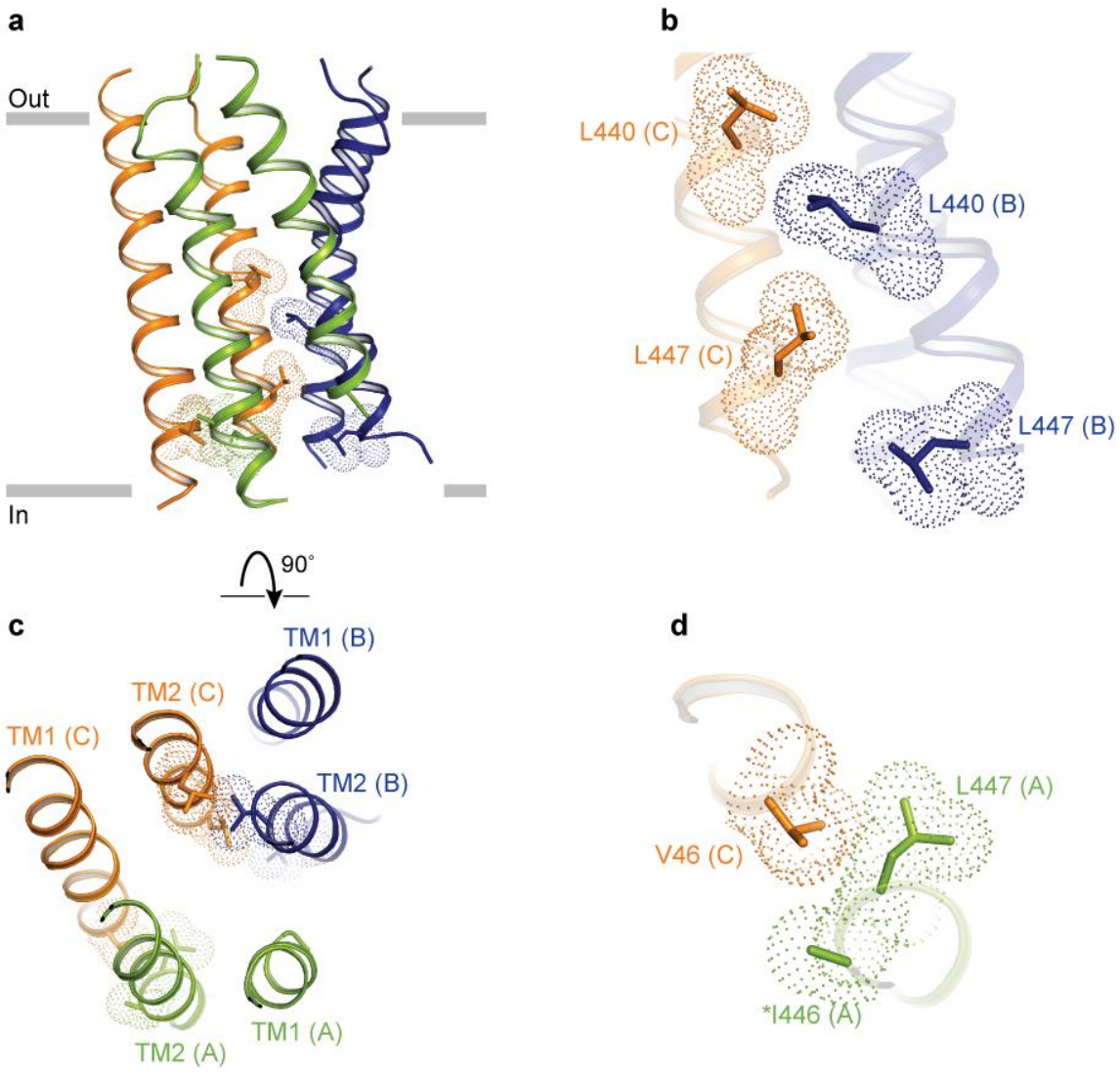

Figure 2.19. Intersubunit contacts of low pH structure in the transmembrane domain.

Figure 2.19. Intersubunit contacts of low pH structure in the transmembrane domain. **a**,**c**, Cartoon representation of the low pH transmembrane domain viewed parallel to the membrane **(a)** and from the extracellular side **(c)**. Highlighted residue side chains are shown in stick representation. **b**, Close-up view of the intersubunit interaction between subunit B, blue, and subunit C (orange). The interaction resembles a leucine zipper motif with leucines at positions i and i+7. **d**, Close-up view of the intersubunit interaction between subunit A, green, and subunit C, orange. This interaction is similar to the high pH intersubunit contact shown in Supplementary Figure 11. Side chains with weak density are modeled as alanine (asterisk).

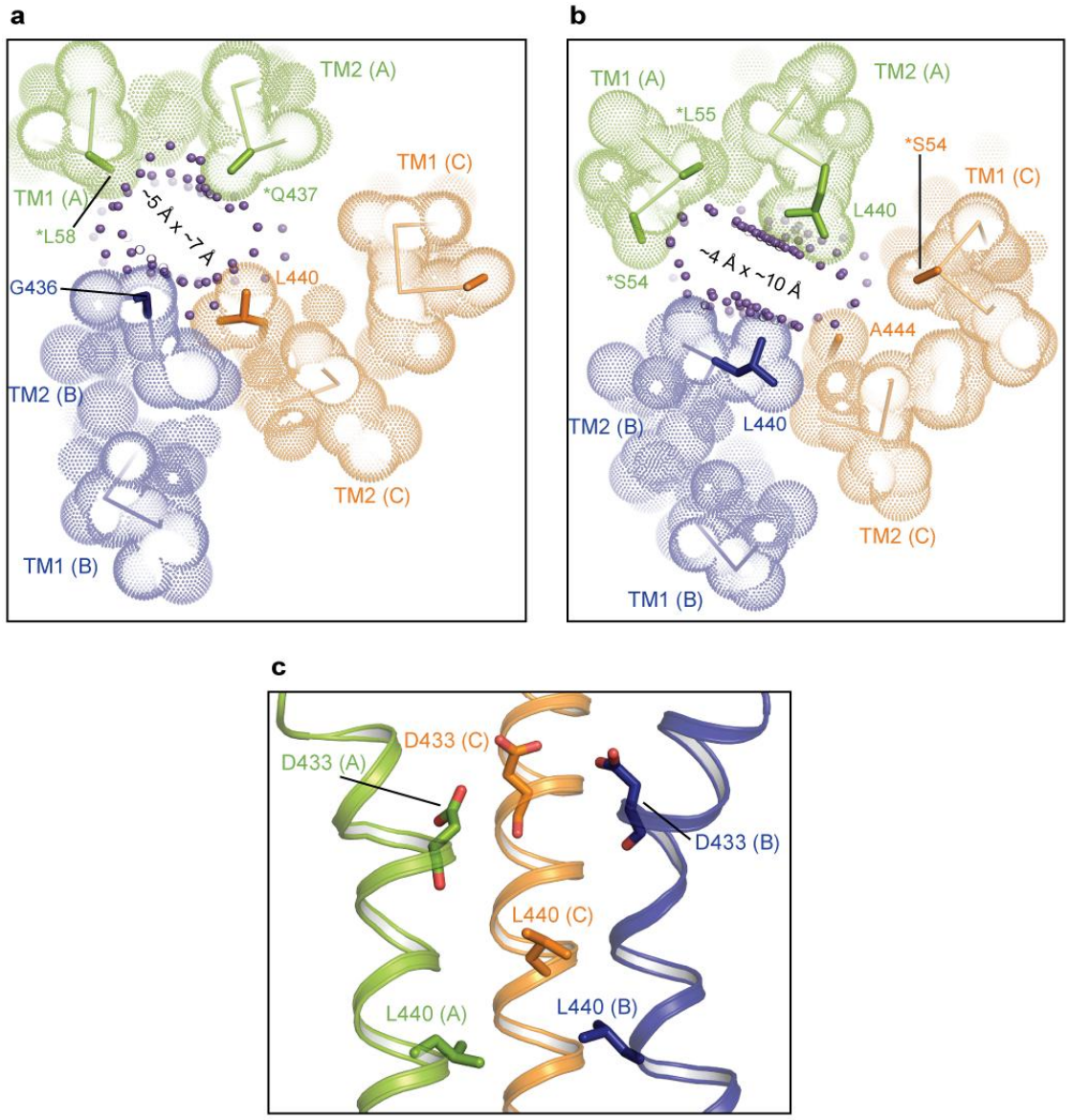

Figure 2.20. Hydrophobic pore constriction in the low pH complex

Figure 2.20. Hydrophobic pore constriction in the low pH complex. Pore constriction in the low pH complex is elliptical and located about halfway across the membrane lined by Leu 440 from subunits C **(a)** and A and B **(b)** viewed from the extracellular side. Residues are drawn in stick and dot representations. Outline of the pore generated by the HOLE software is in purple sphere representation and indicates pore radius larger than 2.3 Å. Estimated dimensions of the minor and major axes are shown. **c**, Acidic residues, Asp 433, positioned above the hydrophobic pore constriction lined by Leu 440 viewed parallel to the membrane. TM1 from all subunits are omitted for clarity. TM2 are shown in cartoon representation and residues are in sticks representation. Residues with weak side chain density are modeled as alanine (asterisk).

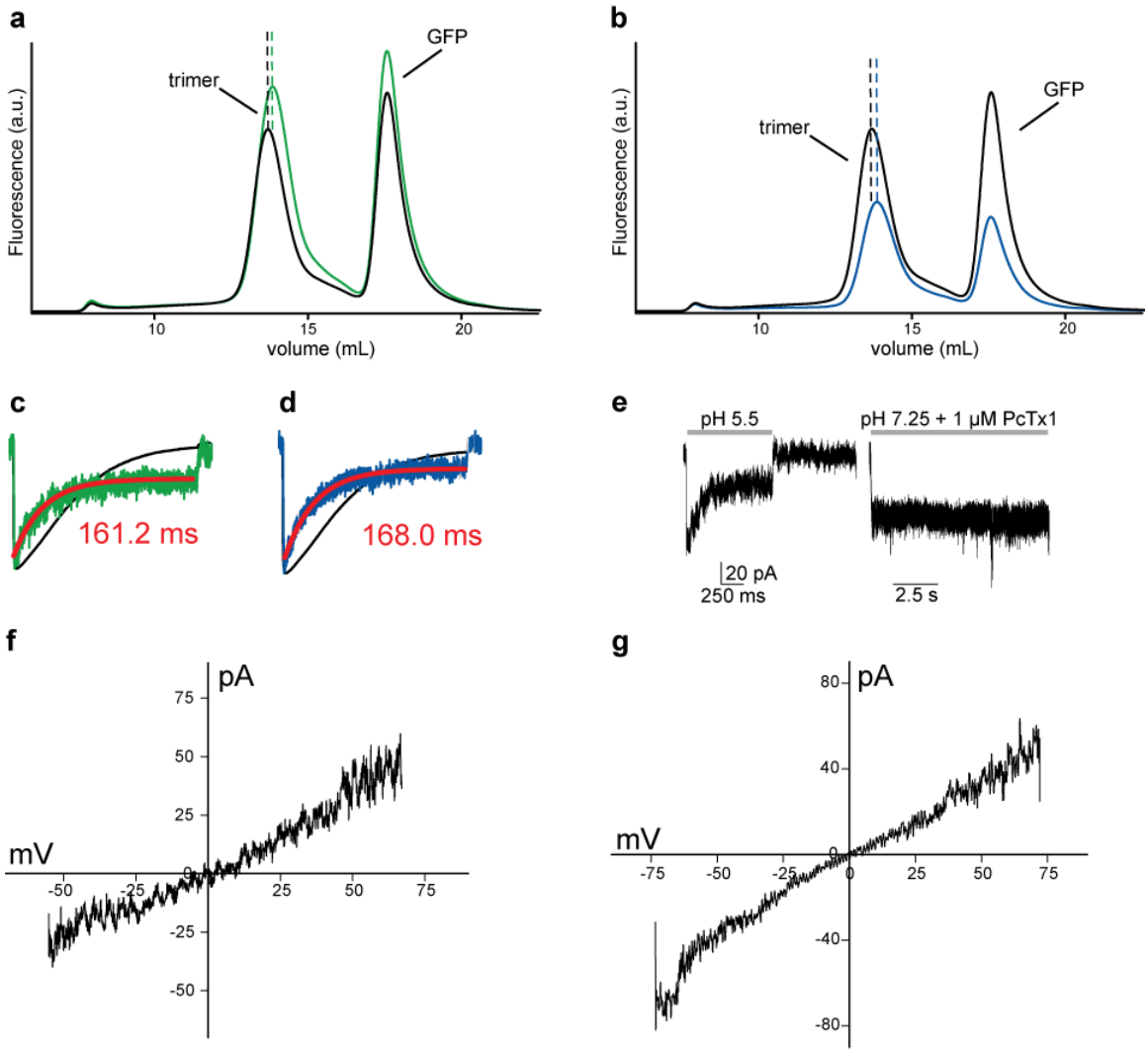

Figure 2.21. Role of L440 in the formation and function of the ion channel pore.

Figure 2.21. Role of L440 in the formation and function of the ion channel pore. a,**b**, Fluorescence-detection size-exclusion chromatography traces of Δ13 (black), Δ13-L440A (**a**, green trace) and Δ13-L440S (**b**, blue). Dashed lines illustrate shifted elution volume of mutants. **c**,**d**, Normalized representative current traces of Δ13 (black), Δ13-L440A (**c**, green trace) and Δ13-L440S (**d**, blue) by whole-cell recording. Measured time constants (red) are ~160 ms for both mutants. Steady-state currents are ~30% and ~20% of the peak current for L440A and L440S, respectively. Channels were opened by a step to pH 5.5 from pH 8.0. **e**, Representative current traces of L440S mutant upon activation by a step to pH 5.5 (left) and pH 7.25 + 1 μM PcTx1 (right). Peak amplitudes of both conditions are similar. Current induced by toxin activation at pH 7.25 does not desensitize. **f-g,** I-V relationships of the L440S mutant generated from ramp experiments of steady-state current following a step from pH 8.0 to pH 5.5 **(f)** or to pH 7.25 + 1 μM PcTx1 **(g)**. Ramp experiments at pH 8.0, where no channel activation was observed, were used for baseline subtraction. Intracellular solution contained 150 mM KCl while the extracellular solution contained 150 mM NaCl.

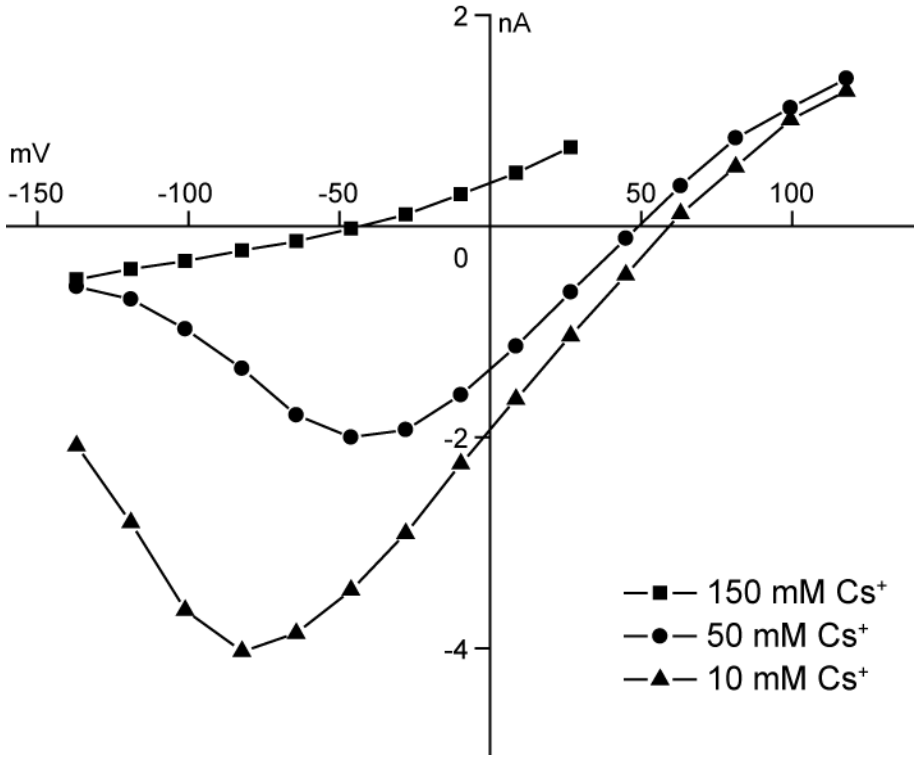

Figure 2.22. Bi-ionic whole cell recordings show voltage-dependent block by Cs^+.

Current-voltage relationships of the Δ13 construct where the external solutions contain (in mM) 150/0, 50/100, and 10/140 Cs+/Na+, respectively. The intracellular solution contains 150 mM K+.

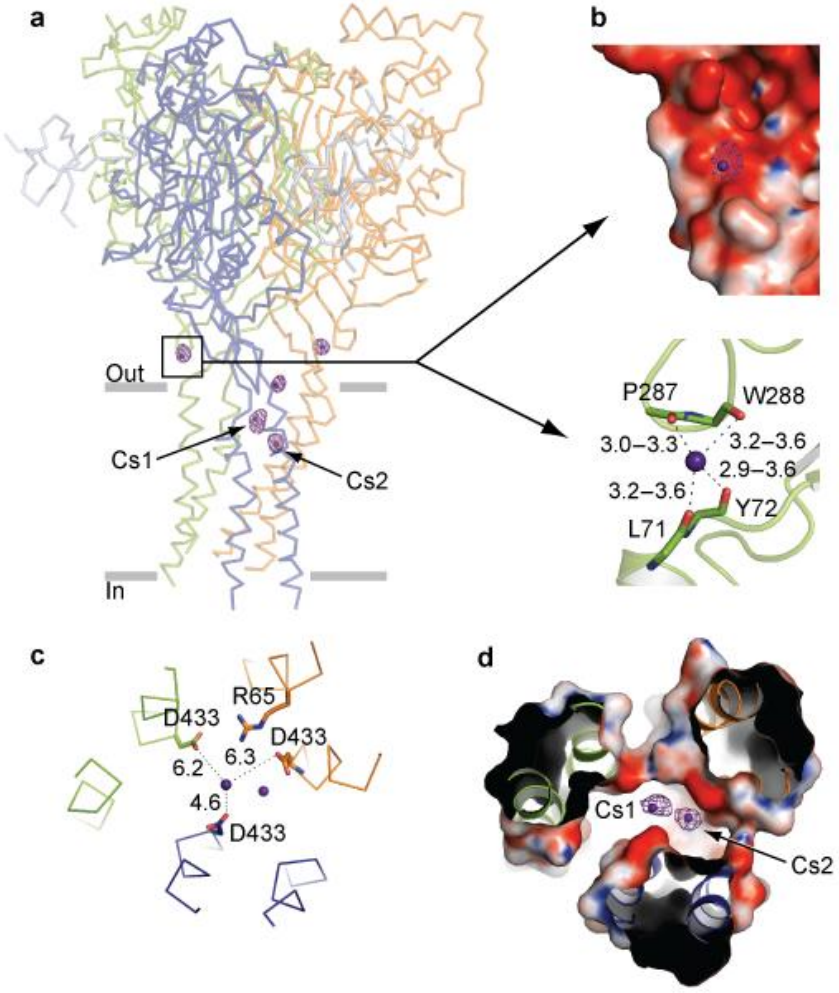

Figure 2.23. Cs^+ binding sites. **a,** Anomalous difference electron density map contoured at 3.5 σ. The low pH complex is in ribbon representation. Cesium sites in the outer pore region are labeled Cs1 and Cs2. **b,** Close-up view of the Cs^+ site in the wrist region. Top, electrostatic potential contoured from -20kT (red) to +20kT (blue). Bottom, Cs^+ coordination by backbone carbonyl oxygens. The main chain is drawn as sticks. **c**,**d**, Close-up view of Cs^+ sites near Asp 433 shown in ribbon and stick representation **(c)** and solvent accessible surface colored by electrostatic potential **(d)** viewed from the extracellular side.

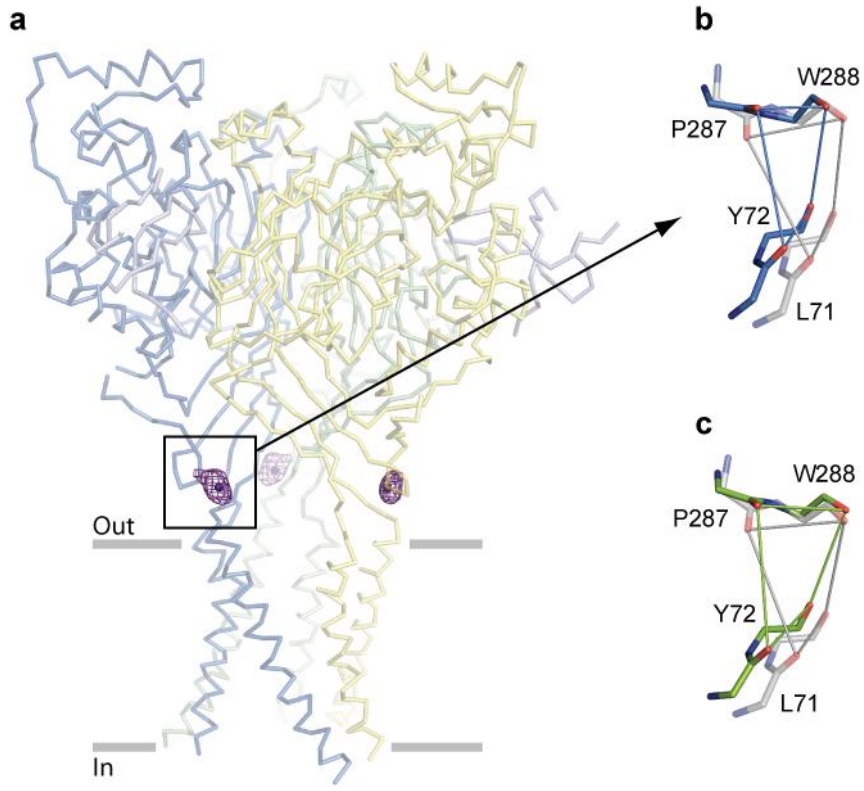

Figure 2.24. Cation binding site in the wrist region. **a**, Anomalous difference electron density map showing Cs+ sites in the wrist region of the high pH complex. The map is contoured at 4.5σ. **b**, **c**, The high pH **(b)** and low pH **(c)** wrist regions are superimposed on the corresponding regions of the structure of the desensitized state (carbon atoms are gray) using Cα positions of Pro 287 and Pro 288 to compare arrangement of backbone carbonyl oxygens coordinating with Cs+. In the superpositions the electron density and spheres representing Cs+ ions have been omitted for clarity.

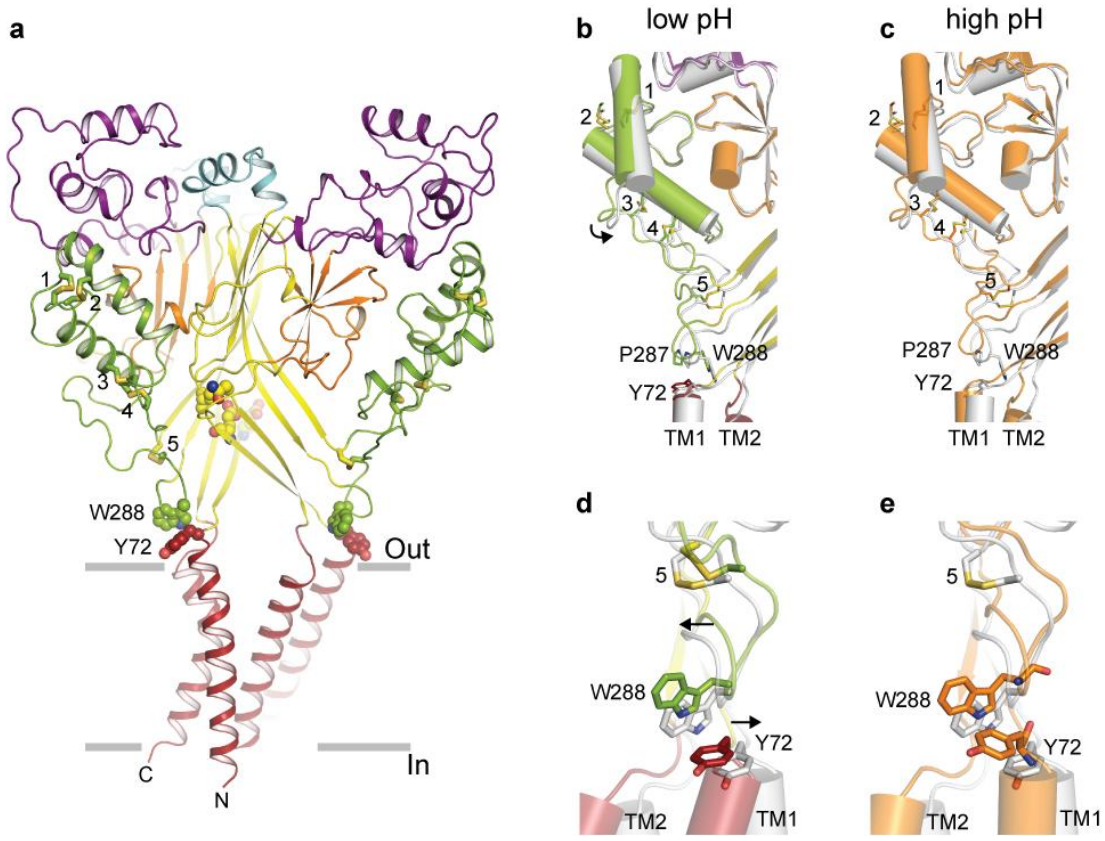

Figure 2.25. Correlated structural movements couple conformational changes between the extracellular and transmembrane domains.

Figure 2.25. Correlated structural movements couple conformational changes between the extracellular and transmembrane domains. **a**, The low pH complex is used as the reference structure, shown in cartoon representation and colored by domain, as in Figure 2. Only two subunits are shown for clarity. Disulfide bonds in the thumb region (green) are numbered, 1(residues 324 and 336), 2(322 and 344). 3(313 and 360), 4(309 and 362), and 5(291 and 366), and shown in stick representation. Residues in the wrist region (W288 and Y72) are shown in spheres. **b**,**c**, Structural rearrangements are illustrated by way of comparisons between the low pH **(b)** and high pH **(c)** structures and the desensitized state structure (gray). Cα positions of the trimer were used for superimpositions. **d**, **e**, Extracellular and transmembrane domains are coupled, in part, through the wrist region. Residues Tyr 72 and Trp 288, implicated in channel gating, are shown in stick representation. Side chains of Tyr 72 and Trp 288 in the desensitized state (gray) show rotational movements relative to the low pH **(d)** and high pH **(e)** that are opposite in direction.

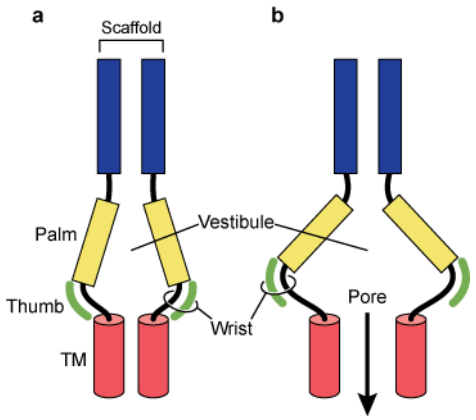

Figure 2.26. Schematic representation of gating. a, The extracellular vestibule in the closed, desensitized state structure adopts a contracted conformation. **b**, In the open pore conformation the vestibule occupies an expanded conformation, stabilized by the thumb domain. The wrist region, in turn, couples the conformational changes of the extracellular domain to the transmembrane domains (red cylinder) of the ion channel pore.

Chapter 3

X-ray structure of acid sensing ion channel – snake toxin complex in an open state

The contents of chapter three are submitted for publication in modified form:

Baconguis, I., **Bohlen, C.**, **Goehring, A.**, **Julius, D.**, & **Gouaux, E.** X-ray structure of acid sensing ion channel – snake toxin complex in an open state. (submitted)

Author Contributions:

I.B. purified Δ13 and crystallized Δ13-MitTx complex, and collected, processed, and refined crystallographic data. C.B. purified MitTx from Texas coral snake while A.G. and E.G. prepared recombinant MitTx. I.B. wrote the manuscript and D.J., C.B., and E.G. edited it.

Abstract

Ion channels are expressed throughout the human body and are implicated in a broad range of physiological activities, including the detection of noxious stimuli. While it has been known for nearly a century that many toxins selectively target ion channels and hijack their normal physiological function, how xenogenous toxins modulate ion channel gating remains largely unknown. We have determined the atomic structure of chicken acid sensing ion channel 1a in complex with the heteromeric Texas coral snake toxin, MitTx, illustrating the mechanism by which this pain-producing toxin opens the channel pore. The α/β heterodimeric toxin acts like a 'churchkey' bottle opener, with the β subunit anchored to the top of the thumb domain, bound near the acidic pocket, and the α subunit positioned below, forming extensive interactions with the base of the thumb and the wrist, 'prying' open the ion channel. The ion channel open conformation reveals a 3-fold symmetric, hour-glass shaped pore and a ~3.6 Å diameter constriction formed by main-chain carbonyl atoms of selectivity-determining residues. Analysis of Cs^+ soaked crystals shows 2 sites in the acidic central vestibule, one site bound via a cation-π interaction in the extracellular fenestrations, and a third site, in the pore, below the ~3.6 Å diameter constriction. Taken together, these studies illuminate the mechanism by which MitTx stabilizes an open-channel conformation of cASIC1a and provide insights into the mechanisms of gating and permeation in acid sensing ion channels.

Introduction

Toxins from venomous animals have captivated our attention from the age of Greek mythology, when Hercules slayed the centaur Nessus with arrows dipped in the blood of the snake-like Hydra [159]. Many venomous toxins act on membrane-embedded ion channels and studies over the past century have elaborated the ion channel targets of classical biological toxins that include α-bungarotoxin and the acetylcholine receptor [160], con-ikot-ikot and AMPA-sensitive glutamate receptors [161], and psalmotoxin [84] or MitTx [91] and acid sensing ion channels. Because these toxins often bind with high affinity and specificity to their cognate channel, typically locking the channel in an open or a shut channel state, they are invaluable probes by which to elucidate ion channel localization, and mechanisms of signal transduction and ion channel gating [162].

Acid sensing ion channels (ASICs) are trimeric, cation permeable channels that belong to the degenerin/epithelial sodium channel (DEG/ENaC) superfamily [21, 28]. Six distinct ASIC subtypes, (1a, 1b, 2a, 2b, 3 and 4) are expressed throughout the central and peripheral nervous system [2, 3, 80, 163]. While all ASIC subtypes are found in sensory neurons [1, 164], and ASIC1a, 2 and 3 have been implicated in multiple pain modalities [132], previous studies have emphasized the role of ASIC3 in acidic, inflammatory, postoperative and ischemic pain [165-167]. Recently, however, experiments utilizing the venomous toxin MitTx from the Texas coral snake [91] have implicated other ASIC subtypes, notably, subunits 1a and 2, in nociception.. MitTx is a heterodimeric polypeptide toxin composed of an α subunit homologous to Kunitz-like protease inhibitors and a β subunit related to phospholipase A2 enzymes, and thus reminiscent of the well known β-bungarotoxin [168, 169]. MitTx potently excites sensory neurons by activating ASIC1

channels in a pH independent manner, thereby eliciting robust acute pain behavior in wild type, but not ASIC1-deficient mice [91]. Moreover, MitTx dramatically slows desensitization in ASIC1 channels, stabilizing an open, sodium-selective conformation of ASIC1. Thus not only does the biological activity of MitTx implicate ASIC1 channels in nociception, but the nearly irreversible binding and activation of ASIC1 channels by MitTx suggests that studies of the molecular complex will shed light on determinants of toxin specificity and mechanisms of ASIC channel gating and permeation.

Methods

Protein expression and purification

The Δ13 cASIC1a protein and native MitTx were expressed and purified as previously described [91, 170]. Prior to crystallization, the complex was formed by mixing Δ13 with MitTx at an approximate molar ratio of 1 Δ13 subunit to 1.5 MitTx, respectively.

Crystallization and cryoprotection

Crystals of the Δ13-MitTx complex were grown by vapor diffusion using a reservoir solution composed of 100 mM sodium acetate (pH 5.5), 6-9% PEG 4000 and drops composed of a ratio of 1:1 and 2:1, protein to reservoir, respectively, at 4 °C and an initial protein concentration of ~2.5 mg/ml. For cryoprotection, crystals were soaked in reservoir solution supplemented with increasing concentrations of glycerol (20-25% v/v final concentration) and 1 mM *n*-dodecyl β-D-maltoside (DDM). For Cs^+ anomalous diffraction experiments, crystals were soaked in reservoir solutions containing 100 mM cesium acetate (pH 5.5) supplemented with 500 mM CsCl and 1 mM DDM.

Structure determination

X-ray diffraction data sets for both native and Cs^+-soaked crystals were collected at the Advanced Light Source (beamline 5.0.2) and diffraction was measured to ~2.70 Å and 2.65 Å resolution, respectively. Diffraction data for crystals soaked in Cs^+-containing solutions were measured using low energy x-rays (9000 eV). Diffraction data sets were indexed, integrated, and scaled using the HKL2000 software[144], with I^+ and I^- from the cesium data scaled separately. The native structure was solved by molecular replacement using the computer program PHASER[145], with the extracellular domain coordinates of the ΔASIC1 structure (PDB code: 2QTS) [24] as a search probe. Resulting electron density maps calculated using amplitudes of $2F_o$-F_c and F_o-F_c and phases from the molecular replacement solution showed strong electron density for the heterodimeric complex of MitTx.

Homology models of the MitTx α and β subunits were built using the 'Automated Mode' of the Swiss-Model homology modeling server (http://swissmodel.expasy.org/) together with the amino acid sequences of the mature polypeptides for the α and β subunits of MitTx [91]. Using the molecular replacement solution obtained with the extracellular domain of the ΔASIC1 structure as described above, truncated homology models of the α subunit, (residues 13-38) and the β subunit (helices α1, α2, and α3) were used in a subsequent round of molecular replacement. Coordinates derived from the subsequent solution were then subjected to iterative rounds of manual model building and crystallographic refinement using the computer programs COOT [146] and PHENIX [147]. Manual building of the transmembrane domains was guided by electron density maps calculated using the crystallographically refined coordinates of the extracellular domain - toxin complex. "Omit"

electron density maps were calculated to validate residue registration in the transmembrane region. Subsequent iterative cycles of model building and refinement were performed after building the transmembrane regions and the α and β subunits of MitTx. The final structure includes residues Trp 47 to Gly 296 and Glu 299 to Asp 454 of the Δ13 construct and residues PCA 1 to Gly 60 and Asn 1 to Cys 118 of the α and β subunits of MitTx. Residues with disordered side chains were built as alanines.

Diffraction data from the Cs^+-soaked crystals and the 'native' Δ13-MitTx structure described above was used in molecular replacement, followed by rounds of manual model building and crystallographic refinement. Inspection of the anomalous difference electron density maps was employed to identify Cs^+ sites and a Cs^+ ion was placed in all peaks that were greater than ~4 σ, resulting in a total of 15 Cs^+ ions. Analysis of the $2F_o$-F_c and F_o-F_c electron density maps, together with the refined structure, indicated that the most significant difference in the protein structure between the 'native' and the Cs^+ soaked structures resided in the transmembrane domain and involved an expansion of the TM helices near Gly 439, near a Cs^+ ion binding site.

Structure validation was performed using MolProbity [148]. Pore surface and dimension were determined using the software HOLE [149] and APBS for calculation of electrostatic potential [171]. AREAIMOL of the CCP4 package was used to calculate buried surface area [172]. Figures were prepared using the program PyMOL.

Expression, refolding and purification of recombinant MitTx-α and MiTx-β

Genes coding for the mature MitTx-α and MitTx-β proteins (Genebank accession numbers JN613325 and JN613326, respectively; [91]) preceded by N-terminal enterokinase cleavage sites were synthesized and subcloned into the pET32b vector for expression in

Escherichia coli. The resulting N-terminal thioredoxin (Trx) MitTx-α and MitTx-β fusion proteins were expressed in *E. coli* RosettagammiB (DE3) pLysS cells following induction with 0.1mM isopropylthiogalactopyranoside for 4 hrs at 30 °C. Cells were collected by centrifugation at 6,200xg and disrupted by sonication in buffer containing 20 mM Tris pH 8, 150 mM NaCl, 1 mM phenylmethylsulfonyl fluoride, 5mM $MgCl_2$, 20ug/ml DNase-I and 0.4mg lysozyme. The cell extracts were centrifuged at 8000g for 15 min, inclusion bodies were collected, washed and solubilized as previously described (Chen and Gouaux, 1997) except that inclusion body solubilization buffer was supplemented with 300mM β-mercaptoethanol.

Refolding of both proteins was carried out using the same method, beginning with dilution of the solubilized inclusion bodies 10-fold into a buffer composed of 50mM Tris pH8.5, 5mM EDTA, 6M GuCl, and 10mM β-mercaptoethanol and clarification of the resulting solution by centrifugation at 125,000g. The supernatant was dialyzed overnight at 4°C against 20mM Tris pH8.5, 1mM EDTA, 200mM NaCl, and 0.5M arginine, followed by an additional overnight dialysis against 20 mM Tris pH 8, 200 mM NaCl, 1 mM EDTA and centrifugation at 125,000g to remove precipitate. Analysis by SDS-PAGE also showed that the refolded samples were composed of >95% MitTx-α or MitTx-β. Using 1.5g of washed inclusion bodies, 116 and 9.2 mg of soluble fusion protein can be obtained for Trx-MitTx-α and Trx-MitTx-β, respectively.

The Trx-tag was removed from both subunits by enterokinase digestion at RT for 2h using ~25 units of enterokinase (Applied Biological Materials) for each 1 mg of Trx-fusion. Purification of the MitTx-α subunit was achieved by dilution of the digested sample with 20 mM MES pH 6, 200 mM NaCl, centrifugation to remove precipitate, concentration and

finally application to a gel filtration column equilibrated in 20 mM MES pH 6, 200 mM NaCl. Monodisperse MitTx-α fractions were pooled and treated with glutaminyl cyclase (R&D Systems) to catalyze N-terminal pyroglutamate formation. Analysis of purified MitTx-α by gel electrophoresis is illustrated in **Figure 3.2a**. Mass spectrumetric analysis shows that the recombinant MitTx-α has a mass of 7104 Da, in ideal agreement with the 7104 Da predicted mass of the native toxin.

Purification of MitTx-β was accomplished by enterokinase digestion as described above, subsequent dialysis against 20 mM MES pH 6, 10 mM NaCl, and chromatographic separation from the Trx tag and other impurities by cation exchange chromatography. Analysis of purified MitTx-β by gel electrophoresis is illustrated in **Figure 3.2b**. The mass of the refolded MitTx-β subunit measured by mass spectrometry is 13736.6 Da, thus comparing favorably with the predicted mass of the native toxin (13738 Da).

Electrophysiology

Whole-cell recordings were carried out with CHO-K1 cells 24 hours after transfection by plasmid DNA encoding the Δ13 construct and GFP expressed from an internal ribosome entry site. Pipettes were pulled and polished to 2-3 MΩ resistance and filled with internal solution containing (in mM): 150 KCl, 2 $MgCl_2$, 5 EGTA and 10 HEPES (pH 7.35). External solution contained (in mM): 150 NaCl, 2 $MgCl_2$, 2 $CaCl_2$, 8 Tris and 4 MES. For ion selectivity experiments, NaCl was substituted with equimolar concentrations of CsCl in the external solution and recombinant MitTx-α and MitTx-β were applied at 300 nM concentration of each toxin subunit. Reversal potentials were measured using voltage ramps from -60 to 90 mV for 100 ms.

Results and discussion

Architecture of the channel-toxin complex

The heterodimeric complex of *Micrurus tener tener* toxin (MitTx) activates the chicken ASIC1a Δ13 construct, a minimal construct of chicken acid sensing ion channel 1a with wild type-like functional properties [170], similar to the MitTx activation of murine ASICs [91]. At pH 7.4, application of MitTx to cells expressing the Δ13 construct induces a slow inward current that reaches a steady-state amplitude that is ~15% of the peak amplitude resulting from a transient step to low pH (**Figure 3.1a**). Further activation by application of pH 5.5 solution produced a fast inward current that is ~2-fold larger than the peak amplitude generated at pH 7.4 in the presence of toxin. Similar to MitTx-induced currents of mouse ASICs, the currents associated with the Δ13-MitTx complex are blocked by micromolar concentrations of amiloride.

To understand how MitTx stabilizes an open channel, amiloride-sensitive conformation of Δ13, MitTx and Δ13 were crystallized as a complex at pH 5.5. Crystals of the complex belong to the space group *R*3, harbor a single Δ13 subunit and toxin α/β heterodimer complex in the asymmetric unit, and diffract x-rays to 2.7 Å resolution. The structure was solved by molecular replacement and subjected to iterative cycles of manual building and refinement, ultimately yielding a structure with good crystallographic statistics (**Table 3.1**).

With one toxin heterodimer radiating from each Δ13 subunit, the toxin-channel complex has a triskelion-like shape when viewed down the 3-fold axis of symmetry (**Figures 3.1b and 3.1c**). Toxin subunits protrude from the 'edges' of the channel trimer with each toxin heterodimer interacting almost exclusively with a single subunit and forming extensive contacts from the ion channel 'wrist', proximal to the extracellular boundary of the

membrane bilayer, to the knuckle and thumb domains, as far as 60 Å from the membrane surface. Consistent with the high affinity of the toxin for the channel [91], one toxin heterodimer buries 1350 $Å^2$ of solvent accessible surface area in the channel-toxin complex, of which 800 $Å^2$ and 550 $Å^2$ are derived from the α and β subunits respectively.

MitTx heterodimer

In the heterodimeric α/β toxin complex, each subunit buries ~500 Å of solvent accessible surface area at the subunit interface (**Figure 3.1c**). Residues near the N- and C-termini of the α subunit play particularly important roles in the nanomolar-affinity heterodimeric complex [91], forming helix-capping contacts to the C-terminus of the α1 helix of the β subunit, as well as mediating interactions with the β-wing domain (**Figures 3.2 and 3.3**). The first five residues of the α subunit form a 'clamp' around the aromatic side chain of Tyr 72 of the β subunit's β-wing with the N-terminal pyroglutamate of the α subunit forming two hydrogen bonds with the backbone amino group of Ala 74 and the carbonyl oxygen of Tyr 72 of the β subunit. Arg 3 of α augments subunit interactions with its guanidinium group forming hydrogen bonds with carbonyl oxygens of Lys 10 and Cys 11 at the C-terminus of the α1 helix of the β subunit and also with carbonyl oxygens of Cys 58 and His 59, and the hydroxyl group of Tyr 8 of the α subunit (**Figure 3.3c**). Cation-π interactions between the guanidinium group of α Arg 3 and Tyr 8 and Phe 26 provide additional contacts within the α-β interface. A Na^+ ion fortifies intersubunit interactions and is coordinated by the backbone carbonyl oxygens of Ser 29 and Phe 68 of the α and β subunits, respectively and by a cation-π interaction with Phe 68 of the β subunit (**Figure 3.3d**).

The 'catalytic loop' of α, reminiscent of the loop in the Kunitz-like protease inhibitors that occludes the catalytic site [173], harbors a crucial lysine residue that insinuates itself into the Δ13 wrist. Akin to the α subunit, the β subunit adopts a phospholipase A2 (PLA_2) fold, stapled together with seven disulfide bonds arranged like those found in group 1A of secreted PLA_2 enzymes [174] (**Figure 3.3b**). Unlike sPLA2 enzymes, however, β lacks the canonical His/Asp catalytic dyad that is crucial to the hydrolysis of phospholipids, as well as the three glycines in the glycine-rich loop that binds Ca^{2+} in $sPLA_2$ enzymes, consistent with its apparent lack of lipase catalytic activity and likely absence of a Ca^{2+} binding site. Nevertheless, we note that the same region of β that is proposed to interact with the membrane in PLA_2 enzymes interacts with the thumb domain of Δ13. Thus both α and β have exploited established scaffolds to evolve new protein domains for modulation of ion channel function.

Δ13-MitTx complex

The heterodimeric MitTx acts like 'churchkey' bottle opener on Δ13, forming extensive interactions with the wrist, palm and thumb domains, supporting the notion that these domains play major roles in gating the ion channel (**Figure 3.4a**). Whereas the β subunit resides at the 'top' of the thumb domain, near the acidic pocket, with its binding footprint overlapping with that of psalmotoxin (**Figure 3.5a**), the α subunit hugs the base of the thumb domain, making contacts with the extracellular end of TM1 and residues of the palm domain on an adjacent subunit.

The β subunit exploits its amino terminus and β-wing 'loop' to snugly adhere to the α4 and α5 helices of the thumb domain. Asn 1 and Asn 3, together with Gln 2 of β-MitTx, form a web of hydrogen bonds with the side chains of Asn 321 and Asn 323 on the α4 helix

of the thumb (**Figure 3.4b**). Positively charged residues, Arg 6 and Lys 60 of the β subunit, augment toxin-channel interactions by forming ionic interactions with Glu 320 on the α4 helix and with Glu 339 and Glu 343 on the α5 helix, respectively (**Figure 3.4c**). Additional reinforcement is provided by the side chain of Phe 65 packing directly alongside the α5 helix, bringing the polypeptide of the β subunit sufficiently close to the thumb so as to allow a direct hydrogen bond between the main chain nitrogen of Phe 65 and the carbonyl oxygen of Glu 343 (**Figure 3.5b**). Interestingly, Asn 3 and Lys 60 of β are aromatic residues at the equivalent positions in sPLA2 enzymes and are involved in interactions with the membrane. Thus the β subunit of MitTx exploits an equivalent surface for binding to ASICs as sPLA2 enzymes use to interact with membranes, with the β subunit harboring positively charged residues for favorable interaction with a negatively-charged ASIC.

The α MitTx subunit is the 'flange' of the toxin 'churchkey bottle opener' positioned on the underside of the thumb domain and insinuating a Phe 14 'hook' into a Δ13 subunit interface and a Lys 16 'barb' into the wrist, at the juncture of the extracellular ends of the transmembrane domains and the base of the palm and thumb domains. Lys 16 of α, situated on the 'reactive loop' of protease inhibitors, juts into the wrist of Δ13 with the ammonium group coordinated by 4 main chain carbonyl oxygens from Δ13 and one from the α subunit (**Figure 3.4d**). Remarkably, the ammonium group occupies the same position as Cs^+ ions occupy in the open-state, Δ13 – PcTx1 complexes [170], thus emphasizing the importance of a monovalent cation binding to this site in open channel states. Phe 14 of α, wedged into a Δ13 subunit interface, is the second crucial interaction. Not only does the aromatic ring appear to splay subunits apart, but it also forms extensive interactions with residues Ala 82 through Thr 84 of the β1-β2 linker, a region of ASICs central to channel gating and, on the

adjacent subunit, with residues Val 361 to Met 364 (**Figure 3.4e**). Phe 13, 20 and 37 supplement the interactions between α and the thumb of Δ13, and together with Arg 28 and 30, which make interactions with residues on α4 and α5 helices, demonstrating the critical role that the α subunit plays in complex formation with Δ13. Finally, the multiple contacts that MitTx makes with Δ13, many of which are to residues that are not conserved between ASIC subtypes, provides a molecular explanation for MitTx's subtype selectivity and illuminates strategies by which one could engineer ASICs with altered toxin sensitivity (**Figure 3.6**).

MitTx expands the extracellular vestibule

Superposition of the Cα positions of the cASIC1a portion of the Δ13-MitTx complex and the desensitized state structure (PDB code 3HGC)[26] reveals prominent conformational changes in the lower palm domain and in subunit interfaces between the thumb of one subunit and the palm of the neighboring subunit. By contrast, there is a conformationally conserved scaffold consisting of the 'upper' β-strands of the palm domain and the knuckle domains, akin to the scaffold observed in the Δ13-PcTx1 complexes (**Figure 3.7a**). Within each subunit, the thumb-finger interface that flanks the acidic pocket and that includes multiple acidic residues implicated in proton sensing, adopts a conformation like that seen in the low pH desensitized state[26] and PcTx1-bound structures [170].

Analysis of the desensitized state and MitTx-Δ13 trimers reveal that conformational changes in the extracellular domain are primarily localized to the lower palm and thumb domains, with rmsd values of 2.0 Å and 1.5 Å, respectively, where the largest difference in Cα position of ~5.1 Å occurs near the extracellular/transmembrane interface (**Figures 3.7a**

and 3.8a). Similarly, superpositions of the PcTx1-Δ13 (PDB codes 4FZ0 and 4FZ1) and MitTx-Δ13 extracellular domains have the greatest conformational differences at the extracellular/transmembrane interface. Indeed, the MitTx-Δ13 complex is distinct from the PcTx1 complexes, with Cα atoms of the wrist region in the low and high pH PcTx1 complexes occupying positions as far as 4.5 Å and 3.0 Å away from their positions in the MitTx complex, respectively (**Figure 3.8b, c**). Despite these differences, the MitTx and PcTx1 complexes show that the open conformations of ASIC involve global shifts at palm-thumb subunit interfaces, expansion of the extracellular vestibule regions, and local conformational changes in the β1- β 2 and β 11- β 12 linkers between the upper and lower palm domains [170].

The α subunit of MitTx plays a fundamental role in locking Δ13 in an open channel, ion conductive state. Extensive interactions of α with the thumb and palm domains not only expands the thumb – palm domain intersubunit interface by ~1 Å at Asn 357 and Thr 210 compared to the desensitized state, but closer to the membrane, near the 'wrist', the separation is greater, as defined by an increase in the separation of Cα atoms of Glu 363 and Val 81 by 3 Å (**Figure 3.8d**). These conformational changes are reminiscent of those observed in the PcTx1 complexes of cASIC1a, thus underscoring the crucial role of intersubunit thumb - palm domain interactions in channel gating [170].

Accompanying the increase in intersubunit separation is a dramatic expansion of the extracellular vestibule, relative to that observed in the desensitized state, due to an 'outward' flexing of the β-strands of the lower palm domain. Using Val 75 as a reference, the intersubunit separation increases from 7 Å in the desensitized state to 14 Å in the MitTx-Δ13 complex (**Figure 3.7b**). The flexing of the palm β-strands also decreases the length of

the constriction, along the 3-fold axis, that occludes a direct, solvent accessible pathway between the central and extracellular vestibules. In the desensitized state, this constriction spans ~12 Å, from Leu 78 to Val 75 whereas in the MitTx bound conformation, the occlusion is only ~ 4 Å and formed by the side chain atoms of 3-fold symmetric Leu 78 residues (**Figure 3.7c, d**). Taken together, these conformational changes are in accord with multiple mutagenesis, chemical modification and ligand binding studies that have previously implicated the central vestibule in the modulation of gating in ASICs [32, 37, 139].

By contrast with the gradual flexing of the lower palm domain β-strands, the binding of MitTx to the Δ13 ion channel promotes discrete 'switching' in the conformation of the β1- β2 and β11- β12 linkers, short regions of polypeptide implicated in ion channel gating [34-36] and residing near the 'pivot points' of the lower palm β -strands. While rearrangements in these linkers were previously noted in complexes of cASIC1a with PcTx1 [170], the superior diffraction of Δ13-MitTx crystals allows us to define these conformational changes with greater accuracy. Relative to the desensitized state, residues 414 and 415 of the β11- β12 linker in the MitTx complex undergo a dramatic conformational change where two molecularly distinct side chains, a hydrophobic Leu and a polar Asn, swap positions (**Figure 3.7c, d**). In the desensitized state, the Leu and Asn side chains are oriented toward the central vestibule and the β1- β2 linker, respectively, yet in the MitTx complex their orientations switch, with the Leu side chain packing against the β1- β2 loop and the Asn primary amide group facing the vestibule and making hydrogen bonds with Tyr 283 of an adjacent subunit, a water molecule and the main chain amide of Asn 415 (**Figure 3.8e**). Together, these changes dilate the lower palm domain, expanding the central and extracellular vestibules.

MitTx stabilizes a symmetric and open pore

Accompanying the expansion of the extracellular vestibules is the opening of the ion channel by way of an iris-like motion of the transmembrane α-helices (**Figure 3.9a**), recalling the apo-to-open conformational changes of the zfP2X4 receptor pore [154]. Comparison of the transmembrane domains between the desensitized and the MitTx-bound conformations demonstrates differential rotational movements of TM1 and TM2 by ~17° and ~4°, respectively, around the 3-fold axis of symmetry (**Figure 3.10**). The larger rotational shift of TM1 modifies contacts with TM2 within each subunit and disrupts interactions with TM2 of an adjacent subunit, while the movements of TM2, albeit smaller in magnitude, disrupt extensive contacts with TM2 of an adjacent subunit. Together, these movements reveal a 3-fold symmetric, hour glass-shaped pore, continuous across the membrane, with a constriction that is ~3.6 Å in diameter and located halfway across the bilayer, near Gly 439 (**Figure 3.9b, c**).

The different rotations of the transmembrane helices around the 3-fold axis cause TM1 and TM2 to undergo a scissor-like movement that modifies intrasubunit interactions on both the extracellular and intracellular portions of the TM domains while preserving interactions in the middle, at the 'pivot.' The immobile pivot involves a clasp of Phe 441 on TM2 by the side chains of Leu 57 and Leu 58 on TM1 (**Figure 3.11a**). By contrast, within the extracellular portion of the TM domains, contacts between Val 61 and Cys 62 (TM1) and Gln 437 (TM2) in the desensitized state are disrupted in the MitTx-bound conformation such that Gln 437 now only forms van der waals contacts with Val 61 (**Figure 3.11b**). On the cytoplasmic side of the pivot, whereas Trp 47 (TM1) is near Thr 448 and Val 449 (TM2) in the desensitized state, in the Δ13-MitTx state, Trp 47 is positioned on the other side of Val 449 completely disrupting contact with Thr 448 (**Figure 3.11c**).

Conformational changes in the TM domains completely disrupt intersubunit contacts between TM1 and TM2 of adjacent subunits while preserving only a few interactions between TM2 subunits, reminiscent of the dearth of contacts found between the TM2 domains in the ATP-bound open channel state of the P2X4 receptor [154]. In fact, contacts between Asn 64/Val 61 (TM1) and Ala 428/Leu 431 (TM2) of adjacent subunits in the desensitized state are entirely ruptured in the Δ13-MitTx complex. In comparison to the desensitized state, where there are extensive intersubunit contacts between TM2 domains, in the Δ13-MitTx structure the sole interactions involve contacts between Leu 440/Leu 447 with Gly 435/ Met 438 on an adjacent subunit (**Figure 3.11d**). The sparse intersubunit contacts result in a dramatic, V-shaped gap between the subunits that is similar to large spaces observed in the ATP-bound P2X4 structure[154]. These fissures are within the membrane-spanning region of the ion channel and thus we suggest that lipids not only participate in extensive interactions with the transmembrane helices, but they also define portions of the ion channel pore.

Inspection of the Δ13-MitTx TM domains reveals a symmetrical pore that converges to a diameter of 3.6 Å near Gly 439. On the extracellular side of the constriction the pore harbors a negative electrostatic potential and is lined by the carboxyl groups of Asp 433, the hydroxyl moieties of Tyr 68 and Tyr 425, and the main chain carbonyl oxygens of Gly 432, Gly 436 and Gly 439. By contrast, this solvent accessible, funnel-shaped pathway does not exist in the desensitized state, where there is an occlusion in the pore from residues Asp 433 to Gly 436 (**Figure 3.9b, c**). The Gly 443 – Ala 444 – Ser 445 residues of the putative "selectivity filter" motif of ASICs and ENaCs [175] [176] [177] [178] are positioned on the cytoplasmic side of the pore constriction, with the carbonyl oxygen of Gly 443 facing the

pore and the hydroxyl of Ser 445 directed toward TM1. Below Gly 443 the pore has a more hydrophobic character, lined by the side chains of Ile 446 and Leu 450. The pore of this toxin complex is primarily lined by residues contributed by TM2, results that are in general agreement with recent accessibility studies [48, 178] but in contrast with earlier studies on FaNaCh [156], and with structures of Δ13 in complex with psalmotoxin [170]. These observations underscore the notion that the transmembrane helices of ASICs exhibit structural plasticity that is dependent, at least in part, on ligands bound to the extracellular domain.

Ion binding sites

To map cation binding sites we soaked crystals in solutions containing Cs^+ and measured anomalous diffraction data. Analysis of the resulting anomalous difference maps revealed many Cs^+ sites, some of which overlap those observed in the desensitized state (**Figure 3.12**) [26]. We observe previously unseen Cs^+ sites in both the extracellular and transmembrane domains (**Figures 3.13 and 3.14**). In the extracellular domain, within the central vestibule, we find two Cs^+ sites positioned on the threefold axis and coordinated by main chain carbonyl oxygens, near Leu 375 (13 σ) and near Lys 373 (7 σ), recalling the Gd^{3+} binding site found within the central vestibule of the apo state of the P2X4 receptor [27] (**Figure 3.13b**). While these results are consistent with the conclusion that the central vestibule provides a favorable site for cation binding, the role of these sites in channel conduction and gating awaits additional experiments.

Strikingly, prominent Cs^+ sites (5 σ) were observed near the triangle-shaped fenestrations in the extracellular vestibule. With one site per subunit, each site is ~5 Å from the aromatic ring of Tyr 68 and thus the ions are bound by cation-π interactions (**Figure**

3.13c) [179]. Both $2F_o$-F_c maps of Cs^+-soaked and native Na^+ crystals show density in this region and we suggest that cations bind to this site as they enter or exit the transmembrane pore (**Figure 3.14a-d**). This cation binding site may also play a role in channel gating, however, as in the desensitized state, the guanidinium group of Arg 65 forms a cation-π interaction with Tyr 68 (**Figure 3.15a**) [26].

We observed a single anomalous difference peak in the Cs^+- soaked crystals within the pore region (6.5 σ), located on the 3-fold axis and situated on the same plane as residues within the 'GAS' selectivity filter sequence (**Figure 3.13d**). The carbonyl oxygen of Gly 439 is the closest atom, approximately 5 Å from the Cs^+ peak, while Gly 443 of the GAS selectivity filter is about 6 Å away. Interestingly, we did not observe an anomalous difference peak at the pore constriction, thus suggesting that the constriction does not form a favorable binding site for Cs^+. Considering the relatively large size of the pore, we suggest that cations are hydrated as they permeate through the channel [158], with the constriction at Gly 439 defining a barrier, as opposed to binding site, for permeant ions. In the Cs^+-bound structure TM2 shows a small yet substantial 'flexing' that begins at Phe 441 and that includes the GAS selectivity filter sequence, extending to the C-terminus and increasing the diameter of the pore (**Figure 3.16a**).

To probe the selectivity of the Δ13-MitTx pore we carried out whole cell patch clamp experiments, showing that replacement of external Na^+ by Cs^+ at -60 mV diminishes inward current to baseline, suggesting that Cs^+ is a weakly permeant ion (**Figure 3.16b**). Voltage ramp experiments reinforce this conclusion yet also demonstrate that the pore is permeable to the smaller K^+ ion (**Figure 3.13e**). Indeed, with K^+ and Cs^+ in the intracellular and extracellular solutions, respectively, the complex primarily exhibits an outward current.

By comparison, with Na^+ on the extracellular side, the current reverses at ~20 mV, consistent with a pore that is modestly selective for Na^+ over K^+ by approximately 2:1, respectively. In accord with the observation that Cs^+ is a weakly permeant ion and that the crystal structure in the presence of Cs^+ shows a 'flexing' of the TM2 helices, we conclude that the basis for ion selectivity in the Δ13-MitTx complex largely involves a barrier mechanism where hydrated cations are selected on the basis of size, with Cs^+ simply being too large for efficient conduction.

Δ13-MitTx complex versus Δ13-PcTx1 complexes

The complexes of the Δ13 ASIC1a ion channel with the PcTx1 and MitTx toxins provide unprecedented insights into the mechanism of toxin action and the principles of ion channel gating and selectivity in ASICs. Undoubtedly the most striking difference between the two toxins is simply that MitTx is much larger and, as a consequence of its size, makes substantially more contacts with the ion channel, spanning an area from the acidic pocket to the wrist. Thus even though PcTx1 and the β subunit of MitTx share an overlapping binding site (**Figure 3.4**), the larger size of β and the presence the MitTx α subunit allow MitTx to make extensive contacts with the thumb and palm domains. Because PcTx1 makes few contacts, by comparison to MitTx, near the 'top' of the thumb domain, the palm domain is able to undergo pH-dependent conformational changes, and thus the Δ13-PcTx1 complexes exhibit dramatic, pH-dependent structure and functional changes. By contrast, MitTx surrounds the palm domain, participating in crucial contacts at subunit interfaces and at the wrist by way of interactions with α subunit residues Phe 14 and Lys 16, respectively, thus stabilizing palm domain, the central vestibule and the extracellular end of TM1 in a single

conformation that largely precludes conformational changes upon pH changes from 7.4 to 5.5.

Summary and conclusion

Mechanism of gating and ion permeation in ASICs

Comparison of Δ13-MitTx with the desensitized state and Δ13-PcTx1 structures reveal that the knuckle and upper palm domains define a conformationally conserved scaffold around which the malleable thumb, lower palm, and wrist domains rearrange to gate the channel. MitTx acts like a 'churchkey' bottle opener with the β-subunit locking onto the upper thumb domain and the α-subunit adhering to the lower thumb domain and 'prying' open the lower palm β-strands, expanding the extracellular vestibule and promoting an 'iris'-like movement of the transmembrane helices, opening the ion channel pore (**Figure 3.17**). The β1- β2 and β11- β12 linkers, 'pivot points' between the scaffold and lower palm domain, undergo a binary 'flip' in conformation while the lower palm 'flexes' between the closed and open channel states. MitTx stabilizes an open conformation not only by extensive interactions with the lower thumb domain, but also by deploying the ammonium group of a key lysine residue at the flexible wrist juncture – a site of cation binding - cementing conformational coupling between the thumb and TM1 and underscoring the central role of TM1 in ion channel gating. On the extracellular side of the membrane, ions access the pore by large fenestrations fitted with cation-π ion binding sites. The conductive pathway is lined primarily by TM2, narrowing to a carbonyl oxygen lined constriction of ~3.6 Å approximately halfway across the bilayer, thus suggesting that cations permeate through the channel as hydrated complexes.

In summary, the apo and agonist-bound complexes of the P2X4 receptor, together with the desensitized, PcTx1- and MitTx1-bound states of cASIC1a, illuminate common principles of architecture and mechanism in ATP-gated P2X receptors and acid sensing ion channels, illustrating how structural scaffolds, malleable central vestibules and six transmembrane helices undergo conformational changes in response to ligand or toxin binding, opening and closing an ion channel pore.

Table

Table 3.1. Data collection and refinement statistics (Δ13-MitTx)

Data collection		
Dataset	Δ13-MitTx	Δ13-MitTx (Cs^+)
Beamline	ALS 5.0.2	ALS 5.0.2
Space group	*R3*	*R3*
Cell dimensions		
a, *b*, *c* (Å)	151.1, 151.1, 124.1	151.5, 151.5, 123.8
α, β, γ (°)	90.0, 90.0, 120.0	90.0, 90.0, 120.0
Wavelength (Å)	1.000	1.378
Resolution (Å)*	50.0-2.7 (2.74-2.70)	50.0-2.65 (2.70-2.65)
R_{sym} or R_{merge}*	0.088 (0.676)	0.093 (0.654)
$I/\sigma I$*	20.1 (2.1)	15.6 (1.5)
Completeness (%)*	100.0 (100.0)	99.9 (100.0)
Redundancy*	5.8 (5.8)	2.9 (2.8)
Refinement		
Resolution (Å)	45.9-2.7	46.0-2.65
No. reflections	26957	58864
$R_{work/}$ R_{free}	0.194/0.237	0.235/0.271
No. atoms		
Total	4725	4757
Δ13	3203	3207
α-MitTx	493	493
β-MitTx	912	916
Cl^-	1	1
Na^+	3	0
Cs^+	0	15
OAc^-	0	4
Water	113	121
Mean B value	53.9	59.9
R.m.s deviations		
Bond lengths (Å)	0.006	0.007
Bond angles (°)	1.085	1.370
Ramachandran		
Most favored (%)	97.4	97.7
Allowed (%)	2.6	2.3
Disallowed (%)	0	0

*Highest resolution shells are shown in parentheses.

Figures and legends

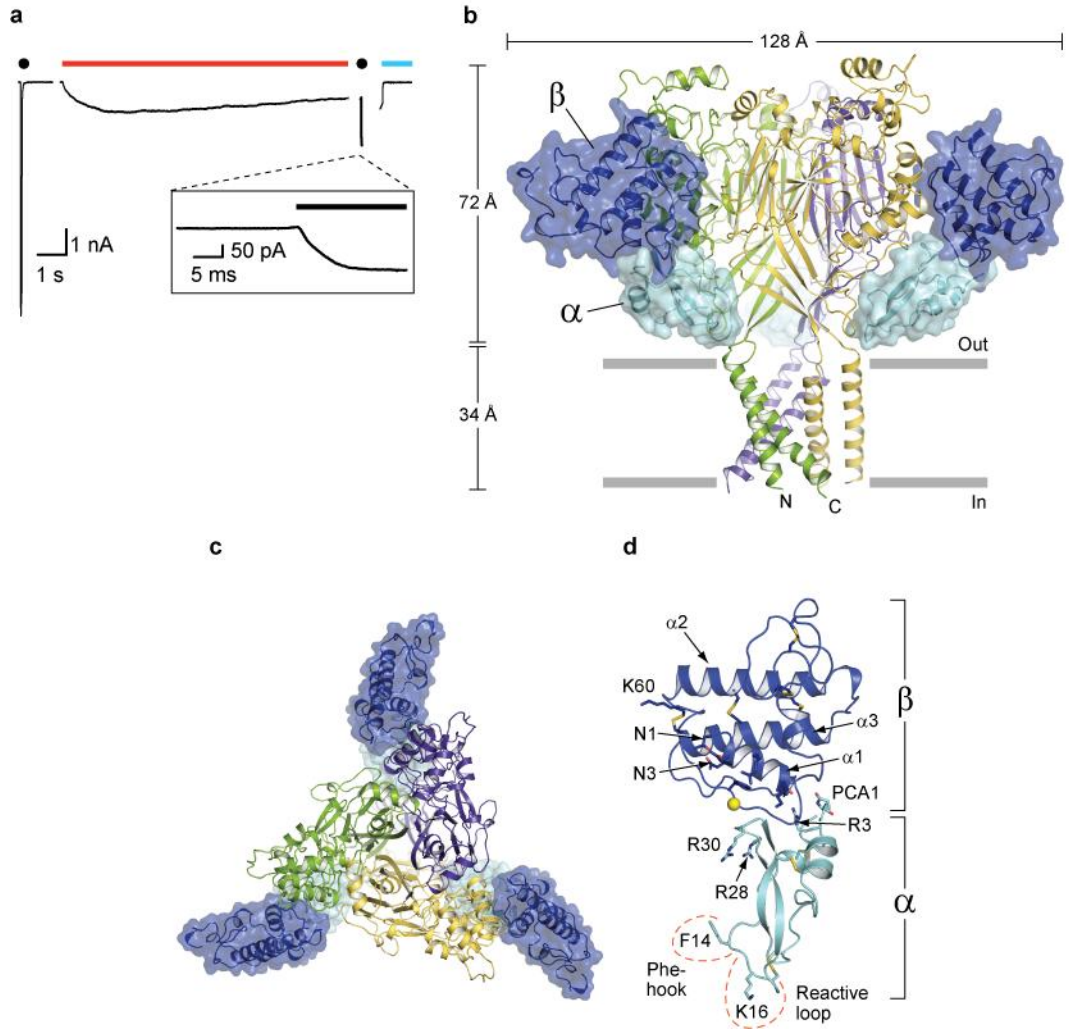

Figure 3.1. Triskelion shaped complex of Δ13 cASIC1a and MitTx.

Figure 3.1. Triskelion shaped complex of Δ13 cASIC1a and MitTx. **a**, Representative current traces of Δ13 upon application of low pH (black dot), 300 nM α/β (red line), and 100 μM amiloride (blue line). **b**, View of complex parallel to the membrane with Δ13 subunits in different colors and in cartoon representation and the α and β MitTx subunits shown in cartoon representation underneath a partially transparent surface. **c**, View of the complex along the 3-fold axis of symmetry and viewed from the extracellular side of the membrane. **d**, Structure of MitTx derived from the complex with Δ13, showing key regions and residues.

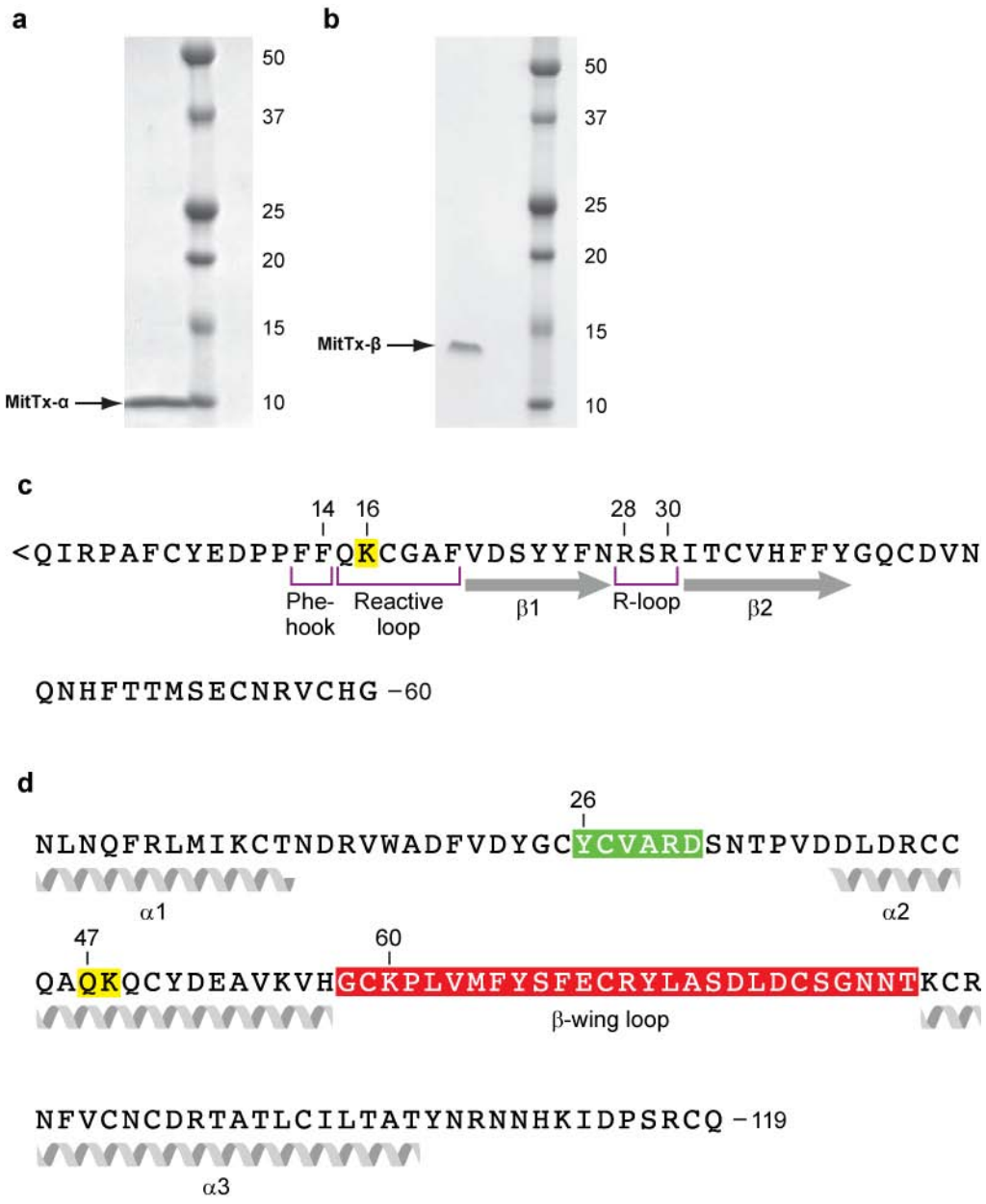

Figure 3.2. Purified recombinant MitTx-α and MitTx-β and structural features of the toxin subunits.

Figure 3.2. Purified recombinant MitTx-α and MitTx-β and structural features of the toxin subunits. Purified MitTx-α (**a**) and MitTx-β (**b**) migrate as single bands on an SDS-PAGE gel. The gel was run under reducing conditions. **c**, Single letter amino acid sequence of the α subunit, where the first residue, shown as '<Q', is a pyroglutamate acid, also known as 5-oxopyrrolidine-2-carboxylic acid (PCA). Lys 16 on the reactive loop, which wedges into the wrist domain, is highlighted in yellow. **d**, Amino acid sequence of the β subunit, also showing key regions and residues. Equivalent positions of the sPLA2 Ca2+ binding site is highlighted in green, equivalent positions of the catalytic dyad in yellow, and the β-wing loop in red.

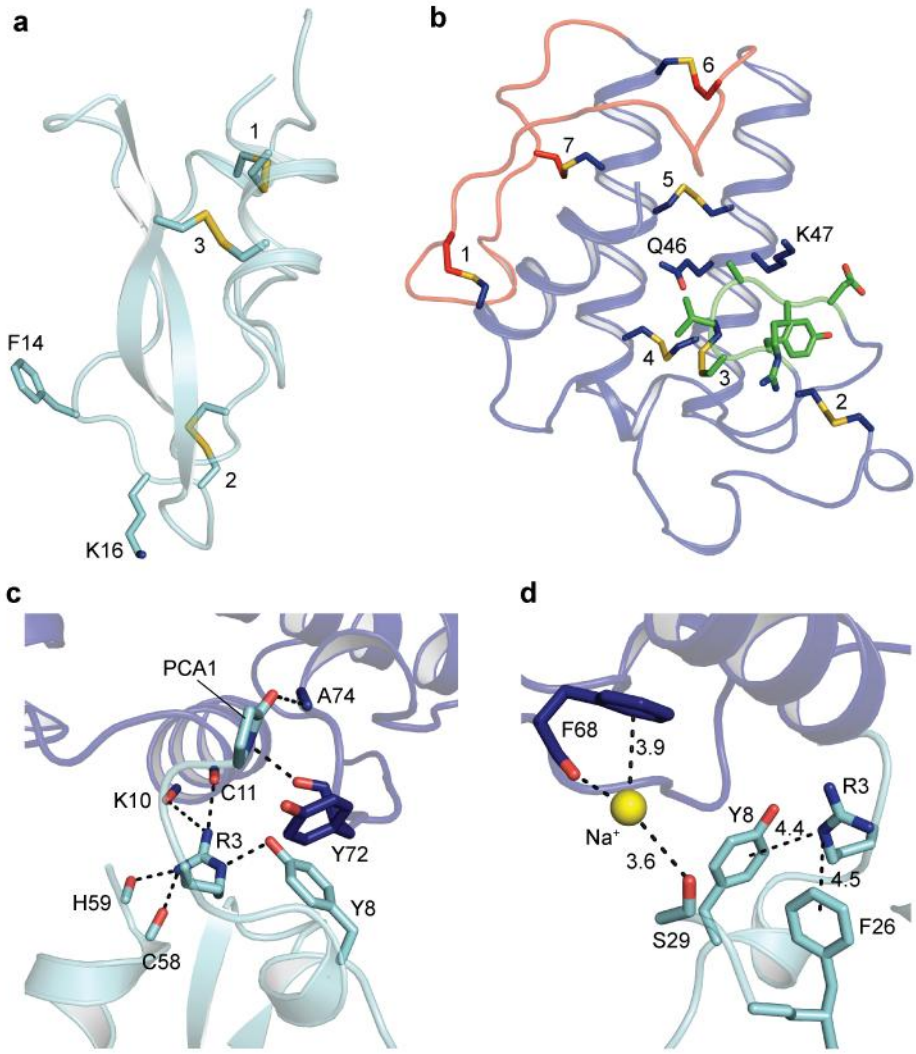

Figure 3.3. Structures of the α and β subunits derived from the Δ13-MitTx complex and illustration of key residues and interactions.

Figure 3.3. Structures of the α and β subunits derived from the Δ13-MitTx complex and illustration of key residues and interactions. **a**, The α subunit, depicting the key Phe 14 and Lys 16 residues, along with the 3 disulfide bonds. **b**, View of the β subunit, showing the 7 disulfide bridges. Shown in green and dark blue are regions that are equivalent to regions in catalytically active sPLA2 enzymes that define a calcium ion binding site and the catalytic site, respectively. The β subunit, however, neither has the conserved amino acids in these regions nor the accompanying calcium binding and catalytic activity. **c**, Interface between the α and β subunits, showing the multitude of hydrogen bonds and also the amino terminal PCA 1 residue. **d**, A sodium ion mediates contacts between the α and β subunits, participating in a cation-π interaction with Phe 68 of the β subunit. Dashed lines indicate bond distances of 2.6-3.5 Å, unless specified.

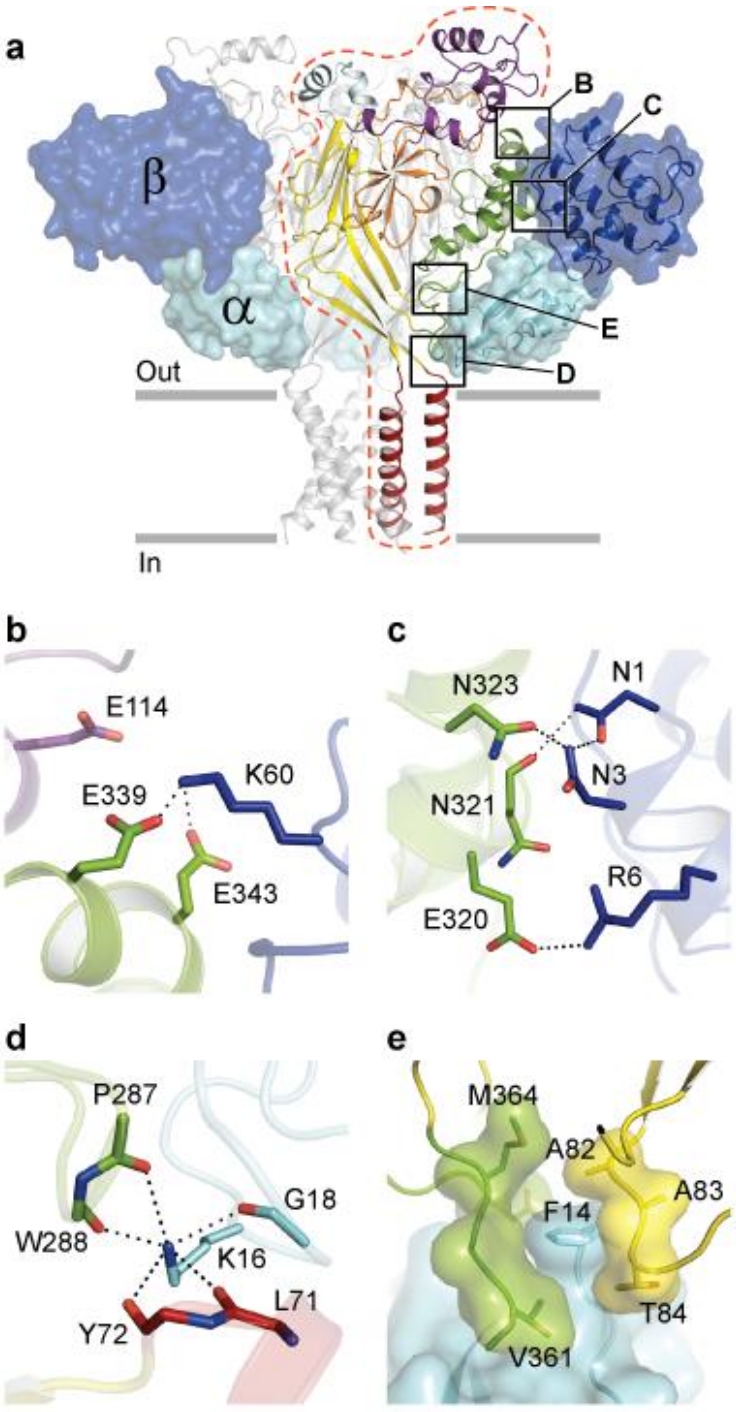

Figure 3.4. MitTx makes extensive interactions with the thumb and wrist domains of Δ13.

Figure 3.4. MitTx makes extensive interactions with the thumb and wrist domains of Δ13. **a**, Overall view of the Δ13-MitTx complex in which one subunit of Δ13 is color-coded by domain: transmembrane, red; palm, yellow; β-ball, orange; knuckle, light blue; finger, purple; and thumb, green. The α and β subunits of MitTx are shown as in Fig. 3.1. Key regions of interactions are boxed. **b**, Lys 60 of the MitTx β subunit forms salt bridge with Glu residues 339 and 343 of the thumb domain. **c**, Asn residues 1 and 3, and Arg 6, participate in a web of hydrogen bonds and a salt bridge to amino acids on the α4 helix of the thumb. **d**, Lys 16 of the MitTx α subunit inserts into a crevice within the Δ13 wrist with the ammonium group making multiple hydrogen bonds to carbonyl oxygen atom at the base of the thumb domain and at the extracellular end of TM1. **e**, The 'Phe hook' of Phe 14 on the α subunit is wedged between the palm and thumb domains of adjacent subunits.

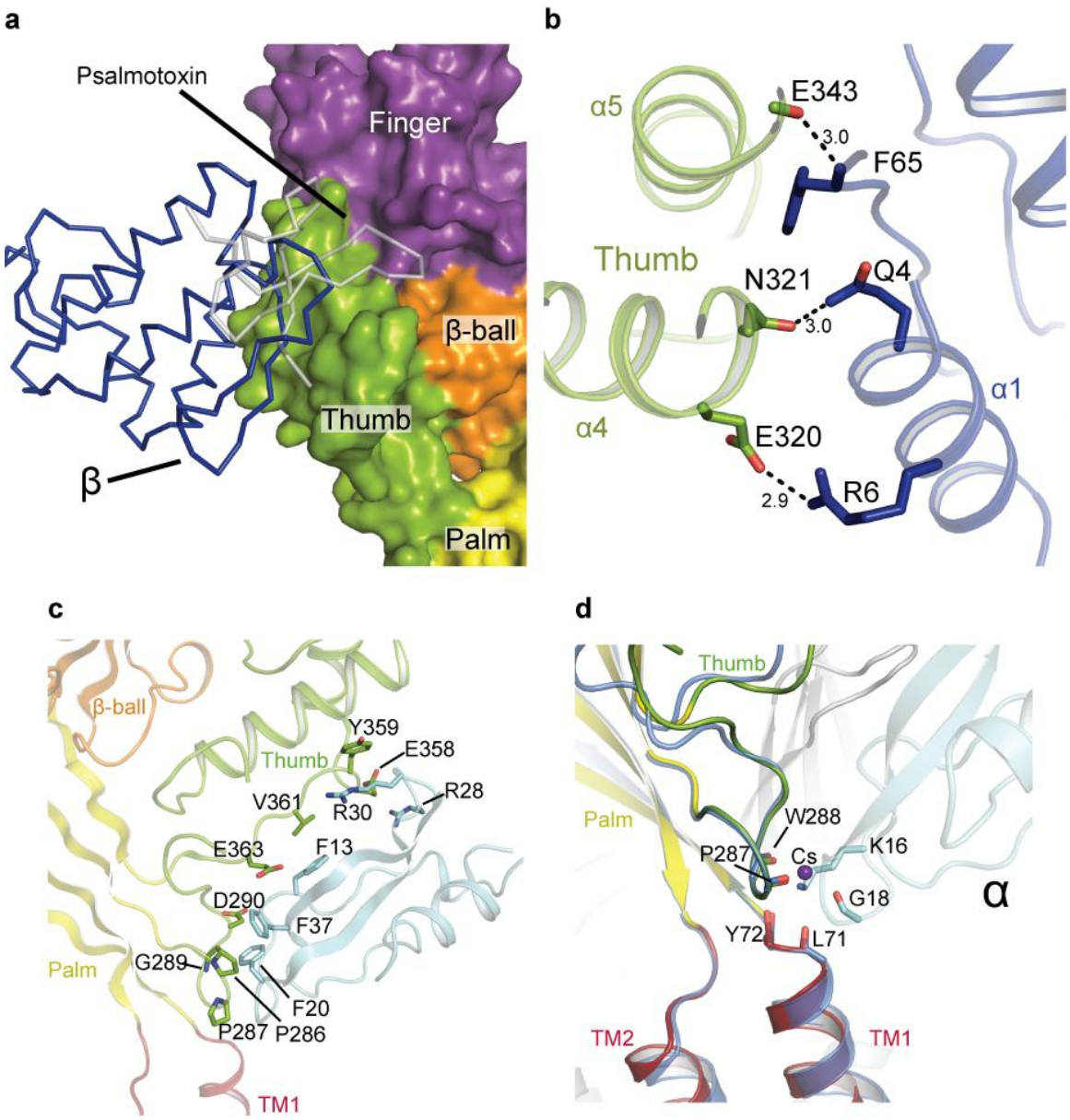

Figure 3.5. MitTx binding site and overlap with psalmotoxin (PcTx1) binding site.

Figure 3.5. MitTx binding site and overlap with psalmotoxin (PcTx1) binding site. **a**, The binding site for PcTx1 (gray α-carbon trace) overlaps with that of the β subunit of MitTx (blue α-carbon trace). Here, the domains of the Δ13 channel are in surface representation and color-coded and labeled according to figure 2 of the main text. **b**, The β subunit of MitTx participates in close contacts with the α5 helix of the Δ13 thumb domain by way of a direct hydrogen bond between the main chain carbonyl oxygen of Glu 343 (Δ13 channel) and the main chain nitrogen of Phe 65 (β subunit), including additional hydrogen bonds between Asn 321 (Δ13) and Gln 4 (β) and a salt bridge between Glu 320 (Δ13) and Arg 6 (β). **c**, Illustration of residues that participate in extensive interactions between the α subunit of MitTx (cyan) and residues on the thumb domain (green) with portions of the Δ13 palm domain (light yellow) and β-ball (light orange) also shown. **d**, View of the 'wrist' region following superposition of Cα positions of residues 285-290 and 70-74 of Δ13-MitTx and low pH Δ13-PcTx1 soaked in Cs+. Note that coordination of the ammonium group of Lys 16 is similar to the carbonyl oxygen coordination with Cs+ in the Δ13-PcTx1 structure.

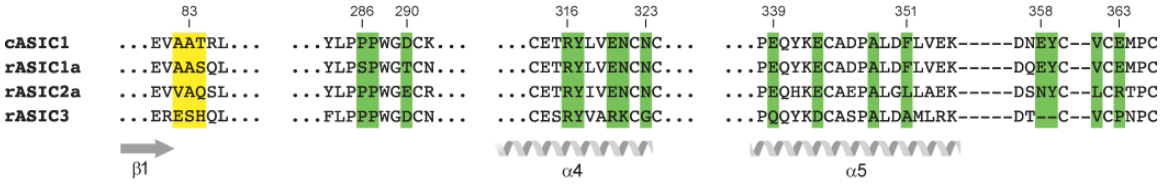

Figure 3.6. Sequence alignment of ASIC subtypes that exhibit different sensitivities to MitTx. Amino acid sequence alignment of ASICs from chicken (cASIC1a) and rat (rASIC1a, 2a, 3) emphasizing residues that in the Δ13 (cASIC1a) complex with MitTx participate in channel – toxin interactions. The highlighted residues define regions of interaction and are color-coded by domain, where yellow is the palm domain and green is the thumb domain. Note that many of the residues in the Δ13 channel that interact with MitTx are not conserved amongst the other ASIC subtypes, thus providing a molecular explanation for the ASIC subtype selectivity of MitTx.

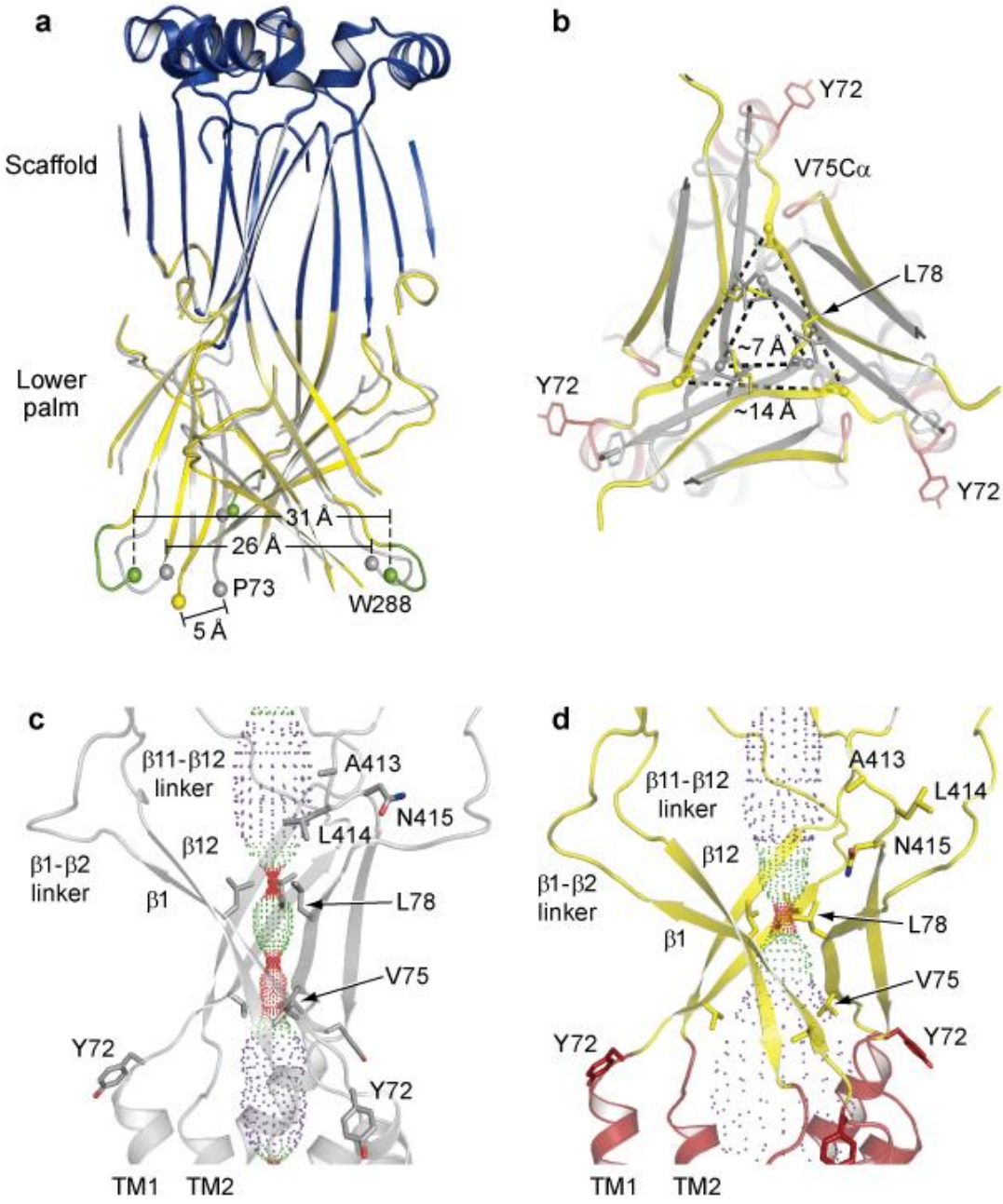

Figure 3.7. MitTx stabilizes the lower palm domain in an expanded conformation.

Figure 3.7. MitTx stabilizes the lower palm domain in an expanded conformation. **a**, Superposition of the upper palm and knuckle domains of the densensitized and MitTx-bound states of cASIC1a. The upper palm and knuckle domains of the MitTx bound state are blue and yellow, respectively, and the densensitized state structure is gray. **b**, View along the 3-fold axis, looking from the extracellular side and toward the membrane, of the superposition from panel (a), showing that the constriction of the lower palm domain undergoes an expansion of ~7 Å at Val 75. **c**, View of the constriction between the central and extracellular vestibules in the desensitized MitTx bound states (**d)** showing the expansion of the low palm and wrist domains and rearrangements of the β1- β 2 and β 11- β 12 linkers.

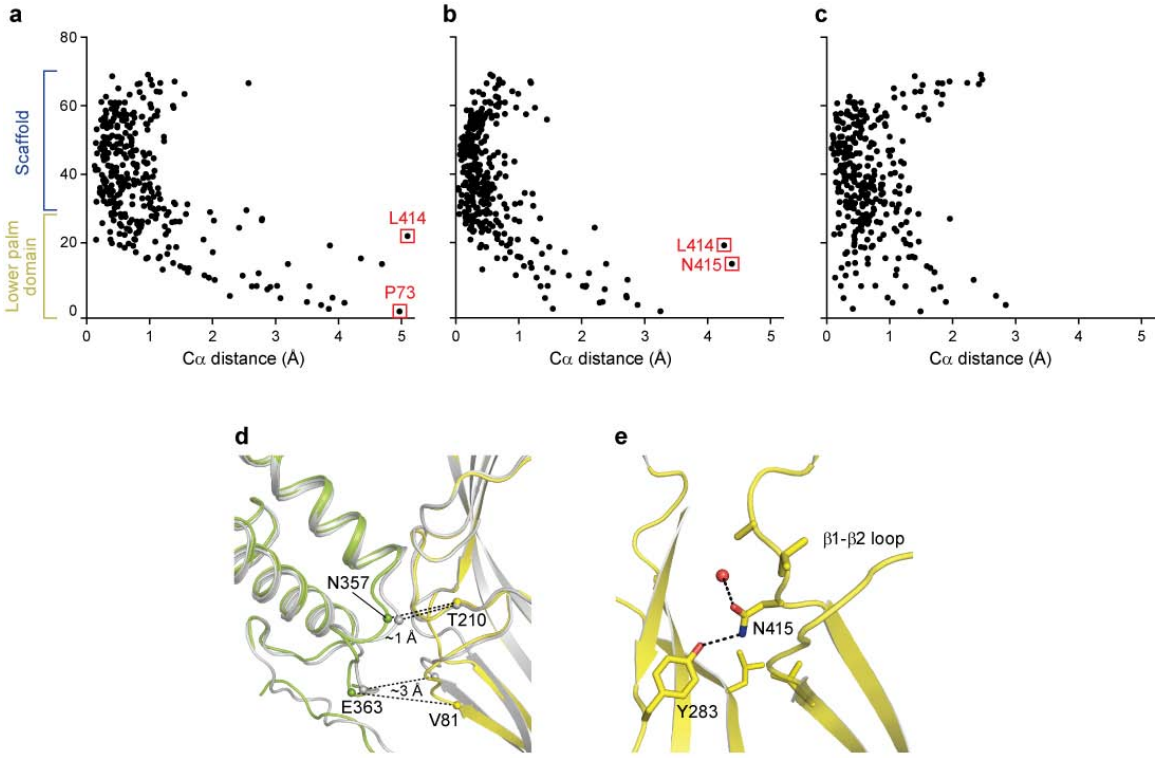

Figure 3.8. Large conformational changes occur in the lower palm domain.

Figure 3.8. Large conformational changes occur in the lower palm domain. Plots showing difference in Cα position indicated as distance following superposition of the desensitized state (PDB code: 3HGC) (**a**), low pH Δ13-PcTx1 (PDB code: 4FZ0) (**b**), and high pH Δ13-PcTx1 (4FZ1) (**c**) structures on Δ13-MitTx structure. The z-axis is positioned along the threefold axis of symmetry with z=0 located at the extracellular and transmembrane interface near Pro 73. Note that residues in the linker region Leu 414 and Asn 415 and residues near the the transmembrane domain exhibit the largest rearrangement in Cα positions. **d**, View of the subunit interface between the thumb and palm domains of adjacent subunits in cartoon representation following superposition of the desensitized state (gray) on the Δ13-MitTx structure (domains colored as in Fig. 2). In the desensitized state, Cα atoms of Asn 357 and Thr 210 are ~8 Å apart while the expanded conformation of Δ13-MitTx separates them by ~1 Å. This expansion is greater towards the extracellular and transmembrane interface where Glu 363 and Val 81 are ~3 Å farther in the Δ13-MitTx than in the desensitized state. Cα atoms are shown as spheres. **e**, Local flipping of the β11-β12 linker changes interaction of residues in the linker. Asn 415 forms polar interactions with Tyr 283 on the adjacent subunit and with a water molecule, whereas in the desensitized state, Asn 415 largely forms hydrogen bonds with Tyr 416 and the backbone nitrogen of Ala 83 within the subunit.

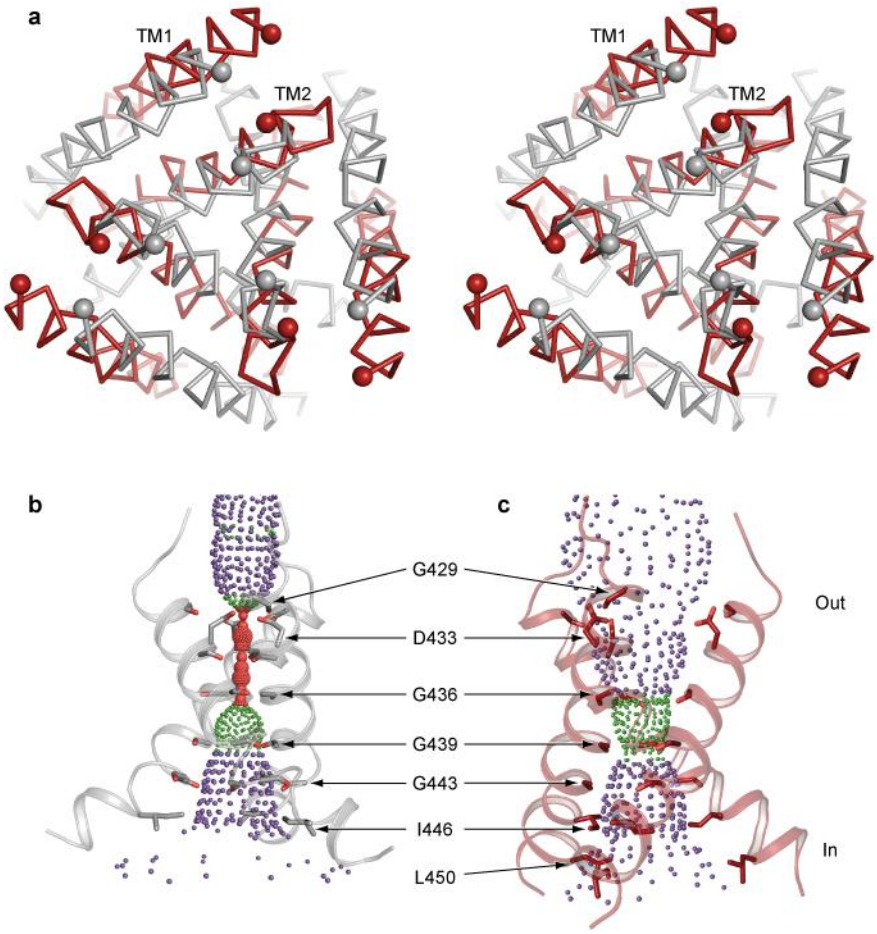

Figure 3.9. Iris-like movement of the transmembrane helices opens the transmembrane pore. **a**, A stereo, α-carbon representation of TM1 and TM2 of the desensitized (gray) and MitTx-bound (red) structures showing the clockwise rotation and expansion of the helices in going from the desensitized to the MitTx-bound conformations. This view is along the 3-fold axis, from the extracellular side of the membrane. **b**, View of TM2 helices of the desensitized state viewed parallel to the membrane showing the shut conformation of the ion channel pore. **c**, The TM2 helixes of the MitTx-bound conformation define an overall open conformation of the pore yet with a constriction at Gly 439.

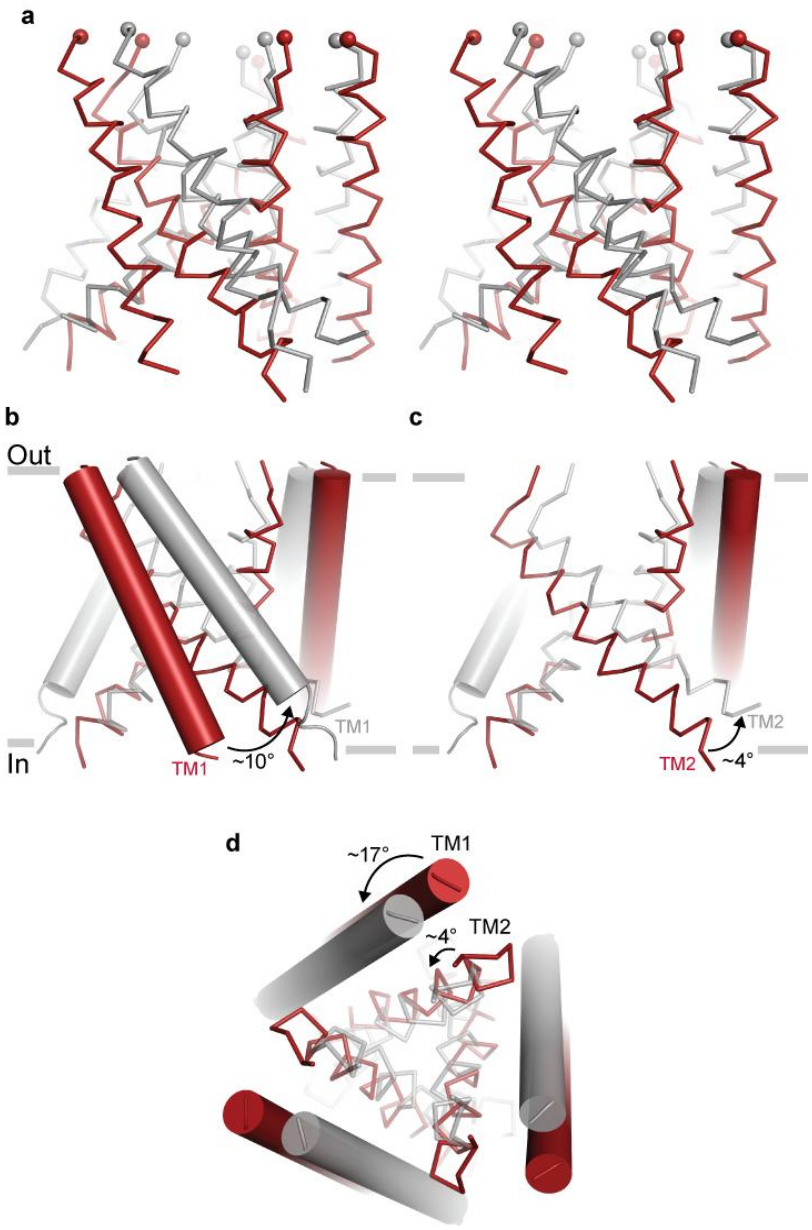

Figure 3.10. Rotational movement and radial expansion of the transmembrane domains open the pore.

Figure 3.10. Rotational movement and radial expansion of the transmembrane domains open the pore. Superposition of the desensitized state (PDB code: 3HGC; gray) and the MitTx-bound state (red) structures emphasizes differences in the conformation of the transmembrane ion channel in shut and open states, respectively. **a**, Stereo view parallel to the membrane. Cα atoms of Tyr 72 and Ala 424 are shown in spheres. View as in (**a**), TM1 (**b**) and TM2 (**c**) in the MitTx-bound state tilts about 10° and 4°, respectively, relative to the desensitized state. TM1 helices are shown in cylinders and TM2 as α-carbon wire tracess. In panel c, TM1 of one subunit is omitted for clarity. **d**, View perpendicular to membrane, seen from the extracellular side of membrane. The transformation from the MitTx-bound state to the desensitized state involves a counter-clockwise, iris-like movement of the transmembrane helices.

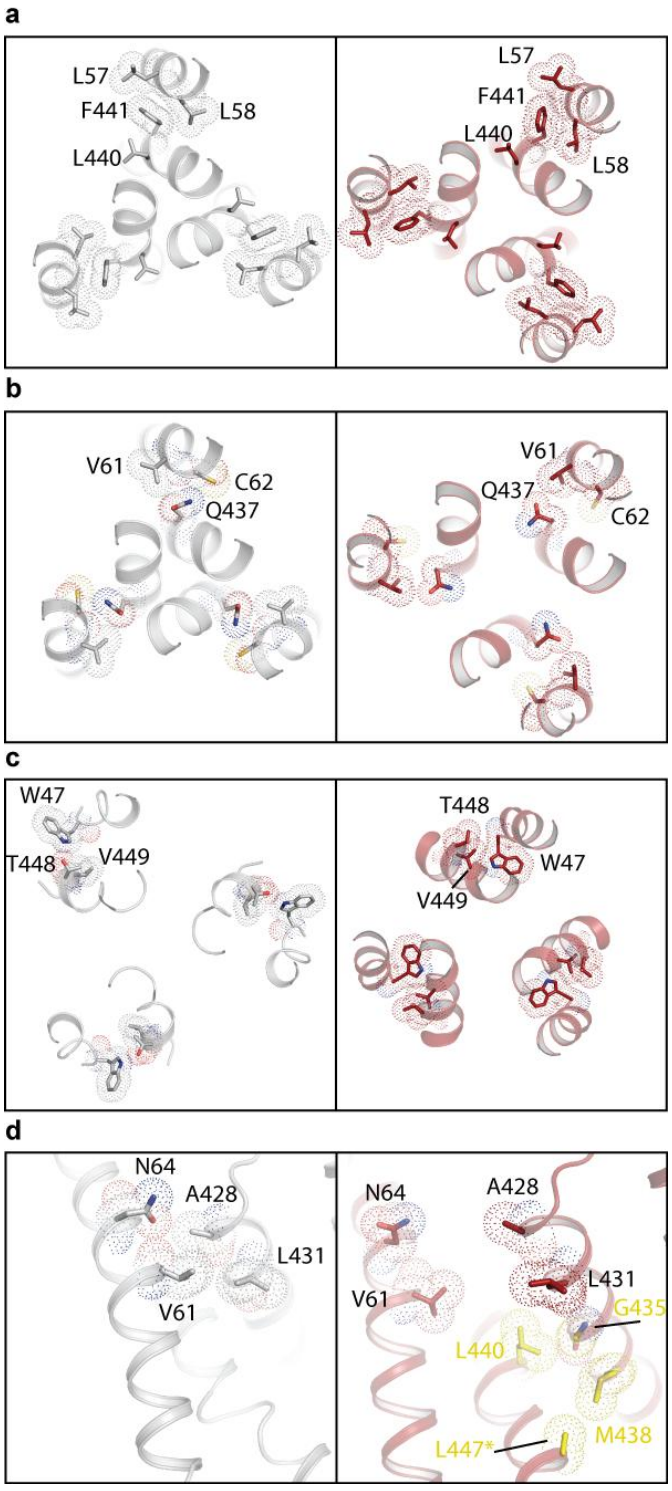

Figure 3.11. Conformational changes in the transmembrane domain modify intra- and intersubunit contacts.

Figure 3.11. Conformational changes in the transmembrane domain modify intra- and intersubunit contacts. Views of the desensitized state (PDB code: 3HGC, gray) and the MitTx-bound state transmembrane domains (red) as 'slabs' along the 3-fold axis of symmetry (**a**, **b**, **c**) or perpendicular to the 3-fold axis (**d**) with an emphasis on residues whose interactions differ between the two states. Panels a, b, and c show how, within a subunit, TM1 and TM2 undergo a scissor-like movement. **a**, Layer near the middle of the membrane showing the 'pivot' of the scissoring movement and how there is minimal movement of Phe 441 relative to Leu 57 and Leu 58. This panel also shows how Leu 440 is situated at the interface between an adjacent TM2 helix and also near the transmembrane pore. **b**, Near the extracellular side of the membrane, the scissoring movement of TM1 and TM2, pivoting around Phe 441 (panel a), gives rise to a substantial shift of Gln 437 relative to Val 61 and Cys 62. **c**, Near the cytoplasmic side of the membrane, we also see how Trp 47 undergoes a substantial movement relative to Thr 448 and Val 449. **d**, In going from the densensitized state to the MitTx-bound state, the intrasubunit interface between TM1 and TM2 that involves Val 61/Asn 64 and Ala 428/Leu 431 ruptures whereas in the MitTx-bound state an intersubunit interface forms between TM2 segments that involves Leu440/Leu447 and Gly 435/Met438, which are colored yellow.

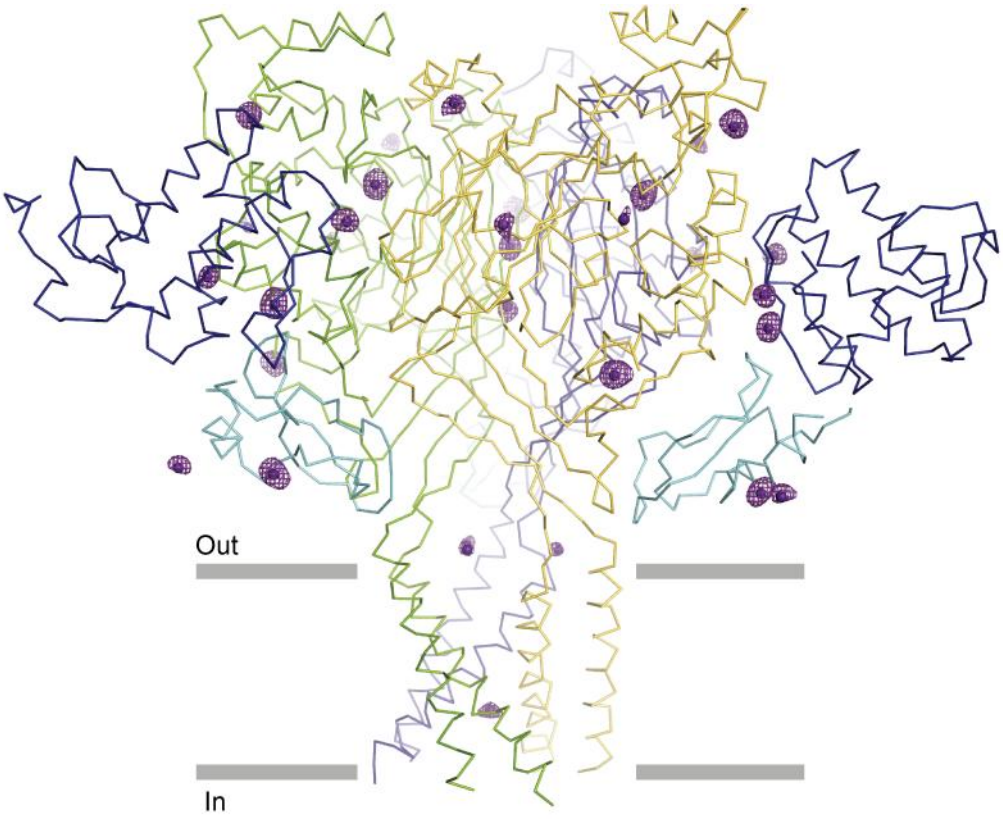

Figure 3.12. Cs^+ binding sites in the Δ13-MitTx complex. Cs^+ ion sites in the Δ13-MitTx complex and the corresponding anomalous difference electron density map calculated from diffraction data measured from the Cs^+-soaked crystals. Each Δ13 subunit is in a different color and the MitTx α and β subunits are in cyan and dark blue, respectively. The map is contoured at 4 σ.

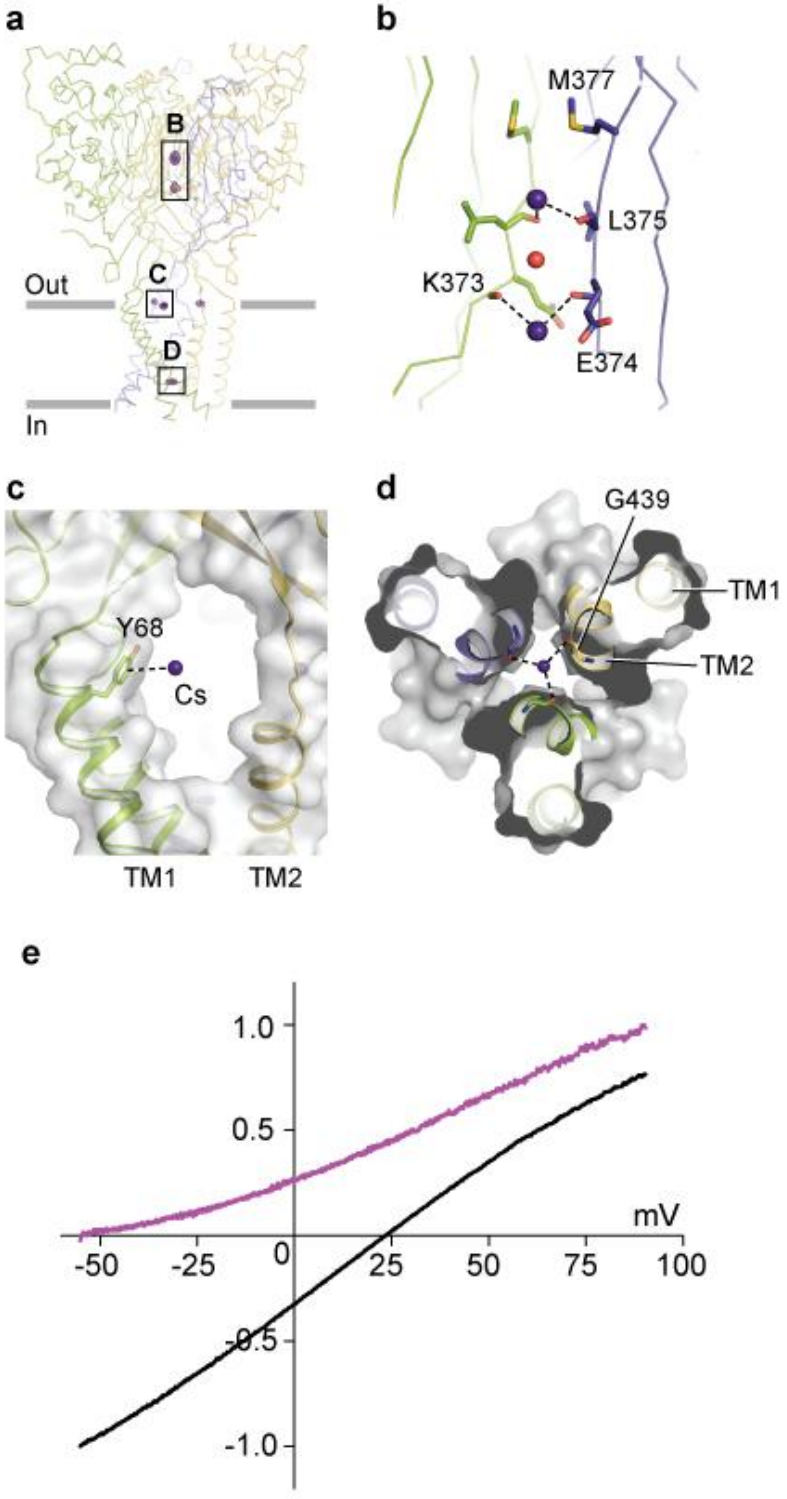

Figure 3.13. Ion binding sites within the vestibules and transmembrane pore.

Figure 3.13. Ion binding sites within the vestibules and transmembrane pore. a, Overall view of an anomalous difference electron density map derived from a crystal soaked in Cs^+ and contoured at 4 σ within the confines of the Δ13 structure. MitTx subunits and corresponding regions of the map have been excluded for clarity. **b**, Cs^+ sites (purple spheres) at the 'top' of the central vestibule are coordinated by main chain carbonyl oxygens from Leu 375 and Lys 373 and separated by a water molecule (red sphere). One subunit has been omitted for clarity. **c**, Cs^+ ions within the lateral fenestrations form a cation-π interaction with Tyr 68. **d**, Cs^+ ion at the constriction of the ion channel pore is coordinated by 3-fold related carbonyl oxygens from Gly 439. **e,** Current/voltage experiment showing that at pH 5.5, Δ13-MitTx is more permeable to Na^+ than K^+. Cs^+ is a weakly permeant ion. Intracellular solution contains 150 mM KCl.

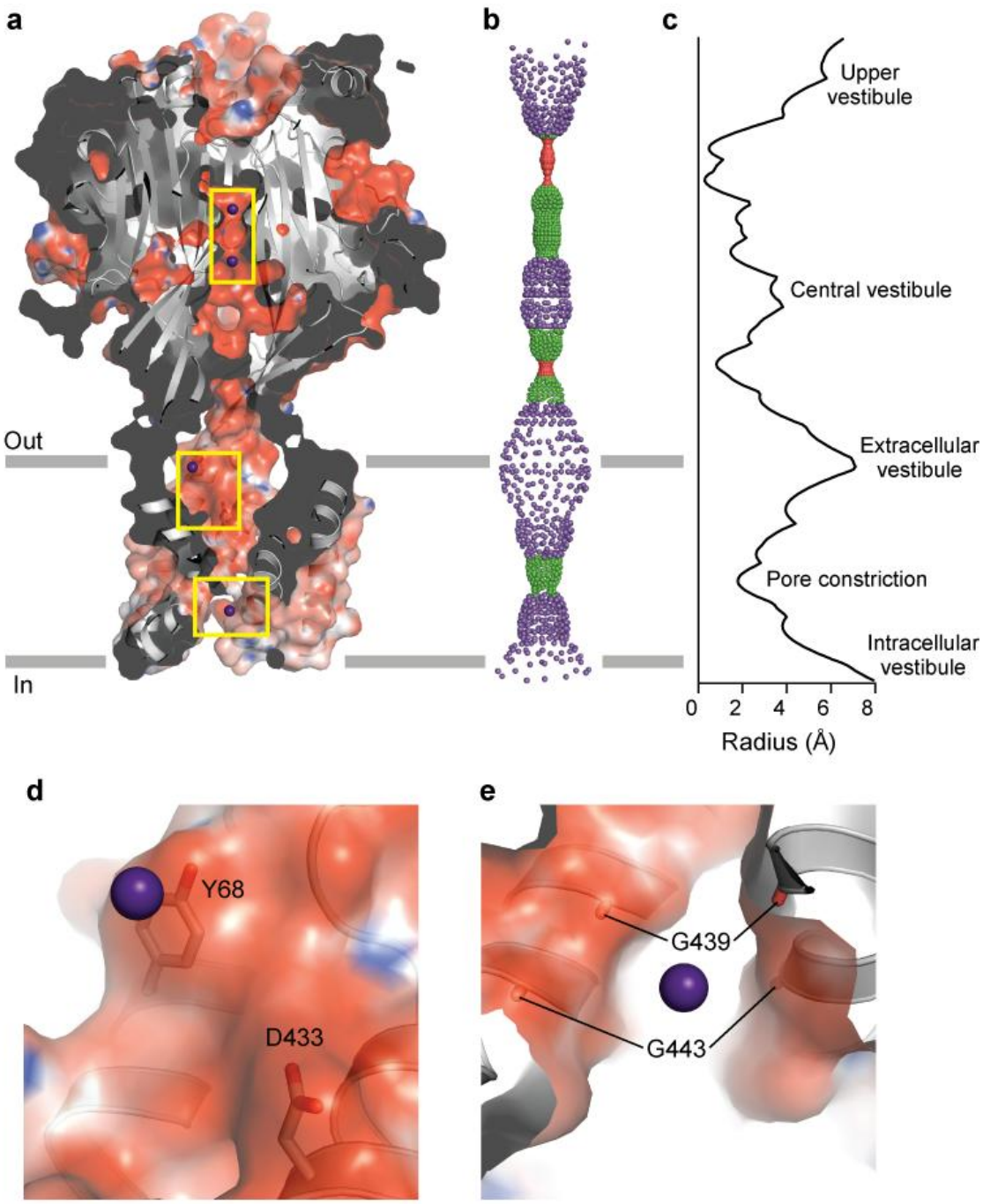

Figure 3.14. Ion binding sites, electrostatic potential and mapping of accessibility along the 3-fold axis of the Δ13-MitTx complex.

Figure 3.14. Ion binding sites, electrostatic potential and mapping of accessibility along the 3-fold axis of the Δ13-MitTx complex. **a**, Sagittal slice of the Δ13 portion of the complex along the 3-fold axis in which the protein is shown in cartoon representation, overlaid with a solvent accessible surface that is color coded by electrostatic potential from -15 kT (red) to +15 kT (blue). Cs+ ions bound to the interior of Δ13 are shown as small purple spheres. **b**, 'HOLE' representation of possible ion pathways along the 3-fold axis of symmetry of the Δ13 channel in the context of the Δ13-MitTx complex, where the different colors define various radii from the pore center (red: <1.15 Å; green: 1.15-2.3 Å; and purple: >2.3 Å). **c**, Plot of pore radius along the 3-fold axis. **d**, Cs+ site adjacent to Tyr 68 in fenestrations of the extracellular vestibule. **e**, Cs+ site at the constriction of the pore, near the carbonyl oxygen atoms of Gly 439.

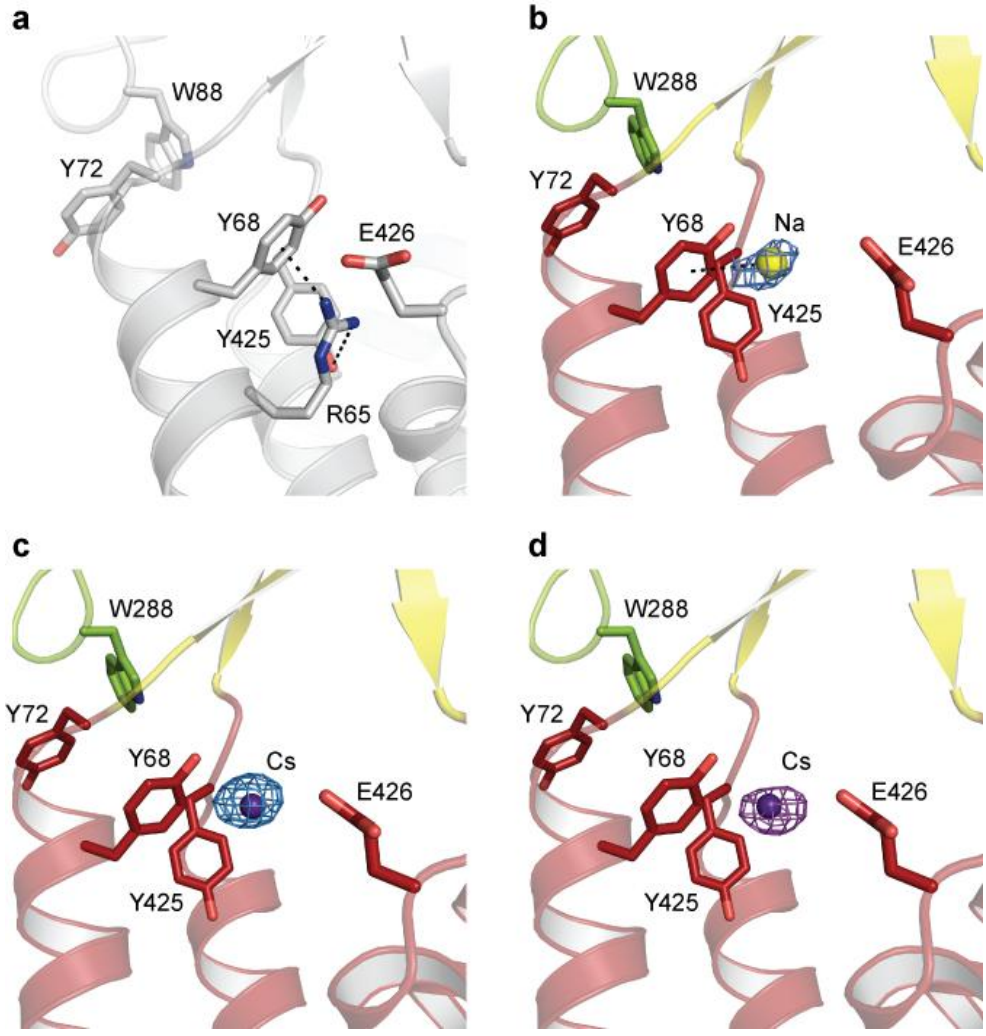

Figure 3.15. Tyr 68 is a site for cation binding by way of cation-π interactions.

Figure 3.15. Tyr 68 is a site for cation binding by way of cation-π interactions. a, In the desensitized state (PDB code: 3HGC), the guanidinium group of Arg 65 forms a cation-π interaction with the aromatic ring of Tyr 68. **b**, In the Δ13-MitTx-bound state, there is a prominent peak in a 2Fo-Fc electron density map derived from 'native' crystals that we suggest is a bound Na^+ ion. Here the map is contoured at 0.9 σ around the putative Na^+ ion. **c**, In Δ13-MitTx crystals soaked in Cs^+ containing solutions, there is also a prominent peak in 2Fo-Fc electron density maps. This map is contoured at 2.0 σ, only around the putative Cs^+ ion. **d**, Most importantly, in anomalous difference electron density maps derived from crystals soaked in Cs^+, there is also a substantial peak adjacent to the aromatic ring of Tyr 68. Here the map is contoured at 3.5 σ, also only immediately around the putative Cs^+ ion.

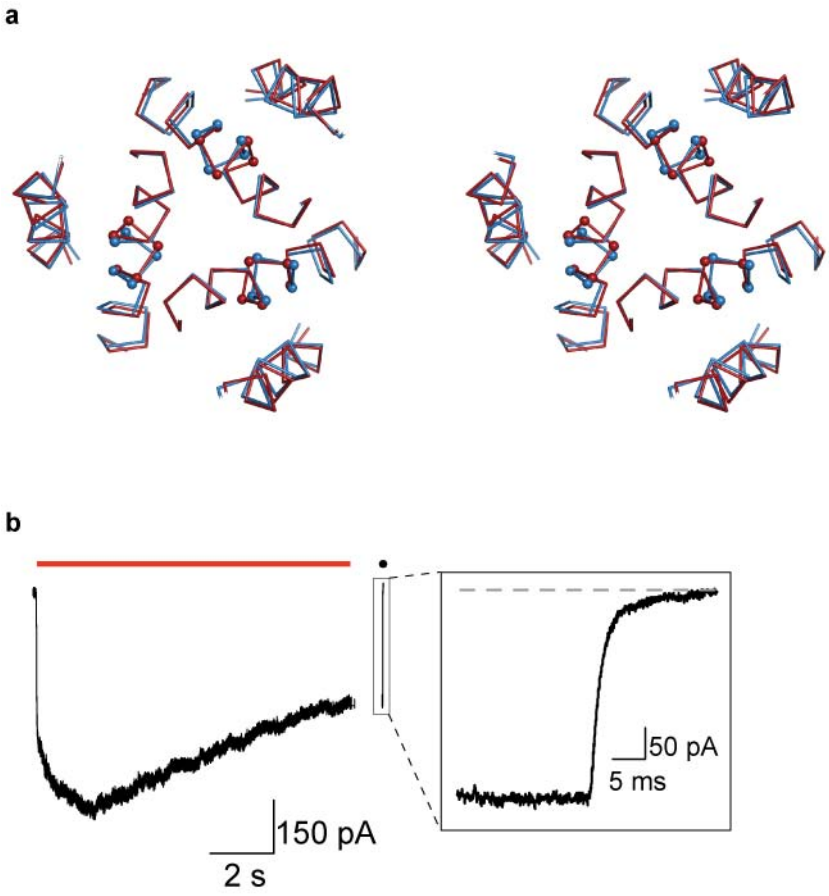

Figure 3.16. Cs^+ blocks MitTx-induced current at pH 5.5. a, A stereo, α-carbon representation of TM1 and TM2 of the native (red) and Cs^+ (blue) MitTx-bound structures showing the 'flexing' of the helices when Cs^+ is bound in the transmembrane region. Greatest displacement occurs near the selectivity filter where distances between Cα atoms of Gly 443 in the native and Cs^+ MitTx-bound structures are ~9 Å and ~10 Å, respectively. This view is along the 3-fold axis, from the extracellular side of the membrane. Cα atoms of residues 441-445 are shown as spheres. **b**, Representative current traces of Δ13 activation by 300 nM recombinant MitTx at pH 7.4 (red line) and pH 5.5 (black dot). Current/amplitude returns to baseline upon application of 150 mM Cs^+ in the extracellular side. Baseline is indicated with gray dotted lines.

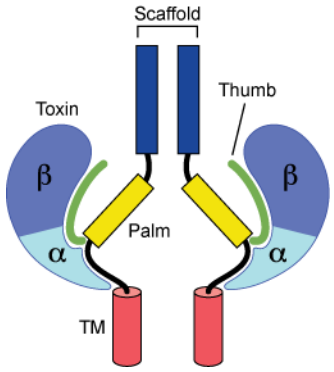

Figure 3.17. Schematic showing how MitTx stabilizes an expanded extracellular vestibule and open channel state of the Δ13 construct of cASIC1a. Extensive contacts between the b subunit and the thumb and palm domains, together with multiple interactions between the a subunit and the thumb, palm, wrist domains and the extracellular end of TM1, lock the Δ13 ion channel in a remarkably pH insensitive, modestly sodium selective and 3-fold symmetric open state.

Chapter 4

Concluding remarks

Summary

Determining molecular mechanisms underlying physiological and pathophysiological processes is challenging. Integral to the development of therapeutic strategies, targeting molecules involved in these processes, like ASICs, with high specificity has been consequently hampered. A cascade of evidence has demonstrated crucial roles for ASICs in the central and peripheral nervous systems, some of which trigger cellular injury such as ischemia or activate nociceptive neural pathways [91, 92, 103, 114-116]. Thus, strategies targeting ASICs hold promise but require extensive knowledge of the ion channel at atomic resolution. At the most basic level, ASICs occupy three different functional states; closed/resting, open, and desensitized. Structural knowledge of the conformations associated with these functional states and how the ion channel responds to specific stimuli will bestow insight into the intricate architecture of ion channel gating within the ENaC/DEG superfamily.

The crystal structures of cASIC1a trapped in the desensitized state[24, 26] were the initial blueprints that laid the foundation for future structural and functional analyses. Subsequent objectives, as focused on in this dissertation, were to obtain different conformations - specifically the open conformation - to ascertain the fundamental basis of channel gating in these trimeric ion channels. The propensity of ASICs to rapidly and profoundly desensitize, however, has complicated crystallization of the channel in the open state. To surmount this hurdle, I exploited the powerful modulatory abilities of toxins, utilizing them to stabilize a non-desensitized conformation of the ion channel. Three distinct crystal structures of cASIC1a in complex with PcTx1 and MitTx have shed light into unanticipated properties of ASICs. These crystal structures outline the toxin binding sites, domains involved in gating of the channel, and ion binding sites.

The first endeavor was determining the structure of the toxin-channel complexes to identify the binding sites that provide high affinity and specificity for the channel. The three structures of the toxin-bound cASIC1a complexes reveal that contacts at the subunit interface are key regions for toxin recognition and transduction to modulate channel activity. For PcTx1, the toxin relies on its positively-charged loops that form polar contacts with the negatively-charged acidic pocket while also anchoring via a hydrophobic embrace with Phe 451 (cASIC1a numbering), a residue that only resides in ASIC1 subunits, thus conferring subunit specificity. The larger MitTx provides a greater array of contacts spanning from the top of the thumb domain, where it forms contacts to residues on both the finger and thumb domains, down to the wrist region, where it forges stable associations via hydrogen bonds and hydropobic interactions. Because many of these interactions involve residues that are not conserved between ASIC subtypes they impart variable modes of subunit recognition and thus are capable of gating ASICs with different subunit composition, with the highest affinity for ASIC1a.

On the basis of these structural studies illustrating that the toxins target the thumb, finger, palm, and wrist domains, they suggest that these domains play critical roles in gating the channel. Comparison of the toxin-bound structures against the desensitized state structure emphasizes a structurally conserved scaffold and dynamic domains that transform upon ligand binding. Common features between the three open conformations include the essential 'flexing' of the lower palm domain that displaces β sheets which, in turn, directly link with the transmembrane domains. The 'flexing' of this β-sheet mantle expands the extracellular vestibule region, located at the extracellular and transmembrane domain

interface. As a consequence of the β-sheet 'flexing', TM1 and TM2 undergo iris-like radial displacements and rotational movements that open the pore region.

The sizes of PcTx1 and MitTx, along with their mechanisms of binding to ASIC1a, correlate with their gating of the channel. The smaller PcTx1 forms contacts primarily at the top of the thumb and palm domains of ASIC1a thus imparting less restriction on the lower palm domain, allowing it to undergo pH-dependent 'flexing' of the β sheets. By constrast, the larger heterodimeric MitTx extends to the wrist region, with the α subunit wedged between ASIC subunits in the lower palm domain and fastened the β sheets of the lower palm domain in a 'flexed' configuration; stabilizing the ion channel in an open, pH-independent conformation.

Contrasting features between the toxin complexes extend to distinctions in the arrangements of the transmembrane domains which in turn are strongly correlated with the differences in ion selectivity. The influence of the extracellular domain in gating the ion channel extends to the extracellular half of the transmembrane domain where the degree of rotation is proportional to the scale of expansion mediated by the 'flexing' of lower palm domain. The arrangement of the intracellular half of the transmembrane domain, however, is still not well-understood. Indeed, crystal contacts alone do not explain the variation of conformations observed in the previous ASIC1a structures because the regions preceding the first residues modeled in the structures are disordered. Though not observed in calculated electron density maps, the amino terminus must influence the arrangement of the transmembrane domains. Previous functional studies characterized the N-terminal region preceding the first transmembrane domain as crucial for gating and selectivity of ENaC/DEG channels.

Mapping ion binding sites in the pore domain and measurements of pore dimensions demonstrate that ions must be hydrated to traverse an ASIC pore, in contrast with the mechanism by which K^+ channels coordinate with K^+ ions. Furthermore, a mapped ion binding site revealed a surprising site in the wrist region which likely modulates channel gating through its coordination with the backbone carbonyl oxygens at the base of the thumb and at the extracellular end of the TM1 domain. The Cs^+ sites in the Δ13-PcTx1structures emphasize the role of the cation site through differences in the Cs^+ anomalous signal observed from different conformations of transmembrane domains within a single trimeric channel. Reinforcing the importance of this cation site at the juncture of the wrist and TM1, we note that the α subunit of MitTx positions the ammonium group of a lysine residue at the same site.

The structures of cASIC1a in desensitized and open conformations have defined domains important for gating and have mapped the toxin sites, thus providing the basis for designing compounds for therapeutic strategies. We have amassed useful information from analyzing these structures and this data will facilitate our efforts directed to uncovering the relationships between atomic structure and molecular mechanism in ASICs and in the ENaC/DEG superfamily.

Future Directions

Structural analysis of ASIC-blocker complex

Exploiting the stabilizing properties for crystallization endowed by the complex formation with MitTx, structural studies in complex with different compounds that modulate ASIC activity, like amiloride and its derivatives, would plot binding sites within the pore region. Because currents from Δ13-MitTx are efficiently blocked by amiloride, co-

crystallization with the open channel blocker would map residues involved and offer possible explanations for the basis of the absence of specificity among amiloride-based pore blockers, which is present in ENaC.

Identification of ASIC-lipid interactions

The open conformations of the toxin-channel complexes harbor V-shaped gaps within the transmembrane domain and thus we suggest that lipids are integral parts of ion channel arrangement and perhaps influence the gating properties of ASICs. To determine how lipids interact with the transmembrane domains, crystallization employing bicelles presents opportunities for investigating multiple interactions between the channel and the bilayer, along with understanding how these interactions influence gating properties. Furthermore, crystallization in bicelles mimicks a physiological lipid-enriched environment offering more stability to the plastic ASIC transmembrane domains.

Apart from stabilizing the transmembrane region of the channel, bicelle crystallization could restore regions with which the elusive N-terminal region interacts. Perhaps extraction of ASICs from the membrane and maintaining their solubility through micelles eliminates properties that preserve the structure of the N-terminal region. Visualizing interactions involving the N-terminal region will provide explanation as to how it influences gating and selectivity properties of ASIC, and by extension, of the ENaC/DEG family.

Understanding the principles of ASIC gating

Among the different states of ASIC, the closed/resting conformation of the channel has remained intangible. To understand how protons, Ca^{2+} and other ligands modulate the activity of the channel, determining the closed conformation of the channel would be an invaluable addition to understanding the mechanism underlying ASIC gating. At present, the conformations derived from different conditions of ASICs are of the proton-bound or activated conformation. Obtaining the structure of the resting/closed state will elucidate how domains rearrange upon activation, desensitization, and recovery.

Insight into heteromeric ASIC assembly

ASICs arrange in homomeric and heteromeric forms in physiological conditions and display a variety of gating kinetics, which allows ASICs to participate in a range of gating acitivities over a broad range of pH conditions. Determining the structure of a heteromic ASIC will provide vital insight into how ASICs arrange in heteromeric configurations and how each subunit influences gating properties and ion permeability.

References

1. Krishtal, O.A. and V.I. Pidoplichko, *A receptor for protons in the membrane of sensory neurons may participate in nociception.* Neuroscience, 1981. **6**: p. 2599-2601.

2. Krishtal, O.A. and V.I. Pidoplichko, *A receptor for protons in the nerve cell membrane.* Neuroscience, 1980. **5**: p. 2325-2327.

3. Waldmann, R., G. Champigny, F. Bassilana, C. Heurteaux, and M. Lazdunski, *A proton-gated cation channel involved in acid-sensing.* Nature, 1997. **386**: p. 173-177.

4. Waldmann, R., G. Champigny, N. Voilley, I. Lauritzen, and M. Lazdunski, *The mammalian degenerin MDEG, an amiloride-sensitive cation channel activated by mutations causing neurodegeneration in C. elegans.* J. Biol. Chem., 1996. **271**: p. 10433-10436.

5. Akopian, A.N., C.C. Chen, Y. Ding, P. Cesare, and J.N. Wood, *A new member of the acid-sensing ion channel family.* Neuroreport, 2000. **11**: p. 2217-2222.

6. Babinski, K., K.T. Le, and P. Seguela, *Molecular cloning and regional distribution of a human proton receptor subunit with biphasic functional properties.* J. Neurochem., 1999. **72**: p. 51-57.

7. Bassler, E.L., T.J. Ngo-Anh, H.S. Geisler, J.P. Ruppersberg, and S. Gründer, *Molecular and functional characterization of acid-sensing ion channel (ASIC) 1b.* J. Biol. Chem., 2001. **276**: p. 33782-33787.

8. Chen, C.C., S. England, A.N. Akopian, and J.N. Wood, *A sensory neuron-specific, proton-gated ion channel.* Proc. Natl. Acad. Sci. USA, 1998. **95**: p. 10240-10245.

9. de Weille, J.R., F. Bassilana, M. Lazdunski, and R. Waldmann, *Identification, functional expression and chromosomal localization of a sustained human proton-gated cation channel.* FEBS Lett, 1998. **433**: p. 257-260.

10. Garcia-Anoveros, J., B. Derfler, J. Neville-Golden, B.T. Hyman, and D.P. Corey, *BNaC1 and BNaC2 constitute a new family of human neuronal sodium channels related to degenerins and epithelial sodium channels.* Proc. Natl. Acad. Sci. USA, 1997. **94**: p. 1459-1464.

11. Gründer, S., H.S. Geisler, E.L. Bassler, and J.P. Ruppersberg, *A new member of acid-sensing ion channels from pituitary gland.* Neuroreport, 2000. **11**: p. 1607-1611.

12. Ishibashi, K. and F. Marumo, *Molecular cloning of a DEG/ENaC sodium channel cDNA from human testis.* Biochem. Biophys. Res. Commun., 1998. **245**: p. 589-593.

13. Lingueglia, E., J.R. de Weille, F. Bassilana, C. Heurteaux, H. Sakai, R. Waldmann, and M. Lazdunski, *A modulatory subunit of acid sensing ion channels in brain and dorsal root ganglion cells.* J. Biol. Chem., 1997. **272**: p. 29778-29783.

14. Price, M.P., P.M. Snyder, and M.J. Welsh, *Cloning and expression of a novel human brain Na+ channel.* J. Biol. Chem., 1996. **271**: p. 7879-7882.

15. Canessa, C.M., J.-D. Horisberger, and B.C. Rossier, *Epithelial sodium channel related to proteins involved in neurodegeneration.* Nature, 1993. **361**: p. 467-470.

16. Schild, L., E. Schneeberger, I. Gautschi, and D. Firsov, *Identification of amino acid residues in the alpha, beta, and gamma subunits of the epithelial sodium channel (ENaC) involved in amiloride block and ion permeation.* J Gen Physiol, 1997. **109**(1): p. 15-26.

17. Chalfie, M. and E. Wolinsky, *The identification and suppression of inherited neurodegeneration in Caenorhabditis elegans.* Nature, 1990. **345**(6274): p. 410-6.

18. Driscoll, M. and M. Chalfie, *The mec-4 gene is a member of a family of Caenorhabditis elegans genes that can mutate to induce neuronal degeneration.* Nature, 1991. **349**: p. 588-593.

19. Lingueglia, E., G. Champigny, M. Lazdunski, and P. Barbry, *Cloning of the amiloride-sensitive FMRFamide peptide-gated sodium channel.* Nature, 1995. **378**(6558): p. 730-3.

20. Cottrell, G.A., *The first peptide-gated ion channel.* J Exp Biol, 1997. **200**(Pt 18): p. 2377-86.

21. Kellenberger, S. and L. Schild, *Epithelial sodium channel/degenerin family of ion channels: a variety of functions for a shared structure.* Physiol. Rev., 2002. **82**: p. 735-767.

22. Wemmie, J.A., C.C. Askwith, E. Lamani, M.D. Cassell, J.H.J. Freeman, and M.J. Welsh, *Acid-sensing ion channel 1 is localized in brain regions with high synaptic density and contributes to fear conditioning.* J. Neurosci., 2003. **23**: p. 5496-5502.

23. Alvarez de la Rosa, D., S.R. Krueger, A. Kolar, D. Shao, R.M. Fitzsimonds, and C.M. Canessa, *Distribution, subcellular localization and ontogeny of ASIC1 in the mammalian central nervous system.* J. Physiol., 2003. **546**: p. 77-87.

24. Jasti, J., H. Furukawa, E. Gonzales, and E. Gouaux, *Structure of acid-sensing ion channel 1 at 1.9 A resolution and low pH.* Nature, 2007 **449**: p. 316-323.

25. Carnally, S.M., H.S. Dev, A.P. Stewart, N.P. Barrera, M.X. Van Bemmelen, L. Schild, R.M. Henderson, and J.M. Edwardson, *Direct visualization of the trimeric structure of the ASIC1a channel, using AFM imaging.* Biochem Biophys Res Commun, 2008. **372**(4): p. 752-5.

26. Gonzales, E.B., T. Kawate, and E. Gouaux, *Pore architecture and ion sites in acid-sensing ion channels and P2X receptors.* Nature, 2009. **460**: p. 599-604.

27. Kawate, T., J.C. Michel, W.T. Birdsong, and E. Gouaux, *Crystal structure of the ATP-gated P2X4 ion channel in the closed state.* Nature, 2009. **460**: p. 592-598.

28. Kashlan, O.B. and T.R. Kleyman, *ENaC structure and function in the wake of a resolved structure of a family member.* Am. J. Physiol. Renal. Physiol., 2011. **301**: p. F684-F696.

29. Sherwood, T.W., E.N. Frey, and C.C. Askwith, *Structure and activity of the acid-sensing ion channels.* Am J Physiol Cell Physiol. **303**(7): p. C699-710.

30. Wemmie, J.A., M.P. Price, and M.J. Welsh, *Acid-sensing ion channels: advances, questions and therapeutic opportunities.* Trends Neurosci., 2006. **29**: p. 578-586.

31. Askwith, C.C., C.J. Benson, M.J. Welsh, and P.M. Snyder, *DEG/ENaC ion channels involved in sensory transduction are modulated by cold temperature.* Proc Natl Acad Sci U S A, 2001. **98**(11): p. 6459-63.

32. Cushman, K.A., J. Marsh-Haffner, J. Adelman, and E.W. McCleskey, *A conformational change in the extracellular domain that accompanies desensitization of acid-sensing ion channel (ASIC) 3.* J. Gen. Physiol., 2007. **129**: p. 345-350.

33. Snyder, P.M., D.B. Bucher, and D.R. Olson, *Gating induces a conformational change in the outer vestibule of ENaC.* J Gen Physiol, 2000. **116**(6): p. 781-90.

34. Springauf, A., P. Bresenitz, and S. Gründer, *The interaction between two extracellular linker regions controls sustained opening of acid-sensing ion channel 1.* J Biol Chem, 2011. **286**(27): p. 24374-24384.

35. Li, T., Y. Yang, and C.M. Canessa, *Leu85 in the beta1-beta2 linker of ASIC1 slows activation and decreases the apparent proton affinity by stabilizing a closed conformation.* J Biol Chem, 2010. **285**(29): p. 22706-22712.

36. Li, T., Y. Yang, and C.M. Canessa, *Asn415 in the beta11-beta12 linker decreases proton-dependent desensitization of ASIC1.* J Biol Chem, 2010. **285**(41): p. 31285-31291.

37. Li, W.G., Y. Yu, C. Huang, H. Cao, and T.L. Xu, *Nonproton Ligand Sensing Domain Is Required for Paradoxical Stimulation of Acid-sensing Ion Channel 3 (ASIC3) Channels by Amiloride.* J Biol Chem, 2011. **286**: p. 42635-42646.

38. Li, W.G., Y. Yu, Z.D. Zhang, H. Cao, and T.L. Xu, *ASIC3 channels integrate agmatine and multiple inflammatory signals through the nonproton ligand sensing domain.* Mol Pain. **6**: p. 88.

39. Ishikita, H., *Proton-binding sites of acid-sensing ion channel 1.* PLoS One. **6**(2): p. e16920.

40. Li, T., Y. Yang, and C.M. Canessa, *Interaction of the aromatics Tyr-72/Trp-288 in the interface of the extracellular and transmembrane domains is essential for proton gating of acid-sensing ion channels.* J Biol Chem, 2009. **284**(7): p. 4689-94.

41. Hong, K. and M. Driscoll, *A transmembrane domain of the putative channel subunit MEC-4 influences mechanotransduction and neurodegeneration in C. elegans.* Nature, 1994. **367**: p. 470-473.

42. Champigny, G., N. Voilley, R. Waldmann, and M. Lazdunski, *Mutations causing neurodegeneration in Caenorhabditis elegans drastically alter the pH sensitivity and inactivation of the mammalian H+-gated Na+ channel MDEG1.* J. Biol. Chem., 1998. **273**: p. 15418-15422.

43. Tolino, L.A., S. Okumura, O.B. Kashlan, and M.D. Carattino, *Insights into the mechanism of pore opening of acid-sensing ion channel 1a.* J Biol Chem. **286**(18): p. 16297-307.

44. Adams, C.M., M.P. Price, P.M. Snyder, and M.J. Welsh, *Tetraethylammonium block of the BNC1 channel.* Biophys J, 1999. **76**(3): p. 1377-83.

45. Salinas, M., M. Lazdunski, and E. Lingueglia, *Structural elements for the generation of sustained currents by the acid pain sensor ASIC3.* J Biol Chem, 2009. **284**(46): p. 31851-9.

46. Li, T., Y. Yang, and C.M. Canessa, *Two residues in the extracellular domain convert a nonfunctional ASIC1 into a proton-activated channel.* Am J Physiol Cell Physiol, 2010. **299**(1): p. C66-C73.

47. Li, T., Y. Yang, and C.M. Canessa, *Asp433 in the closing gate of ASIC1 determines stability of the open state without changing properties of the selectivity filter or Ca2+ block.* J Gen Physiol. **137**(3): p. 289-97.

48. Li, T., Y. Yang, and C.M. Canessa, *Outlines of the pore in open and closed conformations describe the gating mechanism of ASIC1.* Nat Commun, 2011. **2**: p. 399.

49. Coscoy, S., J.R. de Weille, E. Lingueglia, and M. Lazdunski, *The pre-transmembrane 1 domain of acid-sensing ion channels participates in the ion pore.* J Biol Chem, 1999. **274**(15): p. 10129-32.

50. Garcia-Anoveros, J., C. Ma, and M. Chalfie, *Regulation of Caenorhabditis elegans degenerin proteins by a putative extracellular domain.* Curr Biol, 1995. **5**(4): p. 441-8.

51. Kellenberger, S., M. Auberson, I. Gautschi, E. Schneeberger, and L. Schild, *Permeability properties of ENaC selectivity filter mutants.* J. Gen. Physiol., 2001. **118**: p. 679-692.

52. Kellenberger, S., I. Gautschi, and L. Schild, *A single point mutation in the pore region of the epithelial Na+ channel changes ion selectivity by modifying molecular sieving.* Proc Natl Acad Sci U S A, 1999. **96**(7): p. 4170-5.

53. Kellenberger, S., N. Hoffmann-Pochon, I. Gautschi, E. Schneeberger, and L. Schild, *On the molecular basis of ion permeation in the epithelial Na+ channel.* J Gen Physiol, 1999. **114**(1): p. 13-30.

54. Sheng, S., K.A. McNulty, J.M. Harvey, and T.R. Kleyman, *Second transmembrane domains of ENaC subunits contribute to ion permeation and selectivity.* J Biol Chem, 2001. **276**(47): p. 44091-8.

55. Sheng, S., J. Li, K.A. McNulty, D. Avery, and T.R. Kleyman, *Characterization of the selectivity filter of the epithelial sodium channel.* J Biol Chem, 2000. **275**(12): p. 8572-81.

56. Snyder, P.M., D.R. Olson, and D.B. Bucher, *A pore segment in DEG/ENaC Na(+) channels.* J Biol Chem, 1999. **274**(40): p. 28484-90.

57. Benos, D.J., *Amiloride: a molecular probe of sodium transport in tissues and cells.* Am J Physiol, 1982. **242**(3): p. C131-45.

58. Palmer, L.G., *Ion selectivity of the apical membrane Na channel in the toad urinary bladder.* J Membr Biol, 1982. **67**(2): p. 91-8.

59. Benos, D.J. and B.A. Stanton, *Functional domains within the degenerin/epithelial sodium channel (Deg/ENaC) superfamily of ion channels.* J Physiol, 1999. **520 Pt 3**: p. 631-44.

60. Gründer, S., D. Firsov, S.S. Chang, N.F. Jaeger, I. Gautschi, L. Schild, R.P. Lifton, and B.C. Rossier, *A mutation causing pseudohypoaldosteronism type 1 identifies a conserved glycine that is involved in the gating of the epithelial sodium channel.* EMBO J., 1997. **16**: p. 899-907.

61. Berdiev, B.K., T.B. Mapstone, J.M. Markert, G.Y. Gillespie, J. Lockhart, C.M. Fuller, and D.J. Benos, *pH alterations "reset" Ca2+ sensitivity of brain Na+ channel 2, a degenerin/epithelial Na+ ion channel, in planar lipid bilayers.* J Biol Chem, 2001. **276**(42): p. 38755-61.

62. de Weille, J. and F. Bassilana, *Dependence of the acid-sensitive ion channel, ASIC1a, on extracellular Ca(2+) ions.* Brain Res, 2001. **900**(2): p. 277-81.

63. Chu, X.P., J.A. Wemmie, W.Z. Wang, X.M. Zhu, J.A. Saugstad, M.P. Price, R.P. Simon, and Z.G. Xiong, *Subunit-dependent high-affinity zinc inhibition of acid-sensing ion channels.* J Neurosci, 2004. **24**(40): p. 8678-89.

64. Baron, A., L. Schaefer, E. Lingueglia, G. Champigny, and M. Lazdunski, *Zn2+ and H+ are coactivators of acid-sensing ion channels.* J. Biol. Chem., 2001. **276**: p. 35361-35367.

65. Jiang, Q., K. Inoue, X. Wu, C.J. Papasian, J.Q. Wang, Z.G. Xiong, and X.P. Chu, *Cysteine 149 in the extracellular finger domain of acid-sensing ion channel 1b subunit is critical for zinc-mediated inhibition.* Neuroscience. **193**: p. 89-99.

66. Cho, J.H. and C.C. Askwith, *Potentiation of acid-sensing ion channels by sulfhydryl compounds.* Am J Physiol Cell Physiol, 2007. **292**(6): p. C2161-74.

67. Chu, X.P., N. Close, J.A. Saugstad, and Z.G. Xiong, *ASIC1a-specific modulation of acid-sensing ion channels in mouse cortical neurons by redox reagents.* J Neurosci, 2006. **26**(20): p. 5329-39.

68. Immke, D.C. and E.W. McCleskey, *Protons open acid-sensing ion channels by catalyzing relief of Ca^{2+} block.* Neuron, 2003. **37**: p. 75-84.

69. Paukert, M., E. Babini, M. Pusch, and S. Gründer, *Identification of the Ca2+ blocking site of acid-sensing ion channel (ASIC) 1: Implications for channel gating.* J. Gen. Physiol., 2004. **124**: p. 383-394.

70. Sherwood, T., R. Franke, S. Conneely, J. Joyner, P. Arumugan, and C. Askwith, *Identification of protein domains that control proton and calcium sensitivity of ASIC1a.* J Biol Chem, 2009. **284**(41): p. 27899-27907.

71. Zhang, P., F.J. Sigworth, and C.M. Canessa, *Gating of acid-sensitive ion channel-1: Release of Ca^{2+} block vs allosteric mechanism.* J. Gen. Physiol., 2006. **127**: p. 109-117.

72. Babini, E., M. Paukert, H.S. Geisler, and S. Gründer, *Alternative splicing and interaction with di- and polyvalent cations control the dynamic range of acid-sensing ion channel (ASIC).* J. Biol. Chem., 2002. **26**: p. 41597-41603.

73. Davies, N.W., H.D. Lux, and M. Morad, *Site and mechanism of activation of proton-induced sodium current in chick dorsal root ganglion neurones.* J Physiol, 1988. **400**: p. 159-87.

74. Immke, D.C. and E.W. McCleskey, *Lactate enhances the acid-sensing Na+ channel on ischemia-sensing neurons.* Nature Neurosci., 2001. **4**: p. 869-870.

75. Adams, C.M., P.M. Snyder, and M.J. Welsh, *Paradoxical stimulation of a DEG/ENaC channel by amiloride.* J Biol Chem, 1999. **274**(22): p. 15500-4.

76. Qadri, Y.J., Y. Song, C.M. Fuller, and D.J. Benos, *Amiloride docking to acid-sensing ion channel-1.* J Biol Chem. **285**(13): p. 9627-35.

77. Hamilton, K.L. and D.C. Eaton, *Single-channel recordings from amiloride-sensitive epithelial sodium channel.* Am J Physiol, 1985. **249**(3 Pt 1): p. C200-7.

78. Palmer, L.G. and G. Frindt, *Amiloride-sensitive Na channels from the apical membrane of the rat cortical collecting tubule.* Proc Natl Acad Sci U S A, 1986. **83**(8): p. 2767-70.

79. Garty, H. and L.G. Palmer, *Epithelial sodium channels: function, structure, and regulation.* Physiol Rev, 1997. **77**(2): p. 359-96.

80. Gründer, S. and X. Chen, *Structure, function, and pharmacology of acid-sensing ion channels (ASICs): focus on ASIC1a.* Int J Physiol Pathophysiol Pharmacol, 2010. **2**(2): p. 73-94.

81. Kleyman, T.R. and E.J.J. Cragoe, *Amiloride and its analogs as tools in the study of ion transport.* J. Membr. Biol., 1988. **105**: p. 1-21.

82. Kuduk, S.D., R.K. Chang, J.M.-C. Wai, C.N. Di Marco, V. Cofre, R.M. DiPardo, S.P. Cook, M.J. Cato, A. Jovanovska, M.O. Urban, M. Leitl, R.H. Spencer, S.A. Kane, G.D. Hartman, and M.T. Bilodeau, *Amidine derived inhibitors of acid-sensing ion channel-3 (ASIC3).* Bioorg. Med. Chem. Lett., 2009. **19**: p. 4059-4063.

83. Kuduk, S.D., C.N. Di Marco, R.K. Chang, R.M. Dipardo, S.P. Cook, M.J. Cato, A. Jovanovska, M.O. Urban, M. Leitl, R.H. Spencer, S.A. Kane, M.T. Bilodeau, G.D. Hartman, and M.G. Bock, *Amiloride derived inhibitors of acid-sensing ion channel-3 (ASIC3).* Bioorg Med Chem Lett, 2009. **19**(9): p. 2514-8.

84. Escoubas, P., J.R. De Weille, L. A., S. Diochot, R. Waldmann, G. Champigny, D. Moinier, A. Menez, and M. Lazdunski, *Isolation of a tarantula toxin specific for a class of proton-gated Na+ channels.* J. Biol. Chem., 2000. **275**: p. 25116-25121.

85. Escoubas, P., C. Bernard, G. Lambeau, M. Lazdunski, and H. Darbon, *Recombinant production and solution structure of PcTx1, the specific peptide inhibitor of ASIC1a proton-gated cation channels.* Protein Sci, 2003. **12**(7): p. 1332-1343.

86. Salinas, M., L.D. Rash, A. Baron, G. Lambeau, P. Escoubas, and M. Lazdunski, *The receptor site of the spider toxin PcTx1 on the proton-gated cation channel ASIC1a.* J. Physiol., 2006. **570**: p. 339-354.

87. Chen, X., H. Kalbacher, and S. Gründer, *The tarantula toxin psalmotoxin 1 inhibits acid-sensing ion channel (ASIC) 1a by increasing its apparent H+ affinity.* J Gen Physiol, 2005. **126**(1): p. 71-79.

88. Chen, X., H. Kalbacher, and S. Gründer, *Interaction of acid-sensing ion channel (ASIC) 1 with the tarantula toxin psalmotoxin 1 is state dependent.* J Gen Physiol, 2006. **127**(3): p. 267-276.

89. Chagot, B., P. Escoubas, S. Diochot, C. Bernard, M. Lazdunski, and H. Darbon, *Solution structure of APETx2, a specific peptide inhibitor of ASIC3 proton-gated channels.* Protein Sci, 2005. **14**(8): p. 2003-10.

90. Diochot, S., A. Baron, L.D. Rash, E. Deval, P. Escoubas, S. Scarzello, M. Salinas, and M. Lazdunski, *A new sea anemone peptide, APETx2, inhibits ASIC3, a major acid-sensitive channel in sensory neurons.* Embo J, 2004. **23**(7): p. 1516-25.

91. Bohlen, C.J., A.T. Chesler, R. Sharif-Naeini, K.F. Medzihradszky, S. Zhou, D. King, E.E. Sanchez, A.L. Burlingame, A.I. Basbaum, and D. Julius, *A heteromeric Texas coral snake toxin targets acid-sensing ion channels to produce pain.* Nature, 2011. **479**(7373): p. 410-414.

92. Diochot, S., A. Baron, M. Salinas, D. Douguet, S. Scarzello, A.S. Dabert-Gay, D. Debayle, V. Friend, A. Alloui, M. Lazdunski, and E. Lingueglia, *Black mamba venom peptides target acid-sensing ion channels to abolish pain.* Nature.

93. Sherwood, T.W. and C.C. Askwith, *Dynorphin opioid peptides enhance acid-sensing ion channel 1a activity and acidosis-induced neuronal death.* J Neurosci, 2009. **29**(45): p. 14371-80.

94. Askwith, C.C., C. Cheng, M. Ikuma, C. Benson, M.P. Price, and M.J. Welsh, *Neuropeptide FF and FMRFamide potentiate acid-evoked currents from sensory neurons and proton-gated DEG/ENaC channels.* Neuron, 2000. **26**: p. 133-141.

95. Catarsi, S., K. Babinski, and P. Seguela, *Selective modulation of heteromeric ASIC proton-gated channels by neuropeptide FF.* Neuropharmacology, 2001. **41**(5): p. 592-600.

96. Chen, X., M. Paukert, I. Kadurin, M. Pusch, and S. Gründer, *Strong modulation by RFamide neuropeptides of the ASIC1b/3 heteromer in competition with extracellular calcium.* Neuropharmacology, 2006. **50**(8): p. 964-74.

97. Deval, E., A. Baron, E. Lingueglia, H. Mazarguil, J.M. Zajac, and M. Lazdunski, *Effects of neuropeptide SF and related peptides on acid sensing ion channel 3 and sensory neuron excitability.* Neuropharmacology, 2003. **44**(5): p. 662-71.

98. Ostrovskaya, O., L. Moroz, and O. Krishtal, *Modulatory action of RFamide-related peptides on acid-sensing ionic channels is pH dependent: the role of arginine.* J Neurochem, 2004. **91**(1): p. 252-5.

99. Sherwood, T.W. and C.C. Askwith, *Endogenous arginine-phenylalanine-amide-related peptides alter steady-state desensitization of ASIC1a.* J Biol Chem, 2008. **283**(4): p. 1818-30.

100. Xie, J., M.P. Price, J.A. Wemmie, C.C. Askwith, and M.J. Welsh, *ASIC3 and ASIC1 mediate FMRFamide-related peptide enhancement of H+-gated currents in cultured dorsal root ganglion neurons.* J. Neurophysiol., 2003. **89**: p. 2459-2465.

101. Duan, B., Y.Z. Wang, T. Yang, X.P. Chu, Y. Yu, Y. Huang, H. Cao, J. Hansen, R.P. Simon, M.X. Zhu, Z.G. Xiong, and T.L. Xu, *Extracellular spermine exacerbates ischemic neuronal injury through sensitization of ASIC1a channels to extracellular acidosis.* J Neurosci. **31**(6): p. 2101-12.

102. Baron, A., N. Voilley, M. Lazdunski, and E. Lingueglia, *Acid sensing ion channels in dorsal spinal cord neurons.* J Neurosci, 2008. **28**(6): p. 1498-508.

103. Xiong, Z.G., X.M. Zhu, X.P. Chu, M. Minami, J. Hey, W.L. Wei, J.F. MacDonald, J.A. Wemmie, M.P. Price, M.J. Welsh, and R.P. Simon, *Neuroprotection in ischemia: blocking calcium-permeable acid-sensing ion channels.* Cell, 2004. **118**: p. 687-698.

104. Baron, A., R. Waldmann, and M. Lazdunski, *ASIC-like, proton-activated currents in rat hippocampal neurons.* J. Physiol., 2002. **539**: p. 485-494.

105. Askwith, C.C., J.A. Wemmie, M.P. Price, T. Rokhlina, and M.J. Welsh, *Acid-sensing ion channel 2 (ASIC2) modulates ASIC1 H+-activated currents in hippocampal neurons.* J. Biol. Chem., 2004. **279**: p. 18296-18305.

106. Zha, X.-m., J.A. Wemmie, S.H. Green, and M.J. Welsh, *Acid-sensing ion channel 1a is a postsynaptic proton receptor that affects the density of dendritric spines.* Proc. Natl. Acad. Sci. USA, 2006. **103**: p. 16556-16561.

107. Zha, X.M., V. Costa, A.M. Harding, L. Reznikov, C.J. Benson, and M.J. Welsh, *ASIC2 subunits target acid-sensing ion channels to the synapse via an association with PSD-95.* J Neurosci, 2009. **29**(26): p. 8438-46.

108. Wemmie, J.A., J. Chen, C.C. Askwith, A.M. Hruska-Hageman, M.P. Price, B.C. Nolan, P.G. Yoder, E. Lamani, T. Hoshi, J.H.J. Freeman, and M.J. Welsh, *The acid-activated ion channel ASIC contributes to synaptic plasticity, learning and memory.* Neuron, 2002. **34**: p. 463-477.

109. Miesenbock, G., D.A. De Angelis, and J.E. Rothman, *Visualizing secretion and synaptic transmission with pH-sensitive green fluorescent proteins.* Nature, 1998. **394**(6689): p. 192-5.

110. Krishtal, O.A., Y.V. Osipchuk, T.N. Shelest, and S.V. Smirnoff, *Rapid extracellular pH transients related to synaptic transmission in rat hippocampal slices.* Brain Res, 1987. **436**(2): p. 352-6.

111. Lee, J.M., G.J. Zipfel, and D.W. Choi, *The changing landscape of ischaemic brain injury mechanisms.* Nature, 1999. **399**(6738 Suppl): p. A7-14.

112. Zipfel, G.J., J.M. Lee, and D.W. Choi, *Reducing calcium overload in the ischemic brain.* N Engl J Med, 1999. **341**(20): p. 1543-4.

113. Wahlgren, N.G. and N. Ahmed, *Neuroprotection in cerebral ischaemia: facts and fancies--the need for new approaches.* Cerebrovasc Dis, 2004. **17 Suppl 1**: p. 153-66.

114. Xiong, Z.G., X.P. Chu, and R.P. Simon, *Ca2+ -permeable acid-sensing ion channels and ischemic brain injury.* J Membr Biol, 2006. **209**(1): p. 59-68.

115. Wang, W.Z., X.P. Chu, M.H. Li, J. Seeds, R.P. Simon, and Z.G. Xiong, *Modulation of acid-sensing ion channel currents, acid-induced increase of intracellular Ca2+, and acidosis-mediated neuronal injury by intracellular pH.* J Biol Chem, 2006. **281**(39): p. 29369-78.

116. Simon, R. and Z. Xiong, *Acidotoxicity in brain ischaemia.* Biochem Soc Trans, 2006. **34**(Pt 6): p. 1356-61.

117. Siesjo, B.K., K.I. Katsura, T. Kristian, P.A. Li, and P. Siesjo, *Molecular mechanisms of acidosis-mediated damage.* Acta Neurochir Suppl, 1996. **66**: p. 8-14.

118. Tombaugh, G.C. and R.M. Sapolsky, *Evolving concepts about the role of acidosis in ischemic neuropathology.* J Neurochem, 1993. **61**(3): p. 793-803.

119. Low, C.M., P. Lyuboslavsky, A. French, P. Le, K. Wyatte, W.H. Thiel, E.M. Marchan, K. Igarashi, K. Kashiwagi, K. Gernert, K. Williams, S.F. Traynelis, and F. Zheng, *Molecular determinants of proton-sensitive N-methyl-D-aspartate receptor gating.* Mol Pharmacol, 2003. **63**(6): p. 1212-22.

120. Tang, C.M., M. Dichter, and M. Morad, *Modulation of the N-methyl-D-aspartate channel by extracellular H+.* Proc Natl Acad Sci U S A, 1990. **87**(16): p. 6445-9.

121. Benveniste, M. and R. Dingledine, *Limiting stroke-induced damage by targeting an acid channel.* N Engl J Med, 2005. **352**(1): p. 85-6.

122. Coryell, M.W., A.E. Ziemann, P.J. Westmoreland, J.M. Haenfler, Z. Kurjakovic, X.M. Zha, M. Price, M.K. Schnizler, and J.A. Wemmie, *Targeting ASIC1a reduces innate fear and alters neuronal activity in the fear circuit.* Biol Psychiatry, 2007. **62**(10): p. 1140-8.

123. Wemmie, J.A., M.W. Coryell, C.C. Askwith, E. Lamani, A.S. Leonard, C.D. Sigmund, and M.J. Welsh, *Overexpression of acid-sensing ion channel 1a in transgenic mice increases acquired fear-related behavior.* Proc. Natl. Acad. Sci. USA, 2004. **101**: p. 3621-3626.

124. Coryell, M.W., A.M. Wunsch, J.M. Haenfler, J.E. Allen, J.L. McBride, B.L. Davidson, and J.A. Wemmie, *Restoring Acid-sensing ion channel-1a in the amygdala of knock-out mice rescues fear memory but not unconditioned fear responses.* J Neurosci, 2008. **28**(51): p. 13738-13741.

125. Ziemann, A.E., J.E. Allen, N.S. Dahdaleh, Drebot, II, M.W. Coryell, A.M. Wunsch, C.M. Lynch, F.M. Faraci, M.A. Howard, 3rd, M.J. Welsh, and J.A. Wemmie, *The amygdala is a chemosensor that detects carbon dioxide and acidosis to elicit fear behavior.* Cell, 2009. **139**(5): p. 1012-1021.

126. Ziemann, A.E., M.K. Schnizler, G.W. Albert, M.A. Severson, M.A. Howard III, M.J. Welsh, and J.A. Wemmie, *Seizure termination by acidosis depends on ASIC1a.* Nature Neurosci., 2008. **11**: p. 816-822.

127. Eskandari, S., P.M. Snyder, M. Kreman, G.A. Zampighi, M.J. Welsh, and E.M. Wright, *Number of subunits comprising the epithelial sodium channel.* J. Biol. Chem., 1999. **274**: p. 27281-27286.

128. Coscoy, S., E. Lingueglia, M. Lazdunski, and P. Barbry, *The Phe-Met-Arg-Phe-amide-activated sodium channel is a tetramer.* J. Biol. Chem., 1998. **273**: p. 8317-8322.

129. Snyder, P.M., C. Cheng, L.S. Prince, J.C. Rogers, and M.J. Welsh, *Electrophysiological and biochemical evidence that DEG/ENaC cation channels are composed of nine subunits.* J. Biol. Chem., 1998. **273**: p. 681-684.

130. Kosari, F., S. Sheng, J. Li, D.-O.D. Mak, J.K. Foskett, and T.R. Kleyman, *Subunit stoichiometry of the epithelial sodium channel.* J. Biol. Chem., 1998. **273**: p. 13469-13474.

131. Waldmann, R., *Proton-gated cation channels--neuronal acid sensors in the central and peripheral nervous system.* Adv Exp Med Biol, 2001. **502**: p. 293-304.

132. Deval, E., X. Gasull, J. Noel, M. Salinas, A. Baron, S. Diochot, and E. Lingueglia, *Acid-sensing ion channels (ASICs): pharmacology and implication in pain.* Pharmacol Ther, 2010. **128**(3): p. 549-558.

133. Krishtal, O.A., *The ASICs: Signaling molecules? Modulators?* Trends Neurosci., 2003. **26**: p. 477-483.

134. Yermolaieva, O., A.S. Leonard, M.K. Schnizler, F.M. Abboud, and M.J. Welsh, *Extracellular acidosis increases neuronal cell calcium by activating acid-sensing ion channel 1a.* Proc Natl Acad Sci U S A, 2004. **101**(17): p. 6752-6757.

135. Schild, L., *The epithelial sodium channel and the control of sodium balance.* Biochim Biophys Acta, 2010. **1802**(12): p. 1159-1165.

136. Snyder, P.M., M.P. Price, F.J. McDonald, C.M. Adams, K.A. Volk, B.G. Zeiher, J.B. Stokes, and M.J. Welsh, *Mechanism by which Liddle's syndrome mutations increase activity of a human epithelial Na+ channel.* Cell, 1995. **83**(6): p. 969-978.

137. Chang, S.S., S. Gründer, A. Hanukoglu, A. Rosler, P.M. Mathew, I. Hanukoglu, L. Schild, Y. Lu, R.A. Shimkets, C. Nelson-Williams, B.C. Rossier, and R.P. Lifton, *Mutations in subunits of the epithelial sodium channel cause salt wasting with hyperkalaemic acidosis, pseudohypoaldosteronism type 1.* Nat Genet, 1996. **12**(3): p. 248-253.

138. Yagi, J., H.N. Wenk, L.A. Naves, and E.W. McCleskey, *Sustained currents through ASIC3 ion channels at the modest pH changes that occur during myocardial ischemia.* Circ Res, 2006. **99**(5): p. 501-509.

139. Yu, Y., Z. Chen, W.G. Li, H. Cao, E.G. Feng, F. Yu, H. Liu, H. Jiang, and T.L. Xu, *A nonproton ligand sensor in the acid-sensing ion channel.* Neuron, 2010. **68**(1): p. 61-72.

140. Khakh, B.S., X.R. Bao, C. Labarca, and H.A. Lester, *Neuronal P2X transmitter-gated cation channels change their ion selectivity in seconds.* Nature Neurosci., 1999. **2**: p. 322-330.

141. Samways, D.S., A.B. Harkins, and T.M. Egan, *Native and recombinant ASIC1a receptors conduct negligible Ca2+ entry.* Cell Calcium, 2009. **45**(4): p. 319-325.

142. Mazzuca, M., C. Heurteaux, A. Alloui, S. Diochot, A. Baron, N. Voilley, N. Blondeau, P. Escoubas, A. Gelot, A. Cupo, A. Zimmer, A.M. Zimmer, A. Eschalier, and M. Lazdunski, *A tarantula peptide against pain via ASIC1a channels and opioid mechanisms.* Nat Neurosci, 2007. **10**(8): p. 943-945.

143. Dukkipati, A., H.H. Park, D. Waghray, S. Fischer, and K.C. Garcia, *BacMam system for high-level expression of recombinant soluble and membrane glycoproteins for structural studies.* Protein Expr. Purif. , 2008. **62**: p. 160-170.

144. Otwinowski, Z. and W. Minor, *Processing of X-ray diffraction data collected in oscillation mode.* Meth. Enzymol., 1997. **276**: p. 307-326.

145. McCoy, A.J., *Solving structures of protein complexes by molecular replacement with Phaser.* Acta Crystallogr. D., 2007. **63**: p. 32-41.

146. Emsley, P. and K. Cowtan, *Coot: model-building tools for molecular graphics.* Acta Crystallogr. D., 2004. **60**: p. 2126-2132.

147. Adams, P.D., R.W. Grosse-Kunstleve, L.W. Hung, T.R. Loerger, A.J. McCoy, N.W. Moriarty, R.J. Read, J.C. Sacchettini, N.K. Sauter, and T.C. Terwilliger, *PHENIX: building new software for automated crystallographic structure determination.* Acta Crystallogr. D., 2002. **58**: p. 1948-1954.

148. Davis, I.W., A. Leaver-Fay, V.B. Chen, J.N. Block, G.J. Kapral, X. Wang, L.W. Murray, W.B.r. Arendall, J. Snoeyink, J.S. Richardson, and D.C. Richardson, *MolProbity: all-atom contacts and structure validation for proteins and nucleic acids.* Nucleic Acids Res., 2007. **35**: p. W375-83.

149. Smart, O.S., J.G. Neduvelil, X. Wang, B.A. Wallace, and M.S. Samsom, *HOLE: a program for the analysis of the pore dimensions of ion channel structural models.* J. Mol. Graph., 1996. **14**: p. 354-360.

150. Hayward, S. and R.A. Lee, *Improvements in the analysis of domain motions in proteins from conformational change: DynDom version 1.50.* J. Mol. Graph Model., 2002. **21**: p. 181-183.

151. Saez, N.J., M. Mobli, M. Bieri, I.R. Chassagnon, A.K. Malde, R. Gamsjaeger, A.E. Mark, P.R. Gooley, L.D. Rash, and G.F. King, *A dynamic pharmacophore drives the interaction between Psalmotoxin-1 and the putative drug target acid-sensing ion channel 1a.* Mol Pharmacol, 2011. **80**(5): p. 796-808.

152. Pietra, F., *Docking and MD simulations of the interaction of the tarantula peptide psalmotoxin-1 with ASIC1a channels using a homology model.* J. Chem. Inf. Model, 2009. **49**: p. 972-977.

153. Dawson, R.J., J. Benz, P. Stohler, T. Tetaz, C. Joseph, S. Huber, G. Schmid, D. Hugin, P. Pflimlin, G. Trube, M.G. Rudolph, M. Hennig, and A. Ruf, *Structure of the acid-sensing ion channel 1 in complex with the gating modifier Psalmotoxin 1.* Nat Commun. **3**: p. 936.

154. Hattori, M. and E. Gouaux, *Molecular mechanism of ATP binding and ion channel activation in P2X receptors.* Nature, 2012. **485**: p. 207-212.

155. Li, J., S. Sheng, C.J. Perry, and T.R. Kleyman, *Asymmetric organization of the pore region of the epithelial sodium channel.* J Biol Chem, 2003. **278**(16): p. 13867-13874.

156. Pöet, M., M. Tauc, E. Lingueglia, P. Cance, P. Poujeol, M. Lazdunzki, and L. Counillon, *Exploration of the pore structure of a peptide-gated Na+ channel.* EMBO J., 2001. **20**: p. 5595-5602.

157. Waldmann, R., G. Champigny, F. Bassilana, N. Voilley, and M. Lazdunski, *Molecular cloning and functional expression of a novel amiloride-sensitive Na+ channel.* J Biol Chem, 1995. **270**(46): p. 27411-27414.

158. Hille, B., *Ion channels of excitable membranes*. 3rd ed. 2001, Sunderland, MA: Sinauer Associates, Inc.

159. Graves, R., *The Greek Myths*. 1955, London: Penguin Books.

160. Changeux, J.P., M. Kasai, and C.Y. Lee, *Use of a snake venom toxin to characterize the cholinergic receptor protein.* Proc. Natl. Acad. Sci. USA, 1970. **67**: p. 1241-1247.

161. Walker, C.S., S. Jensen, M. Ellison, J.A. Matta, W.Y. Lee, J.S. Imperial, N. Duclos, P.J. Brockie, D.M. Madsen, J.T. Isaac, B. Olivera, and A.V. Maricq, *A novel Conus snail polypeptide causes excitotoxicity by blocking desensitization of AMPA receptors.* Curr. Biol., 2009. **19**: p. 900-908.

162. Bohlen, C.J. and D. Julius, *Receptor-targeting mechanisms of pain-causing toxins: How ow?* Toxicon, 2012. **60**: p. 254-264.

163. Sherwood, T.W., E.N. Frey, and C.C. Askwith, *Structure and activity of the acid sensing ion channels.* Am. J. Physiol. Cell Physiol., 2012: p. doi: 10.1152/ajpcell.00188.2012.

164. Lingueglia, E., *Acid sensing ion channels in sensory perception.* J. Biol. Chem., 2007. **doi 10.1074**: p. 1-7.

165. Deval, E., J. Noël, N. Lay, A. Alloui, S. Diochot, V. Friend, M. Jodar, M. Lazdunzki, and E. Lingueglia, *ASIC3, a sensor of acidic and primary inflammatory pain.* EMBO J., 2008. **27**: p. 3047-3055.

166. Deval, E., J. Noël, X. Gasull, A. Delaunay, A. Alloui, V. Friend, A. Eschalier, M. Lazdunzki, and E. Lingueglia, *Acid-sensing ion channels in postoperative pain.* J. Neurosci., 2011. **31**: p. 6059-6066.

167. Sutherland, S.P., C.J. Benson, J. Adelman, and E.W. McCleskey, *Acid-sensing ion channel 3 matches the acid-gated current in cardiac ischemia-sensing neurons.* Proc. Natl. Acad. Sci. USA, 2001. **98**: p. 711-716.

168. Chang, C. and C.Y. Lee, *Isolation of neurotoxins from the venom of Bungarus multicinctus and their modes of neuromuscular blocking action.* . Archives Internationales de Pharmacodynamie, 1963. **144**: p. 241-257.

169. Kwong, P.D., N.Q. McDonald, P.B. Sigler, and W.A. Hendrickson, *Structure of β_2-bungarotoxin: potassium channel binding by Kunitz modules and targeted phospholipase action.* Structure, 1995. **3**: p. 1109-1119.

170. Baconguis, I. and E. Gouaux, *Structural plasticity and dynamic selectivity of acid-sensing ion channel-spider toxin complexes.* Nature, 2012. **489**(7416): p. 400-5.

171. Baker, N.A., D. Sept, S. Joseph, M.J. Holst, and J.A. McCammon, *Electrostatics of nanosystems: application to microtubules and the ribosome.* Proc Natl Acad Sci U S A, 2001. **98**(18): p. 10037-41.

172. *CCP4* Project, N., *The CCP4 suite: programs for protein crystallography.* Acta Crystallogr., 1994. **D50**: p. 760-763.

173. Rühlmann, A., D. Kukla, P. Schwager, K. Bartels, and R. Huber, *Structure of the complex formed by bovine trypsin and bovine pancreatic trypsin inhibitor. Crystal structure determination and stereochemistry of the contact region.* J. Mol. Biol., 1973. **77**: p. 417-436.

174. Dennis, E.A., J. Cao, Y.H. Hsu, V. Magrioti, and G. Kokotos, *Phospholipase A2 enzymes: physical structure, biological function, disease implication, chemical inhibition, and therapeutic intervention.* Chem. Rev., 2011. **111**: p. 6130-6185.

175. Sheng, S., J. Li, K.A. McNulty, D. Avery, and T.R. Kleyman, *Characterization of the selectivity filter of the epithelial sodium channel.* J. Biol. Chem., 2000. **275**: p. 8572-8581.

176. Snyder, P.M., D.R. Olson, and D.B. Bucher, *A pore segment in DEG/ENaC Na+ channels.* J. Biol. Chem., 1999. **274**: p. 28484-28490.

177. Kellenberger, S., I. Guatschi, and L. Schild, *A single point mutation in the pore region of the epithelial Na+ channel changes ion selectivity by modifying molecular sieving.* Proc. Natl. Acad. Sci. USA, 1999. **96**: p. 4170-4175.

178. Carattino, M.D. and M.C.D. Vecchia, *Contribution of residues in second transmembrane domain of ASIC1a protein to ion selectivity.* J. Biol. Chem., 2012. **287**: p. 12927-12934.

179. Dougherty, D.A., *Cation-π interactions in chemistry and biology: A new view of benzene, Phe, Tyr and Trp.* Science, 1996. **271**: p. 163-168.